TECHNISCHE UNIVERSITÄT MÜNCHEN

Lehrstuhl für Molekulare Ernährungsmedizin

Characterisation of stromal interaction molecule 1 (STIM1) in the myocardium

Deepak Prabhu Ramanujam

Vollständiger Abdruck der von der Fakultät Wissenschaftszentrum Weihenstephan für Ernährung, Landnutzung und Umwelt der Technischen Universität München zur Erlangung des akademischen Grades eines

Doktors der Naturwissenschaften

genehmigten Dissertation.

Vorsitzende: Univ.-Prof. Dr. Hannelore Daniel

Prüfer der Dissertation:
                1. Univ.-Prof. Dr. Martin Klingenspor
                2. Univ.-Prof. Dr. Dr. Stefan Engelhardt

Die Dissertation wurde am ……07.06.2013………… bei der Technischen Universität München eingereicht und durch die Fakultät Wissenschaftszentrum Weihenstephan für Ernährung, Landnutzung und Umwelt am ……10.10.2013…… angenommen.

Contents

List of figures

Abbreviations

α-MHC	alpha-myosin heavy chain
AAV	adeno associated virus
AC	adenylyl cyclase
ANF	atrial natriuretic factor
AngII	angiotensinII
ANOVA	analysis of variance
ARCF	adult rat cardiac fibroblasts
ARCM	adult rat cardiomyocytes
AU	arbitrary units
ATP	adenosine triphosphate
ß-AR	ß-adrenergic receptor
BSA	bovine serum albumin
BW	body weight
Ca^{2+}	calcium
CAD	Ca^{2+} activating domain
CALM	calmodulin
CAMKII	calmodulin dependent kinase II
cAMP	cyclic adenosine monophosphate
CASQ2	calsequestrin2
CDI	Ca^{2+} dependent inactivation
CFP	cyan fluorescent protein
CoIP	co-immunoprecipitation
CRAC	Ca^{2+} release activated Ca^{2+}
C-terminus	carboxy terminus
DAG	diacylglycerol
ddH_2O	double distilled water
DMSO	dimethylsulphoxide
DNA	deoxyribonucleic acid
dNTP	deoxyribonucleotidetriphosphate
dn	dominant negative
DTT	dithiothreitol
ECL	enhanced chemiluminescence
EDTA	ethylenediaminetetraacetic acid
EF	ejection fraction
ER	endoplasmic reticulum
FCS	foetal calf serum
FRET	fluorescence resonance energy transfer
FS	fractional shortening
GPCR	G protein-coupled receptor
G_s	stimulatory G protein
HDAC	histone deacetylase
HEK	human embryonic kidney
HW	heart weight
IP_3R	inositol triphosphate receptor
kDa	1000 daltons
LTCC	L-type voltage-gated Ca^{2+} channel
LV	left ventricle
LVID	left ventricular inner diameter
LVPW	left ventricular posterior wall thickness
M	Molar
mA	milli ampere

MAPK	mitogen-activated protein kinase
MBP	myosin-binding protein C
MEF2	myocyte enhancer factor 2
min	minute
Na^+	sodium
NCX	Na^+/Ca^{2+} exchanger
NHE	Na^+/H^+ exchanger
NFAT	nuclear factor of activated T-cells
NRCF	neonatal rat cardiac fibroblasts
NRCM	neonatal rat cardiomyocytes
N-terminus	amino terminus
ORAI	calcium release-activated calcium modulator
PCR	polymerase chain reaction
PE	phenylephrine
pH	power of hydrogen
PIP_2	phosphatidylinositol-4,5-bisphosphate
PKA	protein kinase A
PKC	protein kinase C
PLC	phospholipase C
PLN	phospholamban
PM	plasma membrane
PMCA	plasma membrane Ca^{2+} ATPase
PPP3CA	protein phosphatase 3 (calcineurin A)
PPP3CB	protein phosphatase 3 (calcineurin B)
RNA	ribonucleic acid
ROCC	receptor operated Ca^{2+} channel
RyR	ryanodine receptor
s	second
SAM	sterile α-motif
SERCA	sarcoplasmic reticulum Ca^{2+} ATPase
s.e.m.	standard error mean
sh	short hairpin
siRNA	small interfering RNA
SOAR	STIM1 ORAI1 activating region
SOC	store-operated Ca^{2+}
SOCE	store-operated Ca^{2+}-entry
SR	sarcoplasmic reticulum
STIM1	stromal interaction molecule1
TAC	transverse aortic constriction
TAE	tris-acetate EDTA
TG	thapsigargin
TGFß	tumour growth factor ß
TIRF	total internal reflection fluorescence
TNNI	troponin I
TRPC	transient receptor potential cation channel
UV	ultraviolet
v/v	volume to volume
w/v	weight to volume
YFP	yellow fluorescent protein
°C	degree Celsius

1. Introduction

1.1 Cardiac growth in health and disease

Cardiac hypertrophy is the enlargement of the heart as a result of the *in vivo* adaptive mechanism in response to stress, cardiac injury, valvular dysfunction and genetic defects [1]. Cardiac hypertrophy is typically associated with ventricular remodelling and alterations in the extracellular matrix, which can lead to cardiac dysfunction and cell death [2].

Ventricular remodelling, in particular, is not lethal all the times but allows for compensation of the mechanical overload by hypertrophy while still maintaining cardiac function. This phenomenon, known as compensated hypertrophy, was observed by Krayenbuehl and colleagues in patients with aortic stenosis in which increased fibrosis and myocyte hypertrophy correlated with normal ejection fraction and high left ventricular end diastolic pressure [3].

Ventricular remodelling can be divided into three types – developmental, physiological and pathological hypertrophy. Developmental hypertrophy refers to the enlargement of the heart muscle from birth to adulthood. Physiological hypertrophy is associated to hypertrophy induced by exercise or pregnancy and is thought to be adapted in the long term. It is characterized by myocyte enlargement, no fibrosis and normal heart function. Pathological hypertrophy is disease-inducing and can be further classified into dilation, concentric and eccentric hypertrophy [4].
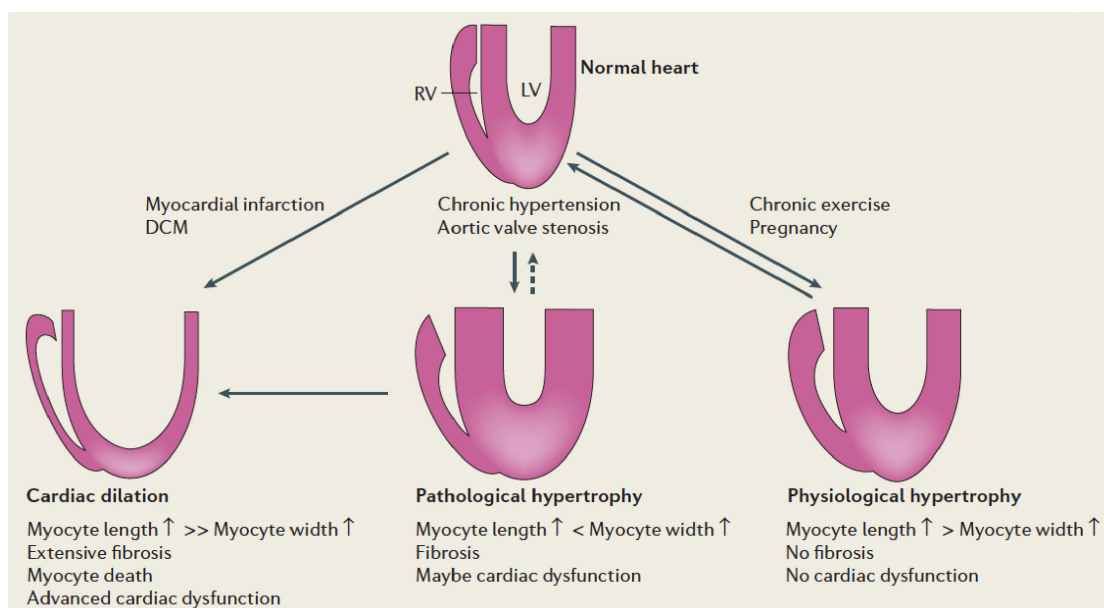
Figure 1. Types of cardiac hypertrophy.
Illustration from Heineke *et al* 2006.

1

1.2. Calcium signalling in the heart

Cardiac excitation-contraction coupling is the process that begins with the electrical excitation of the cardiac myocyte and ends with the contraction of the heart ejecting the blood out of the heart to different parts of the body. Calcium (Ca^{2+}) is the ubiquitous second messenger that moderates the electrical excitation of the cardiac myocyte and subsequent activation of the myofilaments, which leads to muscle contraction [5,6].

During the cardiac action potential, depolarization of the plasma membrane causes an influx of Ca^{2+} into the cytoplasm through sequential opening of L-type voltage-gated Ca^{2+} channels (LTCC). Ca^{2+} entry into the cell then triggers Ca^{2+} release from the sarcoplasmic reticulum (SR) in a Ca^{2+} induced Ca^{2+} release (CICR) manner via ryanodine receptors (RyR2). Ca^{2+} influx into the cell in combination with SR-Ca^{2+} release raises the free intracellular Ca^{2+} ($[Ca^{2+}]_i$) within the cytosol. This then binds to the myofilament protein troponinC facilitating actin-myosin interactions that lead to contraction. Relaxation occurs when there is decline of $[Ca^{2+}]_i$ in the cytoplasm thus allowing for the dissociation of Ca^{2+} from troponinC [5,6].
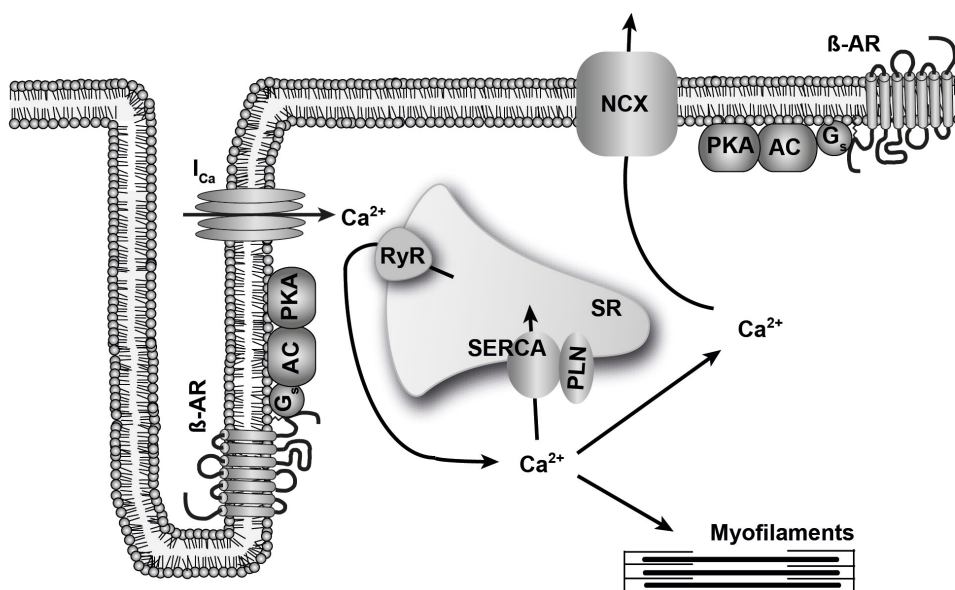
Figure 2. Ca^{2+} transport in ventricular myocytes during excitation-contraction coupling.
AC - adenylyl cyclase; ß-AR - ß-adrenergic receptor; G_s - stimulatory G-protein; I_{Ca} - L-type voltage-gated Ca^{2+} channel; NCX - Na^+/Ca^{2+} exchanger; PKA - protein kinase A; PLN - phospholamban; RyR - ryanodine receptor; SERCA - sarcoplasmic reticulum Ca^{2+} ATPase; SR - sarcoplasmic reticulum.

Ca^{2+} extrusion out of the cell occurs by 4 channels – sarcoplasmic reticulum Ca^{2+}-ATPase (SERCA), sarcolemmal Na^+/Ca^+ exchange (NCX), sarcolemmal Ca^{2+}-ATPase and mitochondrial Ca^{2+} uniporter channel. In rat and mouse ventricles, SR Ca^{2+}-

ATPase and sarcolemmal Na^+/Ca^+ exchanger extrude about 92% and 7% of the Ca^{2+} out of the cytosol. The remaining 1% is extruded out by the slow systems – sarcolemmal Ca^{2+} ATPase and mitochondrial Ca^{2+} uniporter [7,8]. In the case of rabbits and humans, the SR Ca^{2+}-ATPase extrudes about 70% compared to 28% by Na^+/Ca^+ exchanger [9]. This difference is attributed to the higher number of SR Ca^{2+}-ATPase pumps in the rat ventricles compared to rabbit and human ventricles [9].

In a cardiomyocyte cell, 0.1-1 µM Ca^{2+} is generally seen in the bulk of the cytoplasm although the amount of local Ca^{2+} near the channels could be much higher. For every contraction coupling, the cell has to be heavily buffered with high Ca^{2+} (about 150 µM) to increase the diastolic Ca^{2+} concentration of 100 nM to a systolic concentration of 1 µM [10]. For every cardiac beat, the amount of Ca^{2+} extruded out of the cells should be balanced by the same amount of Ca^{2+} influx into the cell. If this balance is not maintained, then the cell either gains or loses Ca^{2+} thereby disrupting the steady state.

1.2.1. Key molecules involved in calcium signalling

1.2.1.1. L-type voltage-gated Ca^{2+} channels

The L-type Ca^{2+} channel is the main entry point of Ca^{2+} influx into the cell and triggers excitation-contraction coupling in excitable cells such as cardiac myocytes. The LTCCs are primarily located at the sarcolemmal-SR junctions (dyadic cleft) such that they are in close proximity to the SR Ca^{2+} release channels like the ryanodine receptors [5,11]. At resting membrane potential, the channel is closed. Ca^{2+} influx into the cell via LTCCs (I_{Ca}) upon membrane depolarization increases the Ca^{2+} sparks in the dyadic clefts, which then triggers the SR Ca^{2+} release via the RyR receptors. The local $[Ca^{2+}]_I$ in these clefts could increase up to 50 µM during the excitation-contraction coupling [12]. This increase in local $[Ca^{2+}]_I$ near the LTCC triggers the Ca^{2+}-dependent inactivation of the LTCC [13] thereby serving as a negative feedback loop for Ca^{2+} influx via LTCC. Ca^{2+}-dependent inactivation of the LTCCs is mediated by binding of active Ca^{2+}-calmodulin to the carboxy terminus of the LTCC channel protein [14]. Taken together, I_{Ca} and SR Ca^{2+}-release serve as local negative feedback loops for high Ca^{2+} influx.

1.2.1.2. IP$_3$ receptor operated Ca^{2+} channels

Receptor operated cation channels are typically gated by binding of agonists to the surface receptors of the cell. This concept of Ca^{2+} entry independent of membrane

3

depolarization and Ca^{2+} influx in smooth muscle cells was first introduced in 1968 [15,16].

Agonist binding to G-protein coupled receptors (G_q) in the plasma membrane activates specific phospholipase C (PLC) isoforms leading to the cleavage of phosphatidylinositol-4,5-bisphosphate (PIP_2) into diacylglycerol (DAG) and inositol-1,4,5-triphosphate (IP_3) [17]. The liberated IP_3 then binds to IP_3 receptors present on the SR membrane triggers intracellular Ca^{2+} release. Although IP_3 mediated Ca^{2+} release does not cause any activation of the cation conductance [18], it can augment the current [19]. In addition to neurotransmitter and hormonal agonists, cardiac $\alpha 1$-adrenergic receptor and muscarinic2 (M2) receptor agonists also increase IP_3 production and muscle contraction [20], but the inotropic effects induced by these agonists are predominantly mediated by protein kinase C and not IP_3 [21]. IP_3Rs are regulated both by IP_3 and also cytosolic Ca^{2+} that forms a positive feedback loop allowing Ca^{2+} release in a Ca^{2+} induced Ca^{2+} release manner. High cytosolic IP_3 and low cytosolic Ca^{2+} trigger activation of IP_3Rs, whereas cytosolic Ca^{2+} concentrations in the range of 1-10 µM can inhibit channel activation [22].

1.2.1.3. Ryanodine receptors

Ryanodine receptors, which are structurally similar to the IP_3Rs, serve both as SR Ca^{2+} release channel and also a scaffolding protein that localizes several key regulatory proteins such as calmodulin to the junctional dyads. These receptors are activated at 1-10 µM cytosolic Ca^{2+} and are inhibited by high cytosolic Ca^{2+} of about 10-100 µM [23]. They play a crucial role during excitation-contraction coupling producing thousands of Ca^{2+} sparks in synchronization with the action potential. Ca^{2+} sparks under resting state is very rare but in cells with high cytosolic and SR Ca^{2+} loads, Ca^{2+} sparks generated at one junction could trigger Ca^{2+} sparks in the neighboring junctions resulting in propagative Ca^{2+} waves.

1.2.1.4. SR Ca^{2+}-ATPase (SERCA)

Sarcoplasmic reticulum Ca^{2+} ATPase (SERCA) is the major Ca^{2+} extrusion pathway (about 70% of the cytosolic Ca^{2+}) from the cytosol causing relaxation of cardiomyocytes [8]. It is a critical molecule that maintains Ca^{2+} homeostasis during excitation-contraction coupling that results in the normal contractility of the heart. The pump activity is regulated by two proteins – phospholamban (PLN) and calsequestrin (CASQ2). Phospholamban is an integral membrane protein present in

the SR that regulates the uptake of cytosolic Ca^{2+} into the SR. In its unphosphorylated form it is bound to SERCA and inhibits its activity. But upon phosphorylation by protein kinase A (PKA), phospholamban dissociates itself from SERCA thereby opening them for Ca^{2+} uptake [24]. This PKA-mediated uptake of Ca^{2+} results in shorter delays between muscle contractions thereby contributing to the lusitropic effects mediated by ß-adrenergic signalling. Calsequestrin (CASQ2) is a high affinity Ca^{2+} binding protein present in the lumen of the SR (40 mol Ca^{2+} per mol of protein) which is responsible for storage and release of Ca^{2+} upon activation of the RyR2 [25]. High load of Ca^{2+} in the SR results in high Ca^{2+} release through the RyR2 receptors [26]. This suggests that the high free Ca^{2+} present in the SR also contributes positively to the open probability of the RyR2 channels.

The function of the pump can be specifically inhibited using four inhibitors and has been listed in the order of their decreasing binding affinities to SERCA – thapsigargin, thapsigarcin, cyclopiazonic acid and 2,5-di-(tert-butyl)hydroquinone. Thapsigargin is a highly specific inhibitor that can targe*t al*l isoforms of protein by forming an irreversible chemical complex with the Ca^{2+}-free SERCA [27].

1.2.1.5. Na$^+$/Ca$^+$ exchanger (NCX)

Na^+/Ca^+ exchanger is the major Ca^{2+} extrusion pathway from the cytosol into the extracellular space. The channel exchanges one Ca^{2+} for three Na^+ ions. The direction and the activity of the channel highly depend on the cytosolic and extracellular concentrations of both Ca^{2+} and Na^+ ions and also on the membrane potential [28]. High cytosolic $[Ca^{2+}]_i$ favours extrusion of Ca^{2+} into extracellular space, whereas high membrane potential and high $[Na^+]_i$ favours Ca^{2+} influx into the cell [29] which can trigger SR Ca^{2+} release when Ca^{2+} influx via LTCC and/or SR Ca^{2+} release is blocked. The rise in Na^+ in the dyadic cleft causes NCX to transiently reverse. Using ventricular-specific NCX knockout mice, Goldhaber *et al* found that NCX was an essential regulator of cardiac contractility independent of SR Ca^{2+} load [30].

1.2.1.6. Modulation of Ca^{2+} by sympathetic activation

Sympathetic stimulation of ß-adrenergic receptor can not only influence increases in developed contraction (inotropy) but also accelerates relaxation with decrease in (lusitropy). Agonist binding to ß-adrenergic receptor activates stimulating G-protein (G_s) which then stimulates adenylyl cyclase (AC) leading to production of cAMP. cAMP then activates PKA that phosphorylates proteins involved in excitation-

contraction coupling. The inotropic effect of PKA is mediated by the phosphorylation of LTCC [31] and RyR2 [32], which increases contractility by enhancing I_{Ca} and SR Ca^{2+} release. PKA phosphorylation of troponin I [33] and myosin-binding protein C [34] modulates Ca^{2+} sensitivity of the myofilaments. The lusitropic effects of PKA, however, are mediated by phosphorylation of phospholamban [35] resulting in its dissociation from SERCA, thereby augmenting speedy uptake of Ca^{2+} and accelerated relaxation.
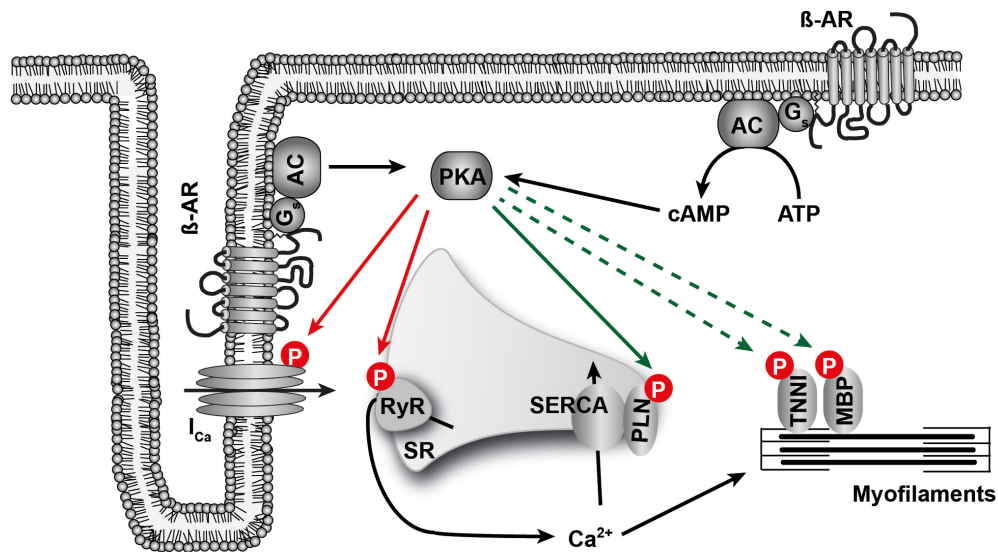
Figure 3. ß-adrenergic stimulation and PKA-mediated phosphorylation of targets during excitation-contraction coupling.
P in red circle indicates phosphorylation. The inotropic and lusitropic effects of ß-adrenergic activation are represented by red and green lines, respectively. PKA-mediated effect on Ca^{2+} sensitivity is represented by green dashed line.
AC - adenylyl cyclase; ATP - adenosine triphosphate; ß-AR - ß-adrenergic receptor; cAMP - cyclic adenosine monophosphate; G_s - stimulatory G-protein; I_{Ca} - L-type voltage-gated Ca^{2+} channel; MBP - myosin-binding protein C; PKA - protein kinase A; PLN - phospholamban; RyR - ryanodine receptor; SERCA - sarcoplasmic reticulum Ca^{2+} ATPase; SR - sarcoplasmic reticulum; TNNI - troponin I.

1.2.2. Calmodulin

Calmodulin (CALM) is the central mediator of Ca^{2+} signalling acting as a Ca^{2+} sensor for many ion channels and a Ca^{2+} transducer for many signalling pathways. Calmodulin is a highly conserved small protein that contains four EF hand-binding motifs that can each bind to calcium [36]. It has a dumbbell-shaped structure with two globular domains at either end linked by a α-helix. Each globular domain has 2 EF hand Ca^{2+} binding motifs.

The two Ca^{2+} binding sites on the C-end have higher Ca^{2+}-affinity at K_d ~1 µM while the two sites on the N-terminal end have lower Ca^{2+} affinity at K_d ~12 µM [37]. Ca^{2+} binding to the N-terminal end has a faster dissociation rate than the C-end. CALM

binds to Ca^{2+} at $K_d \sim 5$ μM which is higher than the average Ca^{2+} concentration of about 0.1 μM in diastole to about 1 μM in systole [37]. This suggests that the average bulk physiologic Ca^{2+} transients during the excitation-contraction coupling cannot trigger CALM mediated Ca^{2+} signalling but is active near the channels where the local Ca^{2+} could be much higher. Ca^{2+} binding to target proteins can significantly alter binding properties of CALM. Ca^{2+} dissociates at a slower rate when bound to proteins and therefore, affinity for Ca^{2+} to be bound with CALM is greatly enhanced. The high affinity for calcineurin to bind the Ca^{2+}-CALM complex, in turn, also enhances the affinity of Ca^{2+} for CALM [38].

Maier *et al* [39] measured the total amount of CALM available in the adult ventricular myocytes at about 6 μM, of which only 1% (~ 50 nM) is available as free CALM [40] that can bind to target proteins. For this reason, CALM has been suggested to be the limiting factor in Ca^{2+} signalling. These freely available CALM are called 'promiscuous' CALM that are typically found in the dyadic clefts and regions near Ca^{2+} channels. The 'dedicated' CALM that lies predominantly bound to the channels even in resting state help in the regulation of the channel activity. For example, Ca^{2+}-dependent inactivation of LTCC is mediated by Ca^{2+} binding to the C-terminus sites of 'dedicated' CALMs [14,41]. 'Dedicated' CALMs also play a crucial role in the inactivation of RyR2 receptors at high Ca^{2+} [42].

'Promiscous' CALM typically requires Ca^{2+} bound to both ends and plays important roles in CamKII-dependent LTCC facilitation [43] and RyR2 leakiness via CamKII-dependent hyperphosphorylation of the receptors [44]. Taken together, major cellular signalling events require locally activated CALM and a high Ca^{2+} buffer.

1.2.3. Calcineurin and NFAT

Calcineurin is a protein phosphatase that is specifically activated by sustained elevations in intracellular Ca^{2+} levels [45,46]. It exists as a heterodimer of a 61 kDa calmodulin binding catalytic subunit A (PPP3CA) and a 19 kDa Ca^{2+} binding regulatory subunit B (PPP3CB) that controls calcineurin activation, and that is highly conserved amongst species [47]. PPP3CA consists of a phosphatase domain, a calmodulin binding site and an auto-inhibitory domain, while PPP3CB shares a similar structure as that of calmodulin with two lobes each containing two Ca^{2+} binding EF hands [48]. As expected, it binds 4 mol of Ca^{2+} with one high affinity Ca^{2+} binding EF hand and three low affinity Ca^{2+} binding EF hands [49]. At low Ca^{2+}, the high affinity Ca^{2+} binding EF hand is occupied and PPP3CB is bound to PPP3CA with the

autoinhibitory domain sterically blocking the active site of the phosphatase. At high Ca^{2+}, Ca^{2+}/calmodulin binds to PPP3CA/B complex and facilitates a conformational shift of the autoinhibitory domain thereby opening up the enzyme active site [46]. Calcineurin exerts its biological effects through two class of transcription factors, nuclear factor of activated T cells (NFAT) and myocyte enhancer factor 2 (MEF2), both of which are implicated in cardiac hypertrophy [50,51].

NFAT are the best-characterized calcineurin-mediated transcription factors. Out of 5 isoforms of NFAT, four are regulated by calcineurin activity (NFATc1-c4). NFAT proteins are present in the cytosol in a hyperphosphorylated inactive state that upon calcineurin-dependent dephosphorylation, translocates to the nucleus and regulates the transcription of genes. The transcription factor MEF2 can be activated either by calcineurin-dependent dephosphorylation or calcineurin-independent CamKII-HDAC inactivation.

1.2.4. Calcium signalling in diseased myocardium

Initiation of cardiac hypertrophy can be broadly categorized into either biomechanical stretch mechanisms or neurohormonal stimulation resulting in production of cytokines, secretory proteins and other growth factors. Cardiac hypertrophy is typically triggered by agonist-mediated stimulation of the GPCRs on the plasma membrane resulting in activation of tyrosine or serine/threonine kinases that are present on their intracellular domains.

Pathological cardiac hypertrophy is typically characterized by activation of Ca^{2+} dependent signalling pathways [52] and re-expression of foetal genes [53]. Intracellular Ca^{2+} levels can be increased through five routes – IP_3 dependent release of internal stores, LTCC, RyR2 leak, reversal of NCX and STIM1-dependent SOCE.

Agonist binding to the G_q-coupled GPCRs activates the phospholipase C bound to their intracellular domain resulting in phosphokinase C activation and IP_3 production. The liberated IP_3 binds to IP_3R on the ER membrane releasing Ca^{2+} from the internal stores. This, in turn, mediates hypertrophic signalling via calcineurin-NFAT activation [54] or CAMKII-HDAC inactivation [55]. Increases in intracellular Ca^{2+} allows for greater diffusion of Ca^{2+}-CALM to move out of the dyadic or local channels clefts thereby resulting in increased Ca^{2+}-CALM in the cytosolic compartment [56] and binding to calcineurin. Binding with calcineurin increases the stability of this complex and de-phosphorylates NFAT transcription factors present in the cytosol thereby triggering their translocation to the nucleus and transcription of the pro-hypertrophic genes.

The coupling effect of the LTCC on the SR Ca^{2+} release channel RyR2 and the feedback of RyR2 on LTCC are crucial for intracellular Ca^{2+} levels. High load of SR Ca^{2+} leads to high release by RyR2 and therefore better inactivation of the LTCC. Despite reduction in the number of channels during heart failure [57], the single channel activity is greatly increased [58] due to ß-adrenergic signalling. T-tubule disorganization during heart failure leads changes in the dyad geometry leading to translocation of LTCC outside of the dyadic clefts [59].

ß-adrenergic induced PKA-mediated hyperphosphorylation of RyR2 in heart failure can lead to diastolic RyR2 leak and therefore lesser SR Ca^{2+} content [32]. High load of SR Ca^{2+} in the presence of high Ca^{2+} also triggers RyR2 leak [60].

Dynamic equilibrium between Na^+ and Ca^{2+} plays a crucial role in maintaining Ca^{2+} homeostasis. G_q-mediated and high intracellular Ca^{2+} increases PKC activation thereby increasing in the Na^+ cytosolic content. This in turn causes a reversal of the NCX pump that increases the Ca^{2+}-influx into the cell.

Ca^{2+} depletion in the stores can also contribute to high cytosolic free Ca^{2+} by increasing Ca^{2+}-influx through STIM1-dependent store-operated channels, which is the topic of interest of this dissertation.
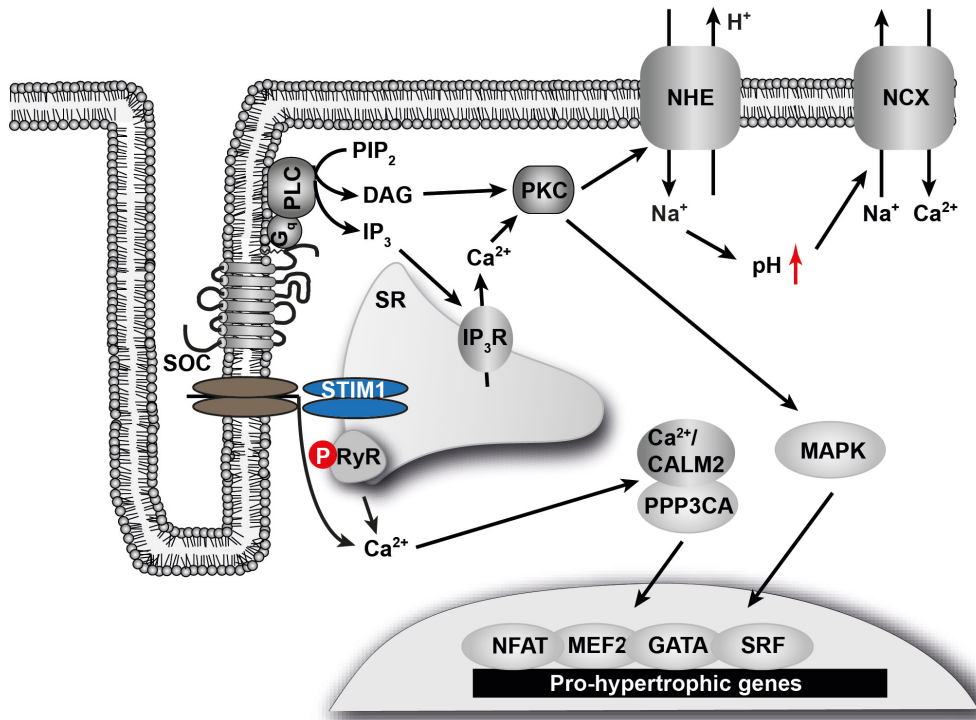
Figure 4. Calcium transport in failing heart.
P in red circle indicates phosphorylation. AC - adenylyl cyclase; ß-AR - ß-adrenergic receptor; CALM2 - calmodulin 2; DAG - diacylglycerol; G_q - G-protein, q-subunit; IP_3 - inositol triphosphate; IP_3R - inositol triphosphate receptor; MAPK - mitogen-activated protein kinase; MEF2 - myocate enhancer factor 2; NCX - Na^+/Ca^{2+} exchanger; NFAT - nuclear factor of activated T-cells; NHE - Na^+/H^+ exchanger; pH - power of hydrogen; PIP_2 - phosphatidylinositol-4,5-bisphosphate; PKC - protein kinase C; PLC - phospholipase C; PLN - phospholamban; PPP3CA - protein phosphatase 3 (calcineurin); RyR - ryanodine receptor; SERCA - sarcoplasmic reticulum Ca^{2+} ATPase; SOC - store-operated Ca^{2+} channel; SR - sarcoplasmic reticulum; SRF - serum reponse factor; STIM1 - stromal interaction molecule 1.

1.3. Store-dependent Ca^{2+} entry (SOCE) as a candidate mechanism for myocardial Ca^{2+} signalling

Store operated Ca^{2+} entry is the major Ca^{2+} entry route in non-excitable cells. It comprises plasma membrane ion channels that are activated upon depletion of the intracellular Ca^{2+} stores in response to the generation of IP_3. When IP_3 binds to the IP_3 receptors in the ER membrane, the Ca^{2+} is released from the ER into the cytosol causing the free Ca^{2+} in the ER to drop significantly from its resting concentration of 600 µM [61]. It was first postulated and identified by Putney and colleagues when they monitored cytosolic Ca^{2+} changes from low to high Ca^{2+} in parotid acinar cells [62,63]. Treatment with muscarinic antagonists resulted in rapid and larger Ca^{2+} transients in the acinar cells.

Apart from maintaining Ca^{2+} homeostasis in non-excitable cells, SOCC regulate a variety of cellular functions such as cell contraction, growth, secretion, adhesion, proliferation, activation of Ca^{2+} dependent enzymes and also gene transcription by activating transcription factors [64–66]. SOC has been identified in a multitude of cells

including T-cells, mast cells, hepatocytes, smooth muscle cells, skeletal muscle cells and neurons [67,68]. Ca^{2+} release activated Ca^{2+} (CRAC) was the first identified subtype of SOC, which is a highly Ca^{2+} selective cation channel. Despite the fact that these channels were well-characterised electrophysiologically in T-cells and mast cells [61,67], it took nearly two decades to identify the molecular composition and nature of these channels. The molecular composition of this channel came into light upon identification of STIM1, a protein on the ER membrane, that serves as a Ca^{2+} sensor for store depletion [69,70] and the gating channel protein, ORAI1, that is present on the plasma membrane [71,72]. It has since then be confirmed by several groups that STIM1 and ORAI1 are both sufficient and necessary for Store operated Ca^{2+} entry [73–75].

The most interesting aspect of SOC is its high selectivity for Ca^{2+} [76]. The channel shows high selectivity towards Ca^{2+} in solutions containing monovalent ions but in the absence of extracellular Ca^{2+} and other divalent ions it can allow permeation of monovalent ions [77,78].

Although SOCE has been extensively studied in non-excitable cells, little is known about its existence, function and physiological relevance in healthy and failing cardiomyocytes. Two independent groups – Hunton and Uehara – showed the existence of SOCE in neonatal cardiomyocytes [79,80]. Hunton also showed that inhibition of SOCE resulted in prevention of NFAT translocation to the nucleus and phenylephrine-induced cardiomyocytes hypertrophy. However, SOCE as well as IP_3-induced Ca^{2+} release was not detected in healthy terminally differentiated adult cardiomyocytes [80,81]. The existence of SOCE in embryonic and neonatal cardiomyocytes but not in adult cells might suggest that SOCE does not contribute to Ca^{2+} regulation during the excitation-contraction coupling but might play a crucial role in the developing heart and also in the heart undergoing pathological remodelling [80,82].
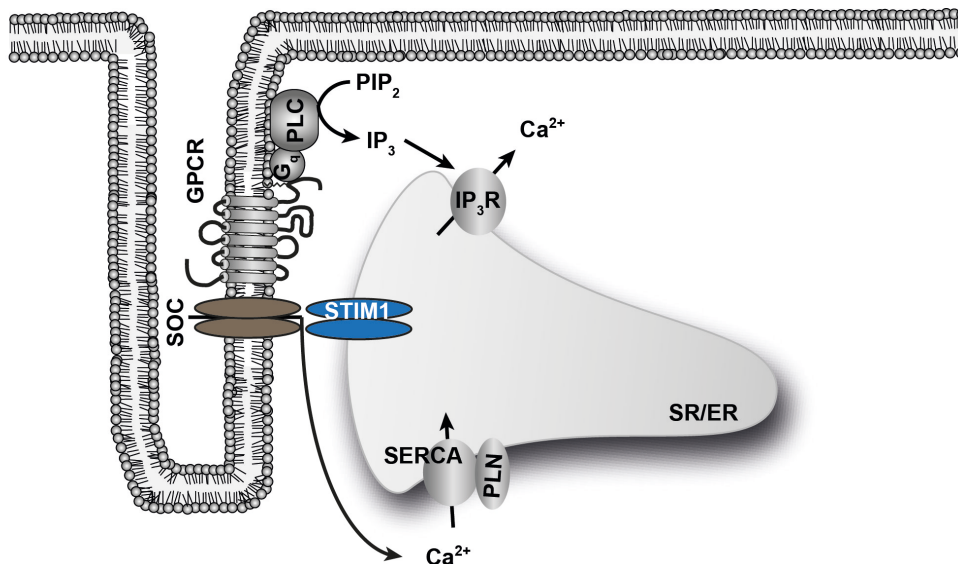
Figure 5. Store-operated Ca^{2+} channels.
GPCR - G-protein coupled receptor; G$_q$ - G-protein, q-subunit; IP$_3$ - inositol triphosphate; IP$_3$R - inositol triphosphate receptor; PIP$_2$ - phosphatidylinositol-4,5-bisphosphate; PLC - phospholipase C; PLN - phospholamban; SERCA - sarcoplasmic reticulum Ca^{2+} ATPase; SOC - store-operated Ca^{2+} channel; SR/ER - sarcoplasmic reticulum / endoplasmic reticulum; SRF - serum reponse factor; STIM1 - stromal interaction molecule 1.

1.3.1. STIM1

Stromal interaction molecule 1 (STIM1) is the ER Ca^{2+} sensor, which is the primary regulator of SOC [69,70,83]. The critical role of STIM1 in SOC was identified by both Roos *et al* and Zhang *et al* by a small interference RNA approach. Even before its discovery as a Ca^{2+} sensor in SOC, it was first identified as 'stromal interacting molecule (SIM)' by Oritani and Kincade [84] in a screen for cell surface receptors in stromal cells. In the study it was identified to be a type I transmembrane protein that helps in the proliferation and survival of the pre B cells. The molecule is highly conserved from roundworms to mammals that emphasize its significance in eukaryotes [62]. STIM1-induced Ca^{2+} influx was identified to regulate biological processes in numerous cell types [85,86]. Mutations in *Stim1* have been known to cause hereditary immunodeficiencies and also auto-immune diseases [85].

STIM1 is a 75 kDa single pass transmembrane protein containing 685 aminoacids and localizes on chromosome 11p15.5. It consists of a 22 kDa N-terminal portion within the lumen of the ER, a single transmembrane segment and a 51 kDa C-terminal portion at the cytosolic side (Figure 6) [85]. The N-terminus portion contains a ER signal peptide, a single canonical EF-hand Ca^{2+} binding domain and a sterile α-motif (SAM) domain which has been identified as a putative protein interaction module, while the C-terminus consists of two coiled-coil domains, a proline/serine rich and a Lys rich region [87,88]. The SAM domain allows STIM1 to homo- or hetero-

oligomerize resulting in self-association architectures [89]. The cytosolic C-terminus is required for the redistribution of STIM1 into punctae in regions very close to the plasma membrane [90,91].
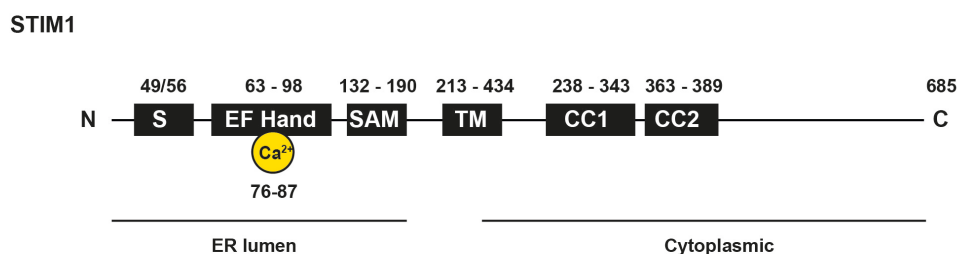
STIM1

Figure 6. Domain structure of STIM1.

1.3.1.1. STIM1 as calcium sensor

The EF hand present on the N-terminus portion is responsible for Ca^{2+} sensing within the lumen of the ER. The canonical EF (cEF1) hand of STIM1 is structurally similar to that of CALM and has a very low affinity for Ca^{2+} at 500 – 600 µM such that it can respond to Ca^{2+} within the ER at range of 100 – 800 µM [71,87]. Stathapulos *et al* [87] also identified another hidden EF hand (hEF2) within the EF-SAM domain, which cannot bind Ca^{2+} but stabilizes the cEF1 hand by formation of an EF-hand pair through hydrogen bonding. The EF-hand pair mediates a tight interaction with the SAM domain to form a stable EF-SAM structure. Ca^{2+} only binds to the first EF hand and the resulting EF-SAM complex bound to Ca^{2+} renders the proteins to exist as monomer [87,92]. The EF hand pair engages the α-helix of the SAM domain to form a stable structure in the same manner as to how Ca^{2+}-CALM engages its target peptides [87,93]. Store depletion would destabilize the EF hand-SAM domain complex exposing the hydrophobic residues and resulting in oligomerization of STIM1 proteins into aggregates called as puncta. The refilling of the stores results in the reformation of the stable EF-Ca^{2+}-SAM resulting in the breaking down of oligomer aggregates into monomers that are then redistributed in the bulk of ER. Contributing to this model of STIM1 as a sensor, mutations in the acidic residues at the Ca^{2+}-binding EF motifs resulted in constitutive activation of CRAC currents in both Drosophila S2 cells and in the T lymphocytes [69,70,73]. Mutations engineered on sites that destabilize the EF-SAM complex induced EF-SAM aggregation [87].

1.3.1.2. Store depletion leads to STIM1 translocation

In resting cells when the stores are replete with Ca^{2+}, STIM1 is distributed diffusely in the bulk of the ER. Upon store depletion, STIM1 oligomerizes and formed distinct puncta-like structures near the plasma membrane – endoplasmic reticulum (PM-ER) junctions (Figure 7). Increases in fluorescence resonance energy transfer (FRET) signal between CFP-STIM1 and YFP-STIM1 observed upon store depletion is direct evidence that STIM1 oligomerizes during Ca^{2+} sensing [94]. Mutations disabling Ca^{2+} binding to the EF hand or targeted substitutions at the hidden EF hand or the SAM domain resulted in constitutive localization of STIM into puncta [69,87]. Also increase in SOCE observed in these EF-SAM domain mutations suggests that disabling Ca^{2+} binding was functionally equivalent to STIM1 oligomerization upon store depletion.
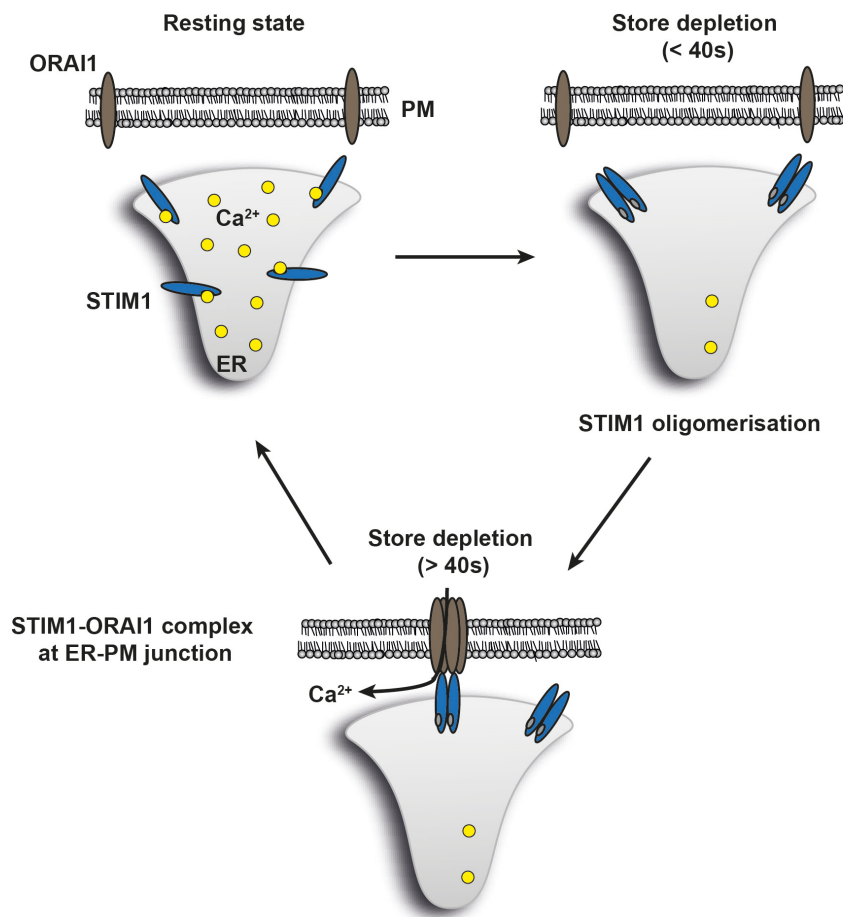
Figure 7. STIM1 interacts with ORAI1 upon store depletion.
ER - endoplasmic reticulum; PM - plasma membrane; ORAI1 - calcium release-activated calcium modulator; STIM1 - stromal interaction molecule 1.

In addition, cytoplasmic C-domain also helps in STIM1 oligomerization. Deletion mutants of the C-terminal end identified a region after the coiled-coil domains at amino acid location 400 – 474 that enhances the ability of STIM1 to oligomerize [95]. Live cell FRET approaches showed that STIM1 formed oligomers upon store depletion and translocated within the ER to ER-PM junctions. Deletion mutants on C-terminal polybasic PM targeting domain oligomerized but failed to translocate to ER-PM junctions [90]. It was also demonstrated using TIRF microscopy in HEK293 cells that STIM1 translocated to regions within 100 nm from the plasma membrane [96]. It was also confirmed by ultrastructure analysis by two independent groups that STIM1 translocated to distances as close as 10 nm from the PM in HeLa [97] and acinar cells [98]. This suggests an 'interactional' model for STIM1 wherein the protein oligomerizes and translocates to ER-PM junction and interacts with its partner proteins in the PM. Overexpression of STIM1 in HEK293 cells induced large SOCE currents without its detection in the PM [73].

1.3.1.3. *Stim1* knockout mice (*Stim1*[ßGeo/ßGeo])

The mice were generated as described previously using the genetrap method [99]. A splice acceptor site 'ßGeo' was inserted 600 bp downstream of exon 7, in the intron 7 of the *Stim1* gene. This resulted in a fusion protein that contained a truncated STIM1 and ß-galactosidase. The protein was not detected by western blot in the knockout mice.

1.3.2. STIM2

There is also another isoform of STIM named STIM2 that is made of 883 amino acids and shares 58% homology with STIM1. It contains similar domain structure as that of STIM1. Silencing *Stim2* abrogated SOC in the RNA interference study conducted by Liou *et al* [69] but did not show any effects in Roos *et al* [83] study. Overexpression of STIM2 alone inhibited SOC influx but upon co-overexpression with ORAI1, SOCE could be activated in both store-dependent and store-independent manner [100,101]. This might suggest that under certain conditions STIM2 can mimic the function of STIM1.

Although STIM2 has a similar Ca^{2+} binding affinity as that of STIM1 ($K_d \sim 500$ μM), it is distributed to puncta at a higher ER Ca^{2+} than that of STIM1 [102]. Even under resting conditions with filled stores, STIM2 are present at the ER-PM junctions in

activated state. It is well established that STIM2 maintains basal cytoplasmic Ca^{2+} levels in several cell types such as HeLa, HUVEC and HEK293T cells[102].

1.3.3. ORAI proteins

ORAI1 is a 33 kDa plasma membrane protein consisting of four transmembrane helices with both the N- and C- termini in the cytosolic side. The N-terminus consists of proline/arginine rich regions and a polybasic domain while the C-terminal contains a coiled-coil domain that is responsible for protein interactions [103]. It consists of two extracellular loops, TM1-TM2 and TM3-TM4, and one intracellular TM2-TM3 loop.

The transmembrane loops render its channel a high selectivity for calcium, which is characteristic of the ORAI channels. The highly negatively charged acidic residues present on the TM1-TM2 loop and on TM3 allows for high Ca^{2+} selectivity against Na^+ that is abundantly present in physiological solutions [104,105]. In the presence of Ca^{2+} and Mg^{2+}, ORAI1 does not conduct Na^+ and Cs^+ but in the absence of divalent ions it conducted monovalent ions [105].

ORAI1 has been identified as the other molecular component of SOC that interacts with STIM1 [71]. The ORAI1 C-terminus has been identified to be necessary for a direct interaction with the second coiled coil domain of STIM1 [106]. The ORAI1 channel functions as a tetramer [107]. There is increasing evidence that ORAI1 can form homo- and hetero- multimers through a series of co-immunoprecipitation experiments and size-exclusion chromatography [74,105]. Mignen *et al* observed that functional ORAI1 channels existed as tetramers by co-expressing tandem multimers of ORAI1 (monomer, dimer, trimer and tetramer) with a dominant-negative ORAI1 in cells stably overexpressing STIM1. SOCE was not inhibited in those cells transfected with tetramers but the current was diminished completely with the other multimers [107]. Highly sensitive photo bleaching experiments showed that ORAI1 existed as dimers in resting state but assembled into tetramers when coexpressed with the C-terminal end of STIM1 [108].

Apart from ORAI1, there also exists two other isoforms of ORAI proteins – ORAI2 and ORAI3. These proteins share more than 60% homology amongst them and have very strong sequence similarity in the transmembrane segments. ORAI2 and ORAI3 coexpressed with STIM1 yielded increases in SOC currents similar to ORAI1 [73,109,110]. Similar to ORAI1, they showed high Ca^{2+} selectivity but differed in their Ca^{2+} dependent inactivation [110]. Reconstitution of recombinant ORAI2 in *Orai1*$^{-/-}$ T cells

did not effectively improve Ca^{2+} influx in these cells, whereas reconstitution of ORAI1 restored the SOC currents [111]. This raises doubts on the contribution of ORAI2 to store-operated Ca^{2+} entry. ORAI1 is the dominant SOC channel in HEK293 cells, human T cells and fibroblasts but can be compensated by ORAI3 in the absence of functional ORAI1 [103].

1.3.4. STIM1-ORAI1 coupling

STIM1-ORAI1 coupling is a well-studied route for store-operated Ca^{2+} entry. STIM1 and ORAI1 are distributed diffusely in the endoplasmic reticulum and plasma membrane, respectively. Upon store depletion, STIM1 and ORAI1 translocate to ER-PM junctions forming a channel through which Ca^{2+} enters into the cell. Overexpression of STIM1 together with ORAI1 has resulted in amplified SOC currents [73,112]. Co-immunoprecipitation of STIM1 with ORAI1 and also FRET-based approaches indicate a direct binding between these molecules [72,113,114]. This was also confirmed by TIRF microscopy in which STIM1 translocation to ER junctions 10-25 nm close to the plasma membrane [115] and their subsequent colocalisation with ORAI1 [91] upon store depletion. A highly conserved C-terminal domain of STIM1, termed as STIM1 ORAI1 activating region (SOAR) or Ca^{2+} activating domain (CAD), was identified to bind and activate ORAI channels [74,116]. However, deletion mutants of a specific 8 amino acids within the SOAR region of STIM1 did not activate ORAI channels but did not prevent it from cluster formation with ORAI1 [74,117]. It was also shown that C-terminus of STIM1 interacted with the N-terminus of ORAI1. Also deletion mutants of N-terminal domains of ORAI1 did not activate SOCE but formed aggregates with STIM1 [74,113,117]. However, ORAI1 lacking C-terminal domains failed to form puncta and therefore did not activate SOCE [113,117]. This suggests that the SOAR domain of STIM1 binds to the C-terminus of ORAI1 and brings together C- and N-termini of ORAI1 for gating of the channels.
It was then required to determine the number of STIM1 and ORAI1 molecules required for proper gating of the channel. It has been previously reported that interaction with STIM1 caused the dimerization of ORAI1 dimers present in the PM to form tetramers [108]. A recent study has implicated a graded activation of the CRAC channels by up to eight molecules of STIM1 binding to ORAI1 tetramers in instigating a maximal SOC response [118].

1.3.5. TRP proteins

The TRP protein was first discovered in *Drosophila* as light-sensitive channel in which the receptor potential was transient upon illumination [119]. They are classified into six sub-families and have been evolutionarily conserved among organisms from worms to humans [120]. They are activated by G-protein-coupled phospholipase C (PLC) signalling cascade, and were initial identified as a Ca^{2+} transporter mediating the refilling of intracellular stores. Before the discovery of STIM1 and ORAI1, these channels had been implicated to play a critical role in capacitative Ca^{2+} entry [121]. The first identified canonical TRP channels were identified as TRPC channels and were further classified into seven isoforms (1-7) out of which TRPC2 is not expressed in humans. Based on structural and functional homologies they can be classified into 2 subfamilies: TRPC1/4/5 (65% sequence homology) and TRPC3/6/7 (70% sequence homology). All TRP proteins share a structural homology consisting of six transmembrane domains that assemble as homo- and hetero-tetramers to form cation permeation pores [122], which is in analogy with voltage-gated K^+, Na^+ and Ca^{2+} channels. They have four ankyrin-repeat domains, one coiled-coil domain and one Caveolin binding site at the N-terminus while has a Na^+/H^+ regulatory domain, a coiled coil domain and calmodulin-IP_3R binding site at its C-terminal end. Both N- and C-terminal ends are present on the cytosolic side. The phosphorylation sites for PKC and PKG are present on the N-terminal stretch of the protein complex. They are non-selective cation channels that allow inward currents of Ca^{2+}, Na^+ and other cations. TRPC channels have been localized to the plasma membrane [123–126] and at T-tubule/SR junction [68]. It has been shown that TRPC1/4/5 are activated by mechanical stretch or store depletion, and TRPC3/6/7 are activated by a second messenger system or G_q-coupled DAG [127]. Based on their modes of activation, TRPC1/4/5 are termed as store operated channels while TRPC3/6/7 were termed as receptor operated channels. Several studies using transgenic overexpression and siRNA silencing have revealed that the TRPC channels are involved in cardiac hypertrophy. It was observed that the TRPC channels preferentially trigger pathological cardiac hypertrophy and remodelling via the calcineurin-NFAT signalling pathway [52]. NFAT stimulation also triggers upregulation of the TRPC channels [125] and consensus NFAT binding sites were identified on TRPC1, 3 and 6. TRPC1 was found to be upregulated in pressure overload induced hypertrophy in rats [124] and mice [123]. It was also reported in the same study that silencing *Trpc1* gene using a siRNA approach prevented phenylephrine-, angiotensinII- and

endothelinI- induced cardiac hypertrophy in addition to reduction of SOCE in cultured cardiomyocytes. TRPC1 was also found to be elevated in aged mice of the Duchenne muscular dystrophy model that suffers from dilated cardiomyopathy with high resting Ca^{2+} levels [128]. TRPC1 knockout mice subjected to pressure overload prevented cardiac hypertrophy and maintained cardiac function, and also did not show an upregulation of TRPC cation current and reduced NFAT activity [123]. They can also serve as stretch activated cation channels [129].

TRPC3 was also upregulated in pressure-overloaded rats [126] and also resulted in increases in cardiomyocyte size, ANP expression and NFAT activation. Transgenic overexpression of TRPC3 in mice resulted in high SOCE in adult cardiomyocytes and developed cardiomyopathy with aging [130]. When these mice were crossed with calcineurin Aß null mice, they prevented hypertrophy in a pressure overload model suggesting the involvement of TRPC-NFAT signalling in pathological remodelling.

In addition to TRPC1 and TRPC3, TRPC6 also contributes to TRPC-NFAT signalling. TRPC6 was upregulated in transgenic mice overexpressing constitutively active calcineurin, pressure overloaded hearts and human failing hearts [125]. Moreover, mice expressing dnTRPC6 completely blocked cardiac hypertrophy [131]. Knockdown of either TRPC3 or TRPC6 inhibited AngII mediated hypertrophy [132] suggesting that heterotetramer formation of these 2 molecules are required for AngII-induced NFAT activation.

Downregulation of SERCA was associated with upregulation of TRPC4 and TRPC5 [126,133]. TRPC5 was also upregulated in end-stage human failure [126] while overexpression of TRPC7 was associated with cardiac apoptosis [134].

Taken together, TRPC channels have an important role in pathological cardiac remodelling preferentially via the calcineurin-NFAT signalling pathway.

1.3.5.1. STIM1-TRPC interactions

Several studies have reported functional interactions between STIM1 and TRPCs. Co-immunoprecipitation experiments have determined direct interaction of STIM1 with TRPC1, TRPC4 and TRPC5, and indirectly with TRPC3 and TRPC6 [135–137]. STIM1 interactions with TRPC3 and TRPC6 are indirect and could be as a result of STIM1-mediated heteromultimerization of TRPC3 with TRPC1 and TRPC6 with TRPC4 [137]. ORAI proteins can interact with both C- and N-termini of TRPCs [138]. Interdependence of STIM1, ORAI1 and TRPC1 in the activation of SOC currents has been observed by several independent groups [139–141]. Reconstitution of ORAI1 in

stably expressing TRPC 1, 3 and 6 HEK cells rendered the SOC channels active [142]. This indicates a functional heteromultimeric complex involving STIM1, ORAI and TRPC proteins for activated SOC currents.

1.4. Aim of the study

The aim of this study was to characterize the function and regulation of STIM1 in the myocardium, and its physiological relevance in diseased heart. In this study, primarily 4 questions were investigated.

First, it was investigated if STIM1 was sufficient and necessary for store-operated Ca^{2+} entry in cardiomyocytes. STIM1 expression in neonatal rat cardiomyocytes (NRCM) was manipulated using adenoviruses either overexpressing or silencing *Stim1*. Store operated Ca^{2+} influx was then measured by Ca^{2+} imaging using FURA-2AM.

Second, it was interesting to determine the localization of endogenous STIM1 in cardiomyocytes and provide evidence on puncta formation by STIM1 upon drug-induced store depletion. Immunofluorescent stainings on endogenous STIM1 was analyzed using confocal and TIRF microscopy.

Third, this study aimed at determining if altering STIM1 expression had functional effects on NRCM such as cardiomyocyte hypertrophy and NFAT activation.

Then, there is increasing evidence that STIM1 interacts with several proteins in inducing SOCE. The study aimed to identify if STIM1 interacts with ORAI and TRP proteins to mediate store operated Ca^{2+} entry.

Finally, the study aimed to investigate if silencing STIM1 could play a protective role in a rat model of pressure overload induced hypertrophy. This aim was addressed by our collaborator, Dr Jean Sebastien Hulot, who conducted these experiments.

2. Materials and methods

2.1. Chemicals

Chemical	Manufacturer
Acetic acid	J.T. Baker (Phillipsburg, USA)
Agar	Applichem (Darmstadt)
Agarose	Peqlab (Erlangen)
Ampicillin	Roth (Karlsruhe)
Ammonium peroxodisulphate (APS)	Sigma-Aldrich (Deisenhofen)
5-bromodeoxyuridine (BrDU)	Sigma-Aldrich (Deisenhofen)
Bovine Serum Albumin (BSA)	Applichem (Darmstadt)
Bromophenol blue	Merck (Darmstadt)
Chloroform	Roth (Karlsruhe)
Complete Mini (Protease inhibitor)	Roche (Mannheim)
Deoxynucleotide triphosphate (dNTP)	Invitrogen (Karlsruhe)
4,6-diamidino-2-phenylindole (DAPI)	Sigma-Aldrich (Deisenhofen)
DNase/RNase-free water	Gibco (Karlsruhe)
Dulbecco's modified eagle medium (DMEM)	Gibco (Karlsruhe)
Dimethylsulphoxide (DMSO)	Roth (Karlsruhe)
Ethylenediaminetetraacetate (EDTA)	Applichem (Darmstadt)
Ethanol	J.T. Baker (Phillipsburg, USA)
Ethidium bromide	Sigma-Aldrich (Deisenhofen)
Fetal bovine serum (FBS)	PAN (Aidenbach)
	Gibco (Karlsruhe)
D-Glucose	Merck (Darmstadt)
Fura-2AM	Invitrogen (Karlsruhe)
Glycerol	Merck (Darmstadt)
Glycine	Applichem (Darmstadt)
Goat serum	Gibco (Karlsruhe)
Haematoxylin	Roth (Karlsruhe)
Hefe extract	Applichem (Darmstadt)
HEPES	Applichem (Darmstadt)
Hydrochloric acid 37% (HCl)	Merck (Darmstadt)
Isofluran	Abbott (Wiesbaden)
Isopropanol	Merck (Darmstadt)

Kanamycin	Fluka (Seelze)
Lipofectamine™ 2000	Invitrogen (Karlsruhe)
Milk powder	Applichem (Darmstadt)
Magnesium chloride ($MgCl_2$)	Merck (Darmstadt)
Magnesium sulphate ($MgSO_4.7H_2O$)	Merck (Darmstadt)
Minimum essential medium (MEM)	Sigma-Aldrich (Deisenhofen)
2-mercaptoethanol	Applichem (Darmstadt)
Methanol	Sigma-Aldrich (Deisenhofen)
Opti-MEM I	Gibco (Karlsruhe)
Paraffin (Paraplast)	Sigma-Aldrich (Deisenhofen)
Paraformaldehyde (PFA)	Sigma-Aldrich (Deisenhofen)
Peptone	Applichem (Darmstadt)
Penicillin/Streptomycin	Gibco (Karlsruhe)
Phenol/chloroform	Roth (Karlsruhe)
Phenylephrine (PE)	Sigma-Aldrich (Deisenhofen)
Phosphate buffered saline (PBS)	Gibco (Karlsruhe)
Potassium chloride (KCl)	Applichem (Darmstadt)
Potassium dihydrogen phosphate (KH_2PO_4)	Roth (Karlsruhe)
Prestained protein ladder	Fermentas (St. Leon-Rot)
ProteinG Dynabeads	Invitrogen (Karlsruhe)
PVDF membrane	Millipore (Billerica USA)
6-ROX	
SKF-96365	Sigma-Aldrich (Deisenhofen)
Sodium acetate ($NaCH_3COO$)	Merck (Darmstadt)
Sodium chloride (NaCl)	Applichem (Darmstadt)
Sodiumdihydrogenphosphate (NaH_2PO_4)	Roth (Karlsruhe)
Sodiumdodecylsulphate (SDS)	Roth (Karlsruhe)
di-sodium hydrogen phosphate (Na_2HPO_4)	Roth (Karlsruhe)
Sodium hydroxide (NaOH)	Roth (Karlsruhe)
Sodium ortho vanadate (Na_3VO_4)	Sigma-Aldrich (Deisenhofen)
SYBR green	
Tetramethylethylenediamine (TEMED)	Sigma-Aldrich (Deisenhofen)
Thapsigargin (TG)	Alexis Biochemicals (Lausen,

	Switzerland)
peqGOLD Trifast	peqLAB (Erlangen)
Toluene	Roth (Karlsruhe)
Triton X-100	Sigma-Aldrich (Deisenhofen)
Trypan blue	Applichem (Darmstadt)
Tween 20	Applichem (Darmstadt)
Vitamine B12	Sigma-Aldrich (Deisenhofen)
Xylene	Roth (Karlsruhe)

2.2. Kits

Kit	Manufacturer
Adeno-X purification kit	Clontech (France)
Adeno-X Rapid titer kit	Clontech (France)
BCA Protein assay kit	Thermo Scientific (Bonn)
BLOCK-iT U6 RNAi entry vector kit	Invitrogen (Karlsruhe)
ECL Plus	GE Healthcare
Endofree plasmid Maxi kit	Qiagen (Hilden)
Luciferase Assay system	Promega (Madison)
NE-PER Nuclear and cytoplasmic extraction kit	Thermo Scientific (Rockford, USA)
Plasmid DNA Maxi kit	Qiagen (Hilden)
Plasmid DNA Midi kit	Qiagen (Hilden)
QIAquick Gel extraction kit	Qiagen (Hilden)
QIAquick PCR purification kit	Qiagen (Hilden)

2.3. Plasmids

The following plasmids were available in the laboratory and were used for the experiments:

Donor vector	Insert	Reference
pDONR-221		Invitrogen (Karlsruhe)
pT-Rex DEST30		Invitrogen (Karlsruhe)
pAd/CMV/V5-DEST30		Invitrogen (Karlsruhe)
pDONR-221	*Stim1*	Pharmakology, Uni Würzburg
pDONR-221	*Orai1*	Pharmakology, Uni Würzburg
pAd/CMV/V5-DEST30	*Stim1*	Pharmakology, Uni Würzburg

pAd/CMV/V5-DEST30	*Orai1*	Pharmakology, Uni Würzburg
pAd/CMV/V5-DEST30	*LacZ*	Pharmakology, Uni Würzburg
pcDNA3-NFAT-luc		(Ref from J. Molkentin)

The following plasmids were constructed by homologous recombination (Gateway Technology, Invitrogen, Karlsruhe) using the BLOCK-iT U6 RNAi Entry Vector Kit (Invitrogen, Karlsruhe).

Donor vector	Insert	Reference
pENTR/U6		Invitrogen (Karlsruhe)
pENTR/U6 and pAd-DEST30	sh*Stim1* sh*Orai1* sh*Orai3* sh*Scr1* sh*Scr2*	

2.4. Enzymes

Enzyme	Manufacturer
Accuprime Pfx DNA Polymerase	Invitrogen (Karlsruhe)
Benzonase	Merck (Darmstadt)
Collagenase II	Worthington (Lakewood, USA)
Difco Trypsin 250	BD (Heidelberg)
DNase	Sigma-Aldrich (Deisenhofen)
Gateway BP Clonase II enzyme mix	Invitrogen (Karlsruhe)
Gateway LR Clonase II enzyme mix	Invitrogen (Karlsruhe)
Platinum Taq DNA Polymerase	Invitrogen (Karlsruhe)
Proteinase K	Fermentas (St. Leon-Rot)
Restriction endonucleases	New England Biolabs (Frankfurt am Main)
Superscript II Reverse transcriptase	Invitrogen (Karlsruhe)
T4 DNA Ligase	New England Biolabs (Frankfurt am Main)
Taq DNA Polymerase	Fermentas (St. Leon-Rot)
Trypsin	Gibco (Karlsruhe)
Trypsin 1:250	PAN (Aidenbach)

2.5. Bacterial strains

Strain	Genotype	Manufacturer
E.coli DH10B (electrocompetent)	F- mcrA Δ(mrr-hsdRMS-mcrBC) φ80lacZ ΔM15 ΔlacX74 recA1 endA1 araD139 Δ(ara, leu)7697 galU galK λ - rpsL nupG tonA	Invitrogen (Karlsruhe)
E.coli TOP10 (chemically competent)	F mcrA Δ(mrr-hsdRMS-mcrBC) φ80lacZΔM15 ΔlacX74 recA1 araD139 Δ(ara-leu) 7697 galU galK rpsL (Str^R) endA1 nupG	Invitrogen (Karlsruhe)

2.6. Buffers and media

Block buffer (milk)

Tris (1M pH 7.5)	3 ml
NaCl	1.75 g
Tween®20	0.3 ml
ddH$_2$O	adjust to 300 ml
Milk powder	5%

Calcium-free HBSS (Hank's Buffered Salt Solution)

KCl	0.4 g
KH$_2$PO$_4$	0.06 g
MgSO$_4$.7H$_2$O	0.19 g
NaHCO$_3$	0.35 g
NaCl	8 g
Na$_2$HPO$_4$.7H$_2$O	0.1 g
ddH$_2$O	adjust to 1 l

CBFHH (Ca^{2+} and HCO^{3-} free Hank's with Hepes) medium

NaCl	137 mM
KCl	5.36 mM
MgSO$_4$.7H$_2$O	0.81 mM
Dextrose	5.55 mM
KH$_2$PO$_4$	0.44 mM
Na$_2$HPO$_4$.7H$_2$O	0.34 mM

Adjust pH to 7.3.

DNA loading buffer (5X)

Xylene cyanol	10 g
0.5 M EDTA	1.4 ml
Glycerol	3.6 ml
ddH$_2$O	7 ml

DNA lysis buffer (for genotyping)

Tris	12.1 g
EDTA	1.87 g
NaCl	11.7 g
SDS	0.2 g
ddH$_2$O	adjust to 1 l

Fura-2AM solution

Fura-2AM (1 mM in DMSO)	1 µl
HBSS	500 µl

Hank's buffered salt solution (HBSS)

CaCl$_2$ anhydrous	0.4 g
KCl	0.4 g
KH$_2$PO$_4$	0.06 g
MgSO$_4$.7H$_2$O	0.19 g
NaHCO$_3$	0.35 g
NaCl	8 g
Na$_2$HPO$_4$.7H$_2$O	0.1 g
ddH$_2$O	adjust to 1 l

IP wash buffer

Tween20	500 µl
PBS pH 7.4	1 l

Lamelli buffer 2X

Tris-HCl 1M pH 6.8	12.5 ml

SDS 10%	40 ml
Glycerol	30 ml
ß-mercaptoethanol	1 ml
Bromophenol blue	traces

LB agar

Peptone	10 g
Yeast extract	5 g
NaCl	5 g
Agar	15 g
1 M NaOH	1 ml
ddH$_2$O	adjust to 1 l

LB medium

Peptone	10 g
Yeast extract	5 g
NaCl	5 g
1 M NaOH	1 ml
ddH$_2$O	adjust to 1 l

Lower buffer 4X (for Western blot)

Tris	182 g
SDS 10%	40 ml
ddH$_2$O	adjust to 1 l

Adjust pH to 8.8 with HCl 37%

NRCM incomplete medium

MEM	10.7 g
NaHCO$_3$	0.35 g
Vitamin B12 67% (w/v)	1 ml
ddH$_2$O	adjust to 1 l

Adjust pH to 7.3 and sterile filtered the solution.

NRCM preplating medium

Penicillin/Streptomycin	1 ml

	FBS	5 ml
	NRCM incomplete medium	94 ml
PBS (10X)		
	NaCl	80 g
	KCl	2 g
	$Na_2HPO_4.7H_2O$	11.5 g
	KH_2PO_4	2 g
	ddH_2O	adjust to 1 l
PBST		
	PBS 10X	100 ml
	Tween® 20	1 ml
	ddH_2O	adjust to 1 l
Protein lysis buffer		
	Tris (1M pH 6.7)	50 mM
	SDS	2%
	Na_3VO_4	1mM
	Complete mini protease inhibitor	1 tablet per 10 ml
Protein IP lysis buffer		
	NaCl 1M	750 µl
	TritonX 10%	500 µl
	Tris-HCl 1M pH 7.4	50 µl
	EDTA 100 mM	50 µl
	Na_3VO_4	10 µl
	ddH_2O	3.64 ml
	Complete mini protease inhibitor	1 tablet per 10 ml
Western running buffer (10X)		
	Tris-HCl	30 g
	Glycine	144 g
	SDS	15 g
	ddH_2O	adjust to 1 l

S.O.C. medium

	Tryptone	2%
	Yeast extract	0.5%
	NaCl	10 mM
	KCl	2.5 mM
	$MgCl_2$	10 mM
	$MgSO_4$	10 mM
	Glucose	20 mM

TAE buffer (50X)

	Tris	242 g
	Acetic acid	57.1 ml
	$Na_2EDTA.2H_2O$	37.2 g
	ddH_2O	adjust to 1 l

Transfer buffer (for Western blot)

	Tris (1M pH 8.3)	25 ml
	Glycine	11.26 g
	Methanol	100 ml
	ddH_2O	adjust to 1 l

Tris-EDTA (TE) buffer

	Tris	10 mM
	EDTA	1 mM

Upper buffer 4X (for Western blot)

	Tris	61 g
	SDS 10%	40 ml
	ddH_2O	adjust to 1 l
	Adjust pH to 6.7 with HCl 37%	

2.7. Oligonucleotide primer

The oligonucleotides were purchased in HPSF-purified lyophilized powder from MWG Eurofins (Ebersberg) and Sigma-Aldrich. The primers were adjusted to a stock concentration of 1 mM using double-distilled autoclaved water (ddH_2O) and were

kept at 55°C and 700 rpm for 10 min. 20 μM working solutions were used for the experiments.

Oligo	Strand	Sequence	Reference
Cloning for shRNA constructs			
sh*Stim1*-1	Top	5'-CAC CGC AGT ACT ACA ACA TCA AGA ACG AAT TCT TGA TGT TGT AGT ACT GC-3'	Clone name: NM_00987.2-1670s1c1
	Bottom	5'-AAA AGC AGT ACT ACA ACA TCA AGA ATT CGT TCT TGA TGT TGT AGT ACT GC-3'	
sh*Stim1*-2	Top	5'-CAC CGC TGC TGG TTT GCC TAT ATC CAC GAA TGG ATA TAG GCA AAC CAG CAG-3'	Origene (GI336191)
	Bottom	5'-AAA ACT GCT GGT TTG CCT ATA TCC ATT CGT GGA TAT AGG CAA ACC AGC AGC-3'	
sh*Stim1*-3	Top	5'-CAC CGC TGA GCA GAG TCT GCA TGA CCC GAA GGT CAT GCA GAC TCT GCT CAG-3'	Origene (GI336192)
	Bottom	5'-AAA ACT GAG CAG AGT CTG CAT GAC CTT CGG GTC ATG CAG ACT CTG CTC AGC-3'	
sh*Orai1*-1	Top	5'-CAC CGC AGT TAC TCC GAG GTG ATC GAA ATC ACC TCG GAG TAA CTC TGG-3'	Clone ID: NM_175423.2-362s1c1
	Bottom	5'-AAA ACC AGA GTT ACT CCG AGG TGA TTT CGA TCA CCT CGG AGT AAC TCT GGC -3'	
sh*Orai1*-2	Top	5'-CAC CGA TGC AGG CGC TGT CCT GGC GCC GAA GCG CCA GGA CAG CGC CTG CAT-3'	Origene (TI304030)
	Bottom	5'-AAA AAT GCA GGC GCT GTC CTG GCG CTT CGG CGC CAG GAC AGC GCC TGC ATC -3'	

sh*Orai1*-3	Top	5'-CAC CGC AGC AGC ACT AGC GGC AGC CGC GAA CGG CTG CCG CTA GTG CTG CTG -3'	Origene (TI569123-3
	Bottom	5'-AAA ACA GCA GCA CTA GCG GCA GCC GTT CGC GGC TGC CGC TAG TGC TGC TGC-3'	
sh*Orai3*	Top	5'-CAC CGT TGA AGC CGT GAG CAA CAT CCC GAA GGA TGT TGC TCA CGG CTT CAA-3'	Origene (TI305362)
	Bottom	5'-AAA ATT GAA GCC GTG AGC AAC ATC CTT CGG GAT GTT GCT CAC GGC TTC AAC-3'	
sh*Scr*-1	Top	5'-CAC CGC GAA TCC TCG TAA TCA TTT CGA AAA ATG ATT ACG AGG ATT CG-3'	Sigma (VC300A2)
	Bottom	5'-AAA ACG AAT CCT CGT AAT CAT TTT CGA AAT GAT TA CGA GGA TTC GC-3'	
sh*Scr-2*	Top	5'-CAC CGA AAT GAT TAC GAG GAT TCG CGA ACG AAT CCT CGT AAT CAT TT-3'	Sigma (VC300B2)
	Bottom	5'-AAA AAA ATG ATT ACG AGG ATT CGT CGC GAA TCC TCC GTA ATC ATT TC-3'	

Genotyping primers

Mouseline	Allele	Sequence	Size (bp)
Stim1^βGeo/βGeo	WT	5'- GTC ATA GCC TGT AAA CTA GA -3' 5'- GTA GCT GCA GGT AGC ACT AG -3'	700
	KO Geo	5'- TTA TCG ATG AGC GTG GTG GTT ATG C -3' 5'- GCG CGT ACA TCG GGC AAA	650

31

		TAA TAT C -3'	
Myh6- AdrB1^{Tg(4)/0}	TG	5'- AGG ACT TCA CAT AGA AGC CTA G -3' 5'- TGT CCA CTG CTG AGA CAG CG -3'	300

Real-time primers

Gene	Sequence	Size (bp)
rStim1	5'- ATA TGC TGA GGA AGA GCT GGA -3' 5'- GCA TAC CAG GAG CTG TGT GA -3'	85
rOrai1	5'- GAC GGA GAG CTG GAA GAA CA -3' 5'- GGC AGA GTG TGG AAG GAA GA -3'	105
rOrai3	5'- GGC TAA GCT CAA AGC CTC CA -3' 5'- GTG GAG ACC ATG AGT GCA AA-3'	177
rTrpc1	5'- GAT GAG CCT CTT GAC AAA CGA -3' 5'- CTG GCA ATT TGA CTG GGA GA -3'	112
rTrpc3	5'- AGA GCG ACC TGA GCG AAG T -3' 5'- AGG GTC AGA AGG AAG CCA TT -3'	83
rTrpc4	5'- GCG GTA CGT GGC AGC CAT GA -3' 5'- TCC CAG AAC TTC GAA GCG AAA GC-3'	112
rTrpc6	5'- TGT GGA ATA TGC TTG ACT TTG G -3' 5'- TGA TCT GAG GAT CGG TAG GG -3'	208
rNppa	5'- CTC CCA GGC CAT ATT GGA G -3' 5'- TCC AGG TGG TCT AGC AGG TT -3'	90
rGapdh	5'- ACA ACT TTG GCA TCG TGG A-3' 5'- AGT GGA TGC AGG GAT GAT GT-3'	138
rRpl32	5'- CCA GAG GCA TCG ACA ACA-3' 5'- GCA CTT CCA GCT CCT TGA CAT-3'	150
mStim1	5'- GGC GTG GAA ATC ATC AGA AGT-3' 5'- TCA GTA CAG TCC CTG TCA TGG-3'	173
mP4hb	5'- GTT TTG CCA CCG CTT CTT AG -3' 5'- CGC CCC AAC CAG TAC TTT TA -3'	103

32

2.8. Small interfering RNA (siRNA)

sIRNA	Sequence	Reference
si*Trpc1*-1	5'- CUG CUC AUC GUA ACA ACU A -3'	Potier *et al* [143]
si*Trpc1*-2	5'- GAG AAA UGC UGU UAC CAU A -3'	Potier *et al* [143]
si*Trpc3*-1	5'- GUG CAA AGA CUU CGU AGU A -3'	Self design
si*Trpc3*-2	5'- CUC AAU CAG CCA ACA CGA U -3'	Self design
si*Trpc4*-1	5'- GGC UCA GUU CUA UUA CAA A -3'	Potier *et al* [143]
si*Trpc4*-2	5'- CCA CGA GGU CCG CUG UAA C -3'	Potier *et al* [143]
si*Trpc6*-1	5'- GGA CCA GCA UAC AUG UUU A -3'	Potier *et al* [143]
si*Trpc6*-2	5'- GUG UGG AUU ACA UGG GCC A -3'	Potier *et al* [143]

2.9. Antibodies

Epitope	Host	Monoclonal / polyclonal	Reference
Primary antibodies			
α-actinin	Mouse	monoclonal	Sigma-Aldrich (Cat. A7811)
Calmodulin	Mouse	monoclonal	Upstate (Millipore) (Cat. 05-173)
G-ß (T20)	Rabbit	polyclonal	Santa Cruz (Cat. sc-378)
GAPDH	Mouse	monoclonal	Calbiochem (Cat. CB1001)
NFATc1 (K-18)-R	Rabbit	polyclonal	Santa Cruz (Cat. sc-1149-R)
ORAI1	Rabbit	polyclonal	Prosci (Cat. 4123)
STIM1	Mouse	monoclonal	BD Biosciences (Cat. 610954)
STIM1	Rabbit	polyclonal	Cell Signalling (Cat. 4196)
STIM1	Rabbit	polyclonal	Sigma-Aldrich (Cat. S6197)
TRPC1	Rabbit	polyclonal	Alomone labs (Cat. ACC-010)
TRPC3	Rabbit	polyclonal	Alomone labs (Cat. ACC-016)
TRPC4	Rabbit	polyclonal	Alomone labs (Cat. ACC-018)
TRPC6	Rabbit	polyclonal	Alomone labs (Cat. ACC-017)
Secondary antibodies			
HRP- anti-mouse IgG	Goat		Jackson Immunoresearch laboratories (Cat. 115-035-003)
HRP- anti-rabbit IgG	Goat		Jackson Immunoresearch laboratories (Cat. 111-035-144)
Cy3- anti-rabbit	Goat		Jackson Immunoresearch

IgG			laboratories (Cat. 111-165-047)
AlexaFluor 488 anti-mouse IgG	Goat		Invitrogen, Karlsruhe (Cat. A11029)

2.10. Molecular biology methods

2.10.1. Polymerase chain reaction (PCR)

For amplification of DNA sequences either from the cDNA or from the plasmid constructs, Accuprime Pfx polymerase was used.

Reaction mixture	10X Accuprime Pfx buffer	5µl
	Forward primer	20 pmol
	Reverse primer	20 pmol
	Template DNA	100 ng
	Accuprime Pfx Polymerase	2.5 Units
	ddH$_2$O	upto 50µl

A 3-step PCR cycle was used for amplification.

Step	Temperature	Time	No. of cycles
Pre-denaturation	95°C	120 s	
Denaturation	95°C	15 s	35 cycles
Annealing	55 – 65°C	20 s	
Elongation	68°C	60 s per kb	
Final elongation	68°C	300 s	

2.10.2. PCR purification

PCR amplified products are purified using the QIAquick PCR purification kit (Qiagen, Hilden). 5 volumes of Buffer QG were added to 1 volume of PCR product. If the colour of the sample turns violet or orange, 10µl of 3M ammonium acetate solution was added (the sample turns yellow). The samples were then applied to QIAquick column and centrifuged at 13000 rpm for 1 min. In the presence of high concentration of salts, the DNA binds to the silica membrane of the column. The flow-throught was discarded and the columns were washed with 750µl of Buffer PE and centrifuged at 13000 rpm for 1 min. The flow-through was discarded and the empty columns were centrifuged to remove any residual solution from the column. The DNA was then eluted using 20µl of ddH$_2$O into a fresh 1.5 ml microfuge tube.

2.10.3. Restriction endonuclease digestion

Restriction endonuclease digestion was performed either to test the clones for insertion of the genes or for cloning. The restriction endonucleases were purchased from New England Biolabs and the digestion was performed in the buffers as per the manufacturers recommendations. 1 µg of DNA was digested with 1 unit of the enzyme for 1 hour at recommended temperatures. The restriction endonucleases were then inactivated by incubating the tubes at 65°C for 20 min.

2.10.4. Agarose gel electrophoresis

To prepare 1% agarose gel, 1g of agarose in 100 ml of 1X TAE buffer was boiled in a microwave oven. After cooling down the solution to 60°C, 10 ml of ethidium bromide was added per 100 ml of solution (final concentration of 0.1 µg/µl), and the solution was poured onto the gel chamber and the respective comb was inserted. The DNA samples were diluted 1:5 times with 5X DNA loading buffer and loaded into the wells. A voltage of 70 – 140 V was applied to the chambers. 100 bp or 1 kb DNA ladders were purchased from New England Biolabs (Frankfurt am Main). Ethidium bromide is a fluorescent dye that intercalates into the DNA, and the bands can be visualized by illuminating the gel with UV light of 312 nm wavelength (DeVision of Decon Science Tec DBOX, Hohengandern).

2.10.5. Gel extraction

The DNA fragments of the respective size were excised from the agarose gel using a sterile scalpel into a 2 ml microfuge tube and QIAquick gel extraction kit (Invitrogen, Karlsruhe) was used to extract the DNA. The DNA was eluted using 20 µl of autoclaved ddH$_2$O.

2.10.6. Precipitation of DNA with sodium acetate

The samples were mixed with 1/10th volume of 3M sodium acetate and 2.5 volumes of 100% ethanol. The samples were incubated at -80°C for 20 min, centrifuged at 14000 rpm and were then incubated at 4°C for 30 min. The pellet was washed with 1 ml of 75% ethanol, centrifuged at 14000 rpm and then kept at 4°C for 15 min. The pellet was dried at room temperature and was resuspended in 15 µl ddH$_2$O.

2.10.7. Generation of shRNA entry clone constructs

RNA interference (RNAi) is a process within living cells that moderate activity of genes. The RNAi pathway is initiated by the enzyme dicer, which cleaves long double-stranded RNAs into short fragments of 20 nucleotides. The cleaved guide strand is then incorporated into the RNA-induced silencing complex (RISC) which then binds to the complementary sequence of a messenger RNA and leads to post-transcriptional gene silencing. The use of diced or synthetic siRNA directly on living cells for RNAi analysis is limited by their transient nature. Therefore, it is necessary to use a vector-based approach for sustained exogenous overexpression of shRNA in mammalian cells.

BLOCK-iT RNAi kit (Invitrogen) was used to generate an entry clone that permits high-level overexpression of the shRNA of interest. The pENTR/U6 vector into which the double-stranded oligo encoding the shRNA of interest was cloned, is controlled by the human U6 promoter that is recognized by Polymerase III and sustains high-level constitutive expression of the shRNA molecules.
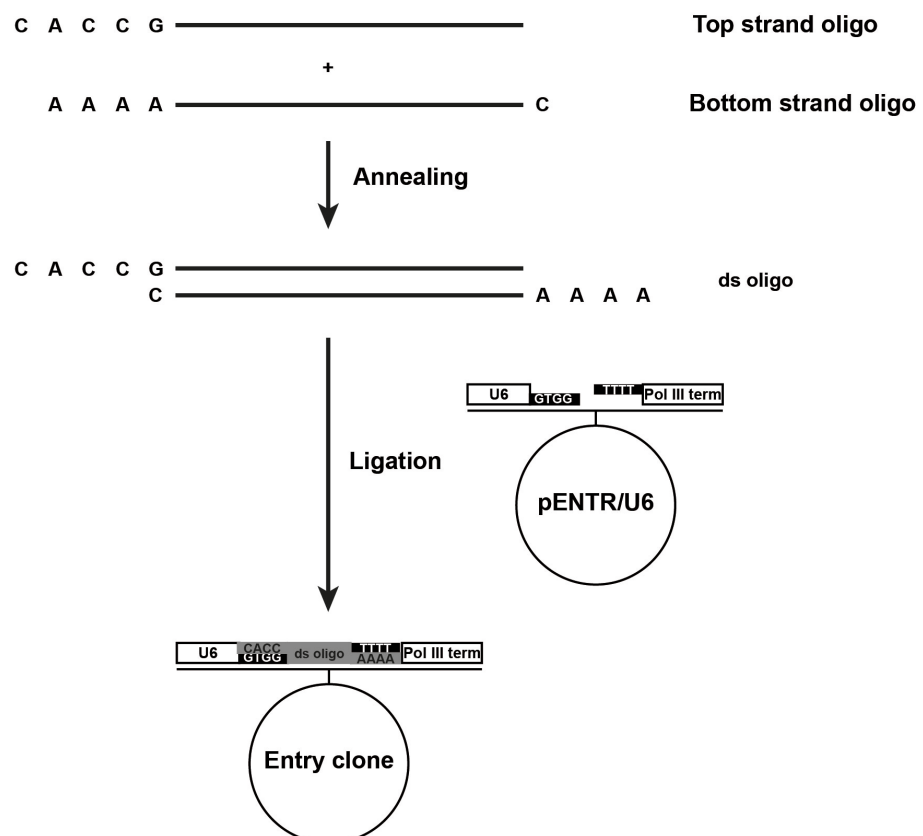

Figure 8. Schematic diagram illustrating generation of shRNA entry clones.

2.10.7.1. Designing the single-stranded oligos

The single stranded oligos were designed according to the manufacturer's guidelines. In the top strand oligo, the transcription initiation site begins at the first nucleotide following the CACC basepairs. It is recommended to initiate the shRNA sequence with a guanosine residue because transcription of native U6 snRNA initiates at 'G'.

When 'G' is part of the target sequence, a complementary 'C' was added to the 3'-end of the top strand oligo. If 'G' was not the first residue of the target sequence, 'G' was added to the 5'-end of the top strand oligo immediately following the CACC overhang but a complementary 'C' was not added to its 3'-end as it was in the first case.

2.10.7.2. Generating double-stranded oligo

The single stranded oligos synthesized by MWG Eurofins (Ebersberg) were annealed to generate a double stranded oligo that was later ligated into a linearized entry vector pENTR/U6 provided in the kit.

Reaction mixture	Top strand oligo (200µM)	5 µl
	Bottom strand oligo (200µM)	5 µl
	10X annealing buffer	2 µl
	ddH$_2$O	8 µl

The tubes were then incubated at 95°C for 4 min. The tubes were then removed from the thermoblock onto the bench and were allowed to cool to room temperature for 10 min. The single stranded oligos will anneal to form double stranded oligo during this incubation. The final concentration of the double stranded oligo would be 50 µM.

The double stranded oligo mixture was subjected to serial dilutions to facilitate ligation.

| First dilution | 50 µM ds oligo | 1 µl |
| | ddH$_2$O | 99 µl |

Second dilution	500 nM ds oligo	1 µl
	10X annealing buffer	10 µl
	ddH$_2$O	89µl

The concentration of the ds oligo after the two dilutions is 5 nM and the oligo stocks were stored at -20°C until ligation was performed.

2.10.8. Ligation of DNA fragments

Ligation was performed using the T4 DNA ligase purchased from New England Biolabs (Frankfurt am Main). The enzyme catalyses the formation of a phosphodiester bond between the 3'-hydroxyl end of one DNA fragment and the 5'-phosphate end of the other DNA fragment. The amount of insert was calculated using the following formula:

$$\text{Insert mass [ng]} = \frac{5 \times \text{Vector mass [ng]} * \text{Insert length [bp]}}{\text{Vector length [bp]}}$$

Reaction mixture	10X Ligase buffer	1 µl
	Vector DNA fragment	10 – 50 ng
	Insert DNA fragment	5 – 250 ng
	T4 DNA Ligase	1 µl
	ddH$_2$O	upto 10 µl

The tubes were incubated at 25°C for 5 hours or at 16°C overnight.

2.10.9. Gateway BP recombination reaction

BP Clonase II enzyme was used to produce the entry clones containing the DNA fragment of interest. The BP clonase II enzyme mix contains bacteriophage lambda rec-Integrase and *E.coli*-encoded protein Integration Host Factor which catalyses the *in vitro* homologous recombination between an attB-flanked DNA fragment and an attP-containing Gateway entry vector.

Reaction mixture	attB-PCR product	15 – 150 ng
	Donor vector	150 ng
	BP Clonase II	2 µl
	TE buffer pH 8.0	upto 10 µl

The tubes were incubated at 25°C for atleast 5 hours. To terminate the reaction, 1 µl of Proteinase K was added and the tubes were incubated at 37°C for 10 min.

2.10.10. Gateway LR recombination reaction

The LR recombination reaction was performed between an attL-containing entry vector and an attR-containing destination vector. The LR Clonase II enzyme mix contains bacteriophage lambda recombinant Integrase and Excisionase, and *E.coli*-encoded protein Integration Host Factor facilitating the *in vitro* recombination reaction.

Reaction mixture	Entry clone	15 – 150 ng
	Destination vector	150 ng
	LR Clonase II	2 μl
	TE buffer pH 8.0	upto 10 μl

The tubes were incubated at 25°C for atleast 5 hours. To terminate the reaction, 1 μl of Proteinase K was added and the tubes were incubated at 37°C for 10 min.

2.10.11. Transformation

Electrocompetent *E.coli* DH10B cells were thawed on ice and 1 – 2 μl of plasmid DNA was added to 50 μl of the cells. The suspension was mixed, transferred into Gene Pulser 0.1 cm cuvettes (Bio-rad) and a short 1.8 kV electromagnetic pulse was applied using the Bio-rad micropulser. The electroporated cell suspension was mixed with 250 μl of S.O.C medium, transferred into an 1.5 ml microfuge tube and was incubated at 37°C and 350 rpm in a thermomixer (Eppendorf) for 1 hour. 50 – 150 μl of the cell suspension was then plated on LB plates containing the corresponding antibiotic (33 μg/μl Kanamycin or 100 μg/μl Ampicillin). The plates were incubated overnight.

Alternatively, chemically competent *E.coli* One Shot TOP10 cells were used. 2 μl of the plasmid DNA was mixed with 50 μl of the cells and incubated on ice for 30 min. Heat-shock was applied by placing the samples at 42°C for 30 s and immediately transferring the tubes to ice. The cells were resuspended with 250 μl S.O.C. medium, incubated at 37°C and 350 rpm in a thermomixer for 1 hour and were plated on LB agar plates.

2.10.12. Mini culture and Mini DNA purification

Clones were picked from the LB agar-plates into 6 ml of LB medium containing the corresponding antibiotics and incubated at 37°C and 180 rpm overnight. 2 ml of the LB culture was then centrifuged at 13000 rpm for 5 min. The supernatant was discarded and the pellet was resuspended in 250 μl of buffer P1. 250 μl of lysis

buffer P2 was added, incubated at RT for 5min for alkaline lysis followed by addition of 300 µl neutralization buffer P3. The samples were centrifuged at 13000 rpm and 4°C for 10 min. The supernatant was then transferred into a fresh 1.5 ml microfuge tube and the DNA was precipitated using 750 µl of isopropanol. The pellet was again washed with 75% ethanol, air-dried and the DNA was resuspended in 20 µl ddH$_2$O.

2.10.13. Maxi/Midi culture and purification

100 µl of the Mini-culture was incubated in 100 ml or 200 ml LB medium containing the corresponding antibiotics at 37°C and 180 rpm for 12 – 16 hours for Midi- and Maxi-cultures, respectively. Maxi- and Midi- DNA purification kits were purchased from Qiagen (Hilden). The DNA pellets were resuspended in 50 µl and 150 µl ddH2O for Midi- and Maxi- DNA preparations, respectively.

2.10.14. Endofree Maxi DNA purification

Endotoxins, also known as lipopolysaccharides (LPS), are cell-membrane components of Gram-negative bacteria such as *E.*coli. Upon lysis of the bacterial culture, the endotoxins are released from the outer membrane into the lysate. The presence of endotoxin can influence the uptake of plasmid DNA in transfection experiments and can also induce non-specific activation of immune cells such as macrophages and B-cells in animal experiments. Endofree Maxi-DNA purification kit (Qiagen, Hilden) was used to produce endotoxin-free plasmids.

2.10.15. Sequencing of plasmid DNA

2 µg of plasmid DNA was diluted in TE buffer to a final volume of 20 µl and the primers at a concentration of 10 pmol/µl in a volume of 10µl was sent to MWG Eurofins Operon (Ebersberg) for sequencing. The sequencing results were analysed using the SDSC Biology workbench software (http://workbench.sdsc.edu) which is available online.

2.10.16. Software

Insilico handling of DNA sequences for the cloning experiments were performed using the softwares - Gene Construction Kit (Textco, New Hampshire, USA) and MacVector 12.0.6 (Cambridge, UK).

2.11. Cell culture methods

2.11.1. Culture of HEK293 cells

HEK293 cells are cultured in DMEM medium containing 10% foetal bovine serum, 1% L-Glutamine and 1% Penicillin (10000U/ml)/Streptomycin (100mg/ml) in a humidified 37°C/5% CO_2 incubator. The cells grew as adherent monolayer in culture dishes (Nunc, Langenselbold) and have a doubling time of about 24 hours. The cells were passaged to a maximal 30 times, after which new aliquots are thawed from the liquid nitrogen storage. The cells were split every 4 days.

For splitting, the culture medium was aspirated from the culture dishes and the cells were washed once with DPBS (Dulbecco's phosphate buffered saline). The cells were trypsinised using trypsin-EDTA solution (0.5 g/l trypsin, 0.2 g/l EDTA) and the plates were monitored under an inverted microscope. As soon as the cells began to detach from the surface of the culture dish, the trypsin solution was removed and the cells were resuspended in fresh culture medium. The cells were then sown in new culture dishes.

2.11.2. Adenovirus generation

Endofree-purified pAd/CMV/V5 plasmid DNA of the gene of interest (6 µg) was digested with PacI restriction endonuclease and incubated at 37°C for 2 hours. The digested plasmid was precipitated with sodium acetate. 2 µg of the plasmid DNA were transfected into HEK cells using the Effectene procedure (Qiagen, Hilden). The DNA was mixed with buffer EC to a total volume of 150 µl and the samples were incubated at RT for 5 min with 16 µl of enhancer. The samples were then incubated at RT for 10 min with 25 µl of Effectene reagent to allow complex formation. The transfection complexes were mixed with 1 ml of growth medium and were added onto a 6-cm dish containing HEK cells which are 80% confluent in 2 ml of medium. The cells were incubated in a humidified 37°C/5% CO_2 incubator until 80% of the cells were cytopathic.

For the first virus amplification, the cell suspension was centrifuged at 850 g at 4°C for 10 min and the pellet was resuspended in 1ml 10 mM Tris (pH 8). The suspension was subjected to freeze-thaw cycle twice by freezing it in liquid nitrogen and thawing using a waterbath at 37°C. The freeze-thaw cycle evokes cell lysis and releases the intracellular viral particles. After centrifugation, the supernatant was stored at -80°C.

For the second amplification, 500 μl of the viral particle from the first amplification was added to a 10-cm dish containing HEK cells. The cell pellet was resuspended in 2 ml of 10 mM Tris (pH 8). The freeze-thaw cycles were repeated and the virus were stored at -80°C.

Finally, 100 μl of virus from the second amplification was used to infect a 15-cm dish containing 90% confluent HEK cells. The cells were kept in a humidified 37°C/5% CO_2 incubator until 80-90% of the cells had rounded up. After centrifugation, the pellet was resuspended in 3 ml 10 mM Tris (pH 8) and the freeze-thaw cycle was repeated thrice, and the final viral particles were stored at -80°C.

2.11.3. Adenoviral purification and titration

The adenoviruses produced were purified and concentrated using the Adeno-X purification kit (Clontech, France) based on a chromatographic technique. HEK293 cells were diluted to a concentration of 1.83 x 10^6 cells/ml in a total volume of 40ml. The virus was mixed with the cells, seeded onto five 150mm cell culture dishes and were cultured in 37°C/5%CO_2 incubator until the cytopathetic effect was observed (typically 3 – 5 days). The cells were harvested by centrifuging at 1500 rpm for 10 min and the pellet was resuspended in fresh medium. The cell suspension was subjected to freeze-thaw cycle thrice to lyse the cells. After centrifugation, the supernatant was incubated with 5μl of Benzonase at 37°C for 30 min. Equal volume of 1X dilution buffer was added to the lysate and was clarified by passing it through a 0.45 μm syringe pre-filter.

The adenovirus loaded into the equilibrated filter assembly was allowed to pass through the filter at a flow rate of 3ml/min. After the wash buffer was passed through the filter, the virus was collected in a sterile tube by passing 3 ml of elution buffer through it. The purified virus were then stored at -80°C.

The Adeno-X rapid titer kit (Clontech, France) was used to titer the produced adenoviruses. HEK cells were infected with serial dilutions of the viral particles for 48 hours. Then, the cells were fixed with ice-cold methanol and incubated with an anti-hexon antibody (1:1000 diluted in 1% BSA/1X PBS) followed by incubation with HRP-conjugated anti-rat antibody (1:500 diluted in 1% BSA/1X PBS). Subsequent exposure of the plate to DAB substrate solution (1:10 diluted in 1X stable peroxidase buffer) caused the infected cells to become brown. The infected cells (brown or black cells) were then counted using an inverted microscope with 20X objective in a

minimum of 3 fields per dilution. The virus titer was then determined using the below formula:

$$\text{Virus titer} = \frac{\underline{(\text{Infected cells per field}) * (\text{fields per well})}}{(\text{Volume of virus}) * (\text{Dilution factor})}$$

2.11.4. Isolation of neonatal rat cardiomyocytes

Whole hearts from newborn Sprague-Dawley rats (1-2 days old) were excised and were transferred into Ca^{2+} and bicarbonate-free HEPES-buffered Hanks' medium (HBSS). After removing the atria, the hearts were cut into pieces, and digested with an enzyme solution containing trypsin (#215240, Becton Dickinson and PAN) and DNase under constant stirring. The suspension was collected over fixed intervals of time into tubes containing 9 ml FBS. The primary cells that were collected after passing through a 40 µm cell strainer were seeded in uncoated plastic dishes for 1 hour at 37°C / 1% CO_2. During the preplating time, the more rapidly adherent fibroblasts attach to the surface. The supernatant containing the cardiomyocytes was collected and the CMs were cultured in MEM containing vitamin B12, $NaHCO_3$, BrdU and 1% FCS. These were almost exclusively cardiomyocytes that stained positive for α-actinin (>95%; data not shown). The plastic dishes containing the cardiac fibroblasts were washed with PBS and cells were cultured in MEM containing vitamin B12, $NaHCO_3$ and 1% FCS. A trained staff carried out the cardiomyocyte isolation from neonatal rats.

Cardiomyocytes from newborn mice (1-2 days old) were also prepared as described above but the cells were cultured in MEM containing L-glutamine, vitamin B12, $NaHCO_3$, BrdU and 5% FCS.

2.11.5. Isolation of adult mouse cardiomyocytes

Langendorff perfusion method was carried out by trained staff for isolation of cardiomyocytes from adult mice (atleast 3 months old). The animals were anesthetised with 4% isoflurane, and an intra-peritoneal injection of xylazine (80 mg/kg) and ketamine (12 mg/kg). The hearts were extracted from the mice, the aorta cannulated and the cannula was attached to the perfusion chamber. The coronary arteries were retrogradely perfused with perfusion buffer for 3 min (flow rate: 4 x 10) and then were digested with a digestion buffer containing Collagenase type II (Worthington) for 11 min (flow rate: 4 x 10) to dissociate ventricular cells. Complete digestion was indicated by a swollen, pale and flaccid appearance of the heart.

Subsequently, atria were excised and the ventricles were cut into small pieces in 2.5 ml of digestion buffer. The torn pieces of the heart were further sheared using a syringe for 1 min. 2.5 ml of buffer P1 was added to inhibit the enzyme activity of collagenases. The suspension was filtered through a 100 µm cell strainer. The homogenate containing the cells were allowed to sediment for 10 min at 37°C. Cardiomyocytes, which are heavier, settle down as a pellet. The supernatant was then transferred into a new tube and centrifuged at 900 rpm for 1 min. The supernatant containing the fibroblasts was transferred into a fresh tube for subsequent isolation of fibroblasts. The pellets were pooled together by resuspending with 10 ml of buffer P2 and transferred into a 25-ml conical flask. Calcium reconstitution was performed by subsequent additions of 50 µl 10 mM $CaCl_2$, 50 µl 10 mM $CaCl_2$, 100 µl 10 mM $CaCl_2$, 30 µl 100 mM $CaCl_2$ and 50 µl 100 mM $CaCl_2$ in time intervals of 4 min between each addition to achieve a final Ca2+ concentration of 100 µM. The cells were sedimented again at 37°C for 10 min and the supernatant was centrifuged at 900 rpm for 1 min. The pellets were pooled together in 2 ml of CM plating medium. For immunofluorescence experiments, the cardiomyocytes were seeded on plates containing laminin-coated overslips. Cardiomyocytes were incubated in 37°C/5% CO_2 incubator. After 6 hours of incubation, the medium was replaced with CM culture medium.

For cardiac fibroblast isolation, the supernatant from the CM centrifugation step was centrifuged at 1200 rpm for 1 min. The supernatant was discarded and the pellet was resuspended in 2 ml of 5% AMCF plating medium. After 1 hour of preplating, the cells were washed with PBS and were incubated with AMCF culture medium.

2.11.6. Stimulation with thapsigargin to induce store depletion

NRCMs isolated by enzymatic digestion were seeded on poly-lysine coated coverslips in MEM containing 1% FCS and were cultured for 24 hours. The medium was then replaced with MEM containing 0.1% FCS and cultured for an additional 24 hours. The cells were then kept in Ca^{2+}-free HBSS solution for 60 minutes and were then treated with 8 µM thapsigargin for 10 min. The cells were then fixed with 4% PFA for 5 min at 4°C for immunofluorescence experiments. To prepare protein lysates the cells were lysed with the appropriate lysis buffer immediately after thapsigargin treatment.

2.11.7. Immunofluorescence

The cells were fixed using 4% PFA for 5 min at 4°C. The cells were washed thrice with PBS to remove excess PFA. The cells were incubated with 100 µl of 0.2% TritonX for 10 min to permeabilise the cells. The cells were then blocked with 1% BSA/1X PBS in a humidified chamber at 37°C for 30 min. The coverslips were incubated with primary antibodies against rabbit anti-STIM1 C-terminal (1:400 diluted in PBS) or rabbit anti-STIM1 N-terminal (1:20 diluted in PBS) and mouse anti-α-actinin (1:1000 diluted in PBS) for 30 min at 37°C. The corresponding Cy3-conjugated AffiniPure goat anti-rabbit (1:200 diluted in PBS) and Alexa488-conjugated goat anti-mouse IgG (1:200 diluted in PBS) were used as secondary antibodies and added for another incubation for 30 min at 37°C. The coverslips were mounted on slides using Vectashield fluorescence mounting medium containing DAPI.

For TIRF microscopy analysis, the coverslips were mounted on slide using PBS.

2.11.8. Transfection of NRCM with siRNA

Transfection was carried out with Lipofectamine™ 2000 (Invitrogen, Karlsruhe) as per the manufacturer's guidelines. These are specially designed cationic lipids which complexes with negatively charged nucleic acids to form liposomes in aqueous conditions. The liposomes carrying a positive charge on its surface can then fuse with the negatively charged plasma membrane thereby facilitating delivery of the nucleic acids into the cell.

50,000 NRCMs per well were seeded into 96-well IBIDI plates in MEM containing 1% FCS and was cultured for 24 hours. The solution A and B for each transfection sample was prepared as below.

Solution A	Lipofectamine™ 2000	0.25 µl
	Opti-MEM	24.75 µl
Solution B	siRNA	10 pmol
	Opti-MEM	upto 25 µl

Solution A was incubated at RT for 5 min following which Solution A was mixed with Solution B containing the siRNA by gentle pipetting. The tubes were then incubated at RT for 20 min to allow siRNA-lipofectamine complex formation. Meanwhile the transfection reagent preparation, the cells were washed with MEM containing 1%

FCS without antibiotics and 50 µl of the medium was added to each well of the plate. 50 µl of the siRNA-lipofectamine complex was then added to the cells. The final concentration of the siRNA in each well is 100 nM. The medium was then replaced with MEM containing 1% FCS and 1% antibiotics after 5 hours of transfection.

2.11.9. Hypertrophy assay

For the hypertrophy assay, 50,000 NRCMs per well were seeded into 96-well IBIDI plates in MEM containing 1% FCS for 24 hours. The cells were infected with respective adenoviruses and were incubated for a further 24 hours in 1% FCS. The medium was then changed to MEM containing 0.1% FCS and after 24 hours, were stimulated with 50 µM phenylephrine (PE) in MEM containing 0.1% FCS for 48 hours. Unstimulated control cells were incubated in MEM containing 0.1% FCS. The cells were fixed with 100 µl 4% PFA for 5 min at RT. To remove the excess PFA, the cells were washed thrice with 200 µl of PBS and were permeabilised with 100 µl of 0.2% TritonX. The plate was then incubated with 100 µl of mouse α-actinin (1:1000 diluted in PBS) in a humidified chamber at 37°C for 30 min. After washing with PBS, the plate was incubated with Alexa488-conjugated goat anti-mouse IgG (1:200 diluted in PBS) and DAPI (1:100 diluted in PBS) for 30 min. The cells were washed thrice with PBS and 150 µl of 50% glycerol was added to the plate. The plate was covered using an aluminium seal cap. The cardiomyocyte area, as visualised by the α-actinin staining, was analysed using an automated microscopy [144].

2.11.10. NFAT-luciferase assay

NFAT activity was detected by luminescence using a luciferase reporter construct containing repetitive NFAT recognition sites (gift from J. Molkentin, University of Cincinatti).

75000 NRCMs were seeded on a 48-well plate in MEM containing 1% FCS. After 2 hours of seeding, the cells were infected with the respective adenoviruses at MOI of 100. On the following day, NRCMs were transfected with 0.2 µg of NFAT-luc plasmid using lipofectamine. The medium was replaced after 5 hours of transfection. After 24 hours, the cells were stimulated with 50 µM PE for 24 hours. The cells were washed with pre-warmed PBS and 70 µl of 1X luciferase lysis buffer was added to the wells.

2.11.11. Proliferation assay

5,000 NRCF were seeded on 96-well IBIDI plates in MEM containing 1% FCS and were culture for 24 hours. The cells infected with the respective adenoviruses were cultured for 24 hours, medium was replaced and after 24 hours were stimulated with 10% FCS for 48 hours. Unstimulated control cells were incubated with 1% FCS. The cells were fixed with 4% PFA at 4°C for 5 min. The cells were washed with PBS thrice and the cells were incubated with 100 µl of DAPI in a humidified chamber at 37°C for 30 min. 150 µl of 50% glycerol was added to the plates and was covered with an aluminium seal. The nuclei count was determined by automated microscopy.

2.12. Microscopy

2.12.1. Confocal microscopy

Confocal images were taken using Zeiss LSM 510 META and were processed using Adobe Photoshop software. Cy3, Alexa-488 and DAPI were excited at 453 nm, 488 nm and 405 nm laserlines, respectively.

2.12.2. Total internal reflection microscopy

For TIRF measurements, the coverslips were mounted on slides using PBS. TIRF images were taken using a TILL Photonics iMIC microscope (Graefelfing, Germany) and were processed using ImageJ software.

2.12.3. Calcium (Ca^{2+}) imaging

Intracellular calcium in the cells is measured using chemical indicators whose spectral properties change depending on their binding to calcium. Fura-2AM is an acetoxymethyl ester derivative of Fura-2 that can be easily loaded into the cells due to their lipophiic nature. The dye is then hydrolysed by cellular esterases that trap them in the cytosol. Upon binding to calcium, the fluorescent excitation maximum of the indicator undergoes an absorption shift from 380 nm (calcium free) to 340 nm (calcium complex). The ratio of the emissions (A340/A380) correlates directly to the amount of intracellular calcium.

500,000 NRCMs were seeded on poly-lysine coated coverslips in a 6-well plate cultured in MEM containing 1% FCS at 37°C/1% CO_2 incubator for 24 hours. The cells were then infected with the respective adenoviruses at an MOI of 100 and were cultured for 24 hours. The medium was replaced and cultured for an additional 24

hours. Cardiomyocytes from neonatal wildtype or *Stim1*$^{-/-}$ mice isolated by enzymatic digestion were cultured in a humidified 37° C/ 1 % CO_2 incubator for 48 hours prior to measurements.

On the day of the measurement, cells were incubated with 750 µl of 2 µM Fura-2 for 45 min at 37° C, followed by washing in HBSS buffer without Ca^{2+} and bicarbonate for 60 min at RT in the dark.

The calcium measurements were carried out on Zeiss Axiovert 35M microscope fitted with a Zeiss Fluor 40X oil-immersion objective. The coverslips containing the cells were taken on a holder and 300 µl of Ca^{2+}-free HBSS/0.5 mM EDTA was added. After taking measurements for 1 min, 200 µl of 20 µM thapsigargin (final concentration of 8 µM) was added on top of the cells followed by the addition of 55 µl of $CaCl_2$ solution (final concentration of 2 mM) and 61 µl of SKF-96365 (final concentration of 10 µM) after 2.5 min and 5 min, respectively. During the entire procedure, cells were imaged through a 40X objective with dual excitation at 340 nm and 380 nm, and monitored at 510 nm. The background fluorescence correction was made and the ratio F340/F380 was determined. The data were then analysed using the Till vision version 4.0 software.

2.12.4. Automated cell-size determination microscopy

The cell size of the cardiomyocytes was determined by automated microscopy and image segmentation. Images were acquired automatically using a 10X objective on an AxioObserver.Z1 (Zeiss, Jena), a motorized scanning stage (Märzhäuser, Wetzlar), Lumen200 fluorescence illumination system (Prior, Cambridge UK) and Retiga4000 CCD fluorescence camera (QImaging, Surrey Canada). Metamorph imaging software (Molecular Devices, Downingtown USA) was used to drive the microscope automatically and also for subsequent analysis of the acquired images. A macro function journal consisting of three subjournals was created. The first subjournal drove the positional scanning of the plate, focusing and image acquisition (4 images per well) in two different fluorescent channels – DAPI and green fluorescence (488 nm). The second journal created separate montage stacks of the images acquired at the two fluorescent intensities and also an overlay montage stack by merging the 2 images together. The third subjournal determined the cell size and number, as indicated by the α-actinin staining for cardiomyocyte area and nuclei staining with DAPI, using the cell scoring plug-in of the software.

For proliferation assay on cardiac fibroblasts, a separate journal that acquired and quantified nuclei staining with DAPI was used.

2.13. Methods for RNA analysis

2.13.1. Isolation of RNA

peqGOLD Trifast[TM] includes phenol and guanidium isothiocyanate in a monophasic solution which on addition of chloroform separates into three phases upon centrifugation. The aqueous phase contains the RNA, the interphase the DNA and the organic phase the protein.

Tissues (50-100 mg) were homogenized in 1 ml of peqGOLD Trifast[TM] using a turrax. In the case of cells on a 3.5 cm dish, the cells were lysed with 1 ml of Trifast by pipetting vigorously. The samples were then incubated at RT for 5 min to allow dissociation of the nucleoprotein complexes. 200 µl of chloroform was added to the samples, vortexed vigorously for 50 sec and were incubated at RT for 10 min. After centrifugation at 12000 x g for 10 min at 4°C, the mixtures separated into three phases – upper aqueous phase (RNA), Interphase (DNA) and lower organic phase (protein). The upper phase containing the RNA was then transferred into a fresh 1.5 ml tube. 500 µl of isopropanol was added to the samples to precipitate the RNA. The samples were kept on ice for 10 min and then centrifuged at 12000 x g for 10 min at 4°C. The supernatant was discarded carefully and the RNA pellet was washed twice with 1 ml of 75% ethanol by vortexing and subsequent centrifugation at 12000 x g for 10 min at 4°C. After discarding the supernatant, the RNA pellet was air-dried to remove excess isopropanol. The RNA samples were then resuspended in 20 µl 55°C-pre-warmed sterile ddH$_2$O and stored at –80°C. The concentration of the samples was determined on the following day using the Nanodrop® ND-1000 spectrophotometer (peqLab, Erlangen).

2.13.2. Reverse transcription

The RNA samples and the reagents were thawed on ice. 2 µl of oligo-dT was taken in fresh 1.5 ml tubes. Then 1 µg of RNA was added to the tubes and the volume was made to 11 µl by adding RNase/DNase-free water. The tubes were incubated at 70°C for 10 min. This allows the annealing of the oligo-dT to the poly-A tail present on the mRNAs and serves as primer for cDNA synthesis.

Reaction mixture	1st Strand buffer	4 µl
	DTT	2 µl
	dNTP (1:10)	1 µl
	RNasin	0.1 µl
	RNase/DNase-free ddH$_2$O	0.9 µl
	Supercript II Reverse Transcriptase	1 µl

9 µl of the prepared mastermix was added to the samples and was incubated at 42°C for 60 min. Then the tubes were incubated directly at 70°C for 10 min and then on ice. The final concentration of the cDNAs was then adjusted to 10 ng/µl using RNase/DNase-free water.

2.13.3. Quantitative real time PCR

Quantitative real time PCR allows both detection and quantification. SYBR green is a non-specific fluorescent dye, which intercalates into the double-stranded DNA. The dye only fluoresces when bound with DNA. With each cycle of amplification, the emitted fluorescence intensity of the SYBR green increases as compared to the reference fluorophore 8-ROX (8-carboxy-X-rhodamine). The number of cycles at which the fluorescence intensity exceeds the threshold is called the cycle threshold (C_t). To quantify the gene expression for RNA of interest, it is normally normalized to the gene expression of a housekeeping gene such as GAPDH ($\Delta\Delta C_t$-method). This normalizes the variation in the amount and the quality of RNA between different samples. However, the expression of the reference gene needs to be similar between the samples.

The reagents for the real time PCR was from Invitrogen (Karlsruhe). The real time PCR was carried out in StepOne Plus instrument (Applied Biosystems, New Jersey).

Reaction mixture	10X PCR buffer	1.25 µl
	50 mM MgCl$_2$	0.375 µl
	Forward primer	0.25 µl
	Reverse primer	0.25 µl
	dNTP	0.2 µl
	1X ROX	0.5 µl
	5X SYBR Green	0.5 µl
	'Platinum' Taq polymerase	0.05 µl

| | ddH$_2$O | 6.625 µl |
| | cDNA (2.5 ng/µl) | 2.5 µl |

Step	Temperature	Time	No. of cycles
Pre-denaturation	94°C	120 s	
Denaturation	94°C	20 s	40 cycles
Annealing	56°C	20 s	
Elongation	65°C	35 s	
Final elongation	65°C	86 s	
Dissociation step			

2.14. Methods for protein analysis

2.14.1. Preparation of protein lysates

Tissues (50-100 mg) were homogenized in 800 µl of protein lysis buffer using a turrax. In the case of adherent cells such as NRCM and NRCF, the stimulated cells were washed with PBS and 250 µl of cold protein lysis buffer was added to the plates. The cells were scraped using a cell scraper and the lysates were transferred into a 1.5 ml tube. The cell lysates were then sonicated.

The lysates were then incubated with 1/10th volume of 5% (v/v) Benzonase at RT for 10 min. Benzonase is a genetically engineered endonuclease which degrades all forms of nucleic acids (DNA, RNA). The tubes were then placed in an ultrasonic bath at 4°C for 5 min. The samples were then centrifuged at 12000 rpm for 20 min at 4°C to clear the lysates and were stored at -80°C until use.

2.14.2. BCA protein quantification

The concentration of the protein lysates was determined by the bicinchoninic acid colorimetric assay using the BCA protein assay kit (Thermo Scientific, Rockford USA). The peptide bonds in the protein reduce the divalent copper ions to monovalent ions, which then chelates with the bicinchoninic acid to form a purple-coloured complex with absorption maximum at 562 nm. The absorbance of the samples at 562 nm was measured using an Infinite 200 spectrophotometer (Tecan, Männedorf). The protein concentration was then evaluated with reference to internal calibration standards such as bovine serum albumin.

2.14.3. Co-immunoprecipitation

The lysates were prepared in IP lysis buffer and the proteins were quantified as described previously. 500 µg of proteins was diluted using IP lysis buffer such that the protein concentration was 1-2 µg/µl. The lysates were then incubated with 4 µg of rabbit anti-STIM1 C-terminal antibody or mouse anti-calmodulin antibody at 4°C for 16 hours on an 'Intelli-mixer' roller (LTF Labortechnik). This allowed for the efficient binding of the primary antibody to the target antigen (Ag-Ab complex). 50 µl of ProteinG dynabeads were taken in 1.5 ml tubes and were placed on the magnet to separate the magnetic beads from the solution. The beads were then washed twice with 100 µl IP wash buffer. The lysate were then transferred to the tubes containing the beads, resuspended and were incubated at 4°C on the roller for 3 hours. The dynabeads-Ag-Ab complex was washed thrice with 200 µl IP wash buffer. After the first wash, the PBS suspension containing the dynabead complex was transferred into a fresh tube. Finally, the beads were resuspended in 45 µl of 1X Lamelli buffer and were boiled at 90°C for 10 min to allow denaturing of the samples. The tubes were then placed on the magnet and the supernatant was then loaded onto the SDS-PAGE gel for protein analysis.

2.14.4. Western blot

Depending on the size of the detected proteins, 8 – 12% polyacrylamide gels were used.

	Stacking gel	Running gel		
		8%	10%	12%
Acrylamide/Bisacrylamide 30%/0.8% (v/v)	0.5 ml	4 ml	4.5 ml	5 ml
Lower buffer (4X)	-	3.8 ml	3.8 ml	3.8 ml
Upper buffer (4X)	1.25 ml	-	-	-
H_2O	3.2 ml	4.7 ml	4.2 ml	3.7 ml
Glycerol (80%)	-	2.5 ml	2.5 ml	2.5 ml
TEMED	6 µl	12 µl	12 µl	12 µl
APS (10%)	48 µl	72 µl	72 µl	72 µl

The gels were casted on Mini-PROTEAN casting stand (Biorad, München). The samples were prepared by boiling at 95°C for 5 min. The gel electrophoresis chamber was filled with 1X running buffer, samples were loaded into the wells and

30 mA current per gel was applied at maximum voltage. Under denaturing conditions, the proteins are separated based on their molecular weight.

The proteins were then transferred onto a PVDF membrane (Millipore, Billerica USA) using wet transfer (Mini-PROTEAN transfer system, Biorad, München). The PVDF membrane was cut to the size of the mini-gel and was activated using methanol. The membrane was placed on the cassette facing the anode and the gel was placed facing the cathode side. The membrane and the gel were sandwiched between 1-2 layers of filter paper. The transfer was carried out at 350 mA current at maximum voltage for 90 min.

The membrane was blocked with 5% non-fat milk for 1 hour at RT on a horizontal shaker and then incubated with the primary antibody for 16 hours at 4°C. The following antibodies diluted in milk block buffer were used: anti-STIM1 (Cell Signalling, 1:1000), anti-Calmodulin (Upstate, 1:1000), anti-GAPDH (Calbiochem, 1:7000), anti-Gß (Santa Cruz, 1:7000), anti-TRPC1 (Alomone labs, 1:200), anti-TRPC3 (Alomone labs, 1:200), anti-TRPC4 (Alomone labs, 1:200), anti-TRPC6 (Alomone labs, 1:200) and anti-NFATc1 (Santa Cruz, 1:200). The membrane was washed thrice with 1X PBST for 10 min at RT. The membranes were then incubated with the appropriate peroxidase-conjugated secondary antibodies (1:10000) at RT for 90 min. The membranes were again washed with the PBST buffer.

The proteins were detected by chemiluminescence. ECL Plus (GE Healthcare, München) was applied to the membrane according to the manufacturer's instructions. The signal was visualized using a Fujifilm LASmini4000 instrument (Fujifilm, Düsseldorf). The blots were then analysed using the Multigauge software (Fujifilm, Düsseldorf).

2.15. Methods for animal experiments

2.15.1. Transgenic mice

Mouse line	Nomenclature	Reference
Stim1 knockout mice	Stim1[ßGeo/ßGeo]	Varga-Szabo *et al* [99]
ß1-transgenic mice	Myh6-*AdrB1*[Tg(4)/0]	Engelhardt *et al* [145]

2.15.2. Animal models

2.15.2.1. ß1-adrenergic receptor transgenic mice (Myh6-AdrB1[Tg(4)/0])

ß1-transgenic was used as one of the heart failure models in the study. The mice were generated by overexpression of ß1-adrenergic receptor under the control of

heart-specific α-MHC promoter [145]. The transgenic mouseline TG4 that had 15-fold increase in its receptor numbers than the wildtype littermates was used in the study. These mice had high cardiac contractility at young age but developed progressive heart failure with myocyte hypertrophy, decreased contractility and reduced cardiac function at 9-months of age.

2.15.2.2. Pressure overload-induced cardiac hypertrophy

Pressure overload hypertrophy can be induced either by constricting the thoracic aorta (TAC) in mice or by placing a tantalum clip on the suprarenal abdominal aorta (AAB) in rats. In order to compensate for the reduction in the aortic flow, the heart begins to pump at a higher left ventricular pressure and gradually develops myocyte hypertrophy. The pressure-overloaded hearts can trigger low-grade infiltration by immune cells (leukocytes and macrophages) that might contribute to increases in cytokine production such as TGFß resulting in reactive fibrosis. Myocyte degeneration triggers transcription of pro-hypertrophic and foetal genes. Further degeneration leading to exhaustion of cellular adaptation causes myocyte loss and replacement fibrosis [146]. The degree of myocyte degeneration influences the transition from compensatory phase into heart failure.
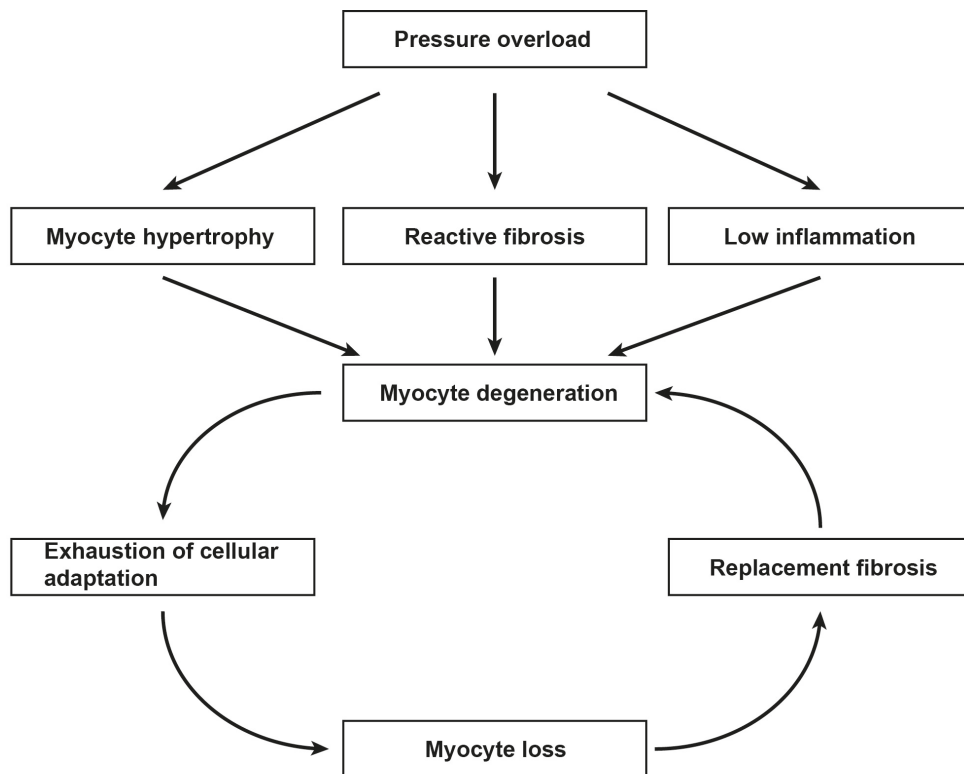
Figure 9. Cardiac remodelling in pressure overload-induced hypertrophy (modified from Hein *et al* 2003).

2.15.3. Isolation of genomic DNA

The tail biopsies were incubated overnight at 55°C and 1100 rpm in 500 µl of DNA lysis buffer (for genotyping) containing 2.5µl of 'Fermentas' Proteinase K. To the tubes, 500 µl of 'Roth' phenol-chloroform was added and were centrifuged at 14000 rpm for 10 min. The upper phase of the cleared lysates were then transferred into fresh 1.5 ml microfuge tubes. The DNA was precipitated by addition of 200 µl of isopropanol and subsequent centrifugation at 14000 rpm at 4°C for 10 min. The supernatant was discarded and the pellet was washed with 500 µl of 70% ethanol. After centrifugation at 14000 rpm at 4°C for 5 min, the pellets were air-dried and resuspended in 20 µl ddH$_2$O.

2.15.4. Genotyping PCR

The PCR reaction was set up as follows.

Reaction mixture	10X PCR buffer	2 µl
	50 mM MgCl$_2$	2 µl
	Forward primer	0.2 µl
	Reverse primer	0.2 µl

dNTP	0.2 µl
'Fermentas' Taq polymerase	0.2 µl
ddH$_2$O	14.2 µl
gDNA (10 ng/µl)	1 µl

The PCR cycle programmes were as described below.

STIM1 knockout mice (*Stim1*$^{\text{ßGeo/ßGeo}}$)

Step	Temperature	Time	No. of cycles
Pre-denaturation	94°C	3 min	
Denaturation	94°C	30 s	35 cycles
Annealing	51°C	30 s	
Elongation	72°C	60 s	
Final elongation	72°C	5 min	

ß1-transgenic mice (Myh6-*AdrB1*$^{\text{Tg(4)/0}}$)

Step	Temperature	Time	No. of cycles
Pre-denaturation	94°C	3 min	
Denaturation	94°C	20 s	35 cycles
Annealing	55°C	30 s	
Elongation	72°C	50 s	
Final elongation	72°C	7 min	

2.15.5. Echocardiography

Vevo 700 was used for echocardiographic measurements (Visual Sonics, Ontario). Mice were subjected to anaesthesia by inhalation (2% isoflurane/98% O$_2$) and were fixed on a hot plate maintained at 37°C. Isoflurane concentration was adjusted such that the heartbeat was in the range of 450±50 beats per min. The chest was shaved and 'Aquasonic' ultrasound transmission gel (Parker laboratories, New Jersey) was applied. The ultrasonic probe in the long axis (B-mode) was placed on parasternal line and the left ventricle, and the position was determined. The echocardiogram was then recorded in the short axis mode (M-mode) by rotating the transducer by 90°C. Left ventricular internal diameter (LVID), left ventricular posterior wall thickness (LVPW) and intraventricular septal thickness (IVS) was determined under both systolic (s) and diastolic (d) phases. The cardiac function parameters such as

ejection fraction (EF) and fractional shortening (FS) were calculated using the below formulae.

$$FS\% = \frac{LVID_d - LVID_s}{LVID_d} * 100$$

$$EF\% = \frac{LV_d - LV_s}{LV_d} * 100$$

where LV represents left ventricular volume.

2.17. Statistics

All quantitative data are reported as mean_SEM. Statistical analysis was performed with the Prism software package (GraphPad version 4). To compare two groups, unpaired student t-test was performed. For comparison of three or more groups, One-way ANOVA was used. Post hoc Bonferonni t-test comparisons were performed to identify which group differences accounted for significant overall ANOVA results. Differences were considered significant when $P < 0.05$, and were represented by * if $P < 0.05$, ** if $P < 0.01$ and *** when $P < 0.001$.

3. Results

3.1. STIM1 expression in heart

In order to characterize the function of STIM1 in the heart, we investigated the expression of the protein in the two predominant cell types in the heart. RNA was isolated from cardiomyocytes (CM) and cardiac fibroblasts (CF) isolated from hearts dissected from neonatal and adult rats, and *Stim1* mRNA expression was analyzed by quantitative real-time PCR. While *Stim1* expression was higher in CMs than CFs in neonatal hearts, it was significantly lower in CMs in adult hearts than CFs (Figure 10A). Similar results were obtained in expression analysis on cell fractions isolated from adult mouse hearts (Figure 10B).

A
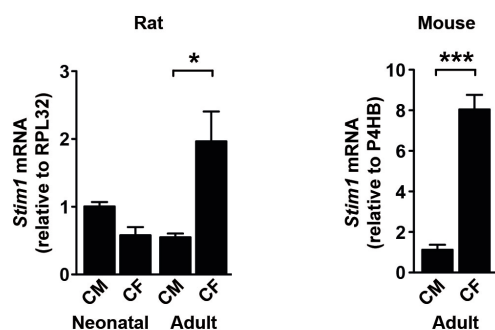
B
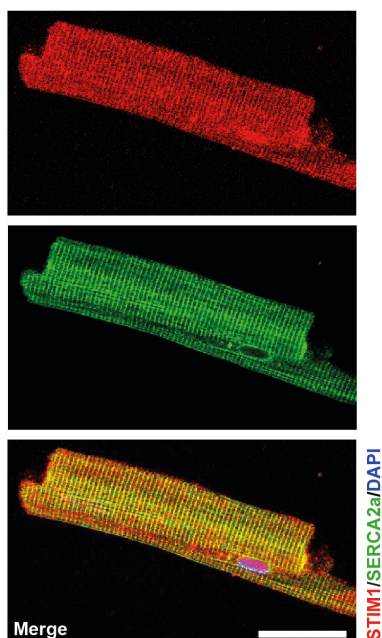
Figure 10. *Stim1* expression and localisation in the heart.
(A) *Right*, relative expression of *Stim1* in neonatal and adult rat cardiomyocytes (CM) and cardiac fibroblasts (CF). *Left*, relative expression in adult mouse cardiomyocytes. n = 3-4 per group. **(B)** Microscopic detection of endogenous STIM1 in adult rat cardiomyocyte. Scalebar represents 50 µm. Data are mean ± s.e.m., and * P<0.05, ** P< 0.01 and *** P<0.001.

Next, we performed immunofluorescence staining on endogenous STIM1 to determine if STIM1 was present in the sarcoplasmic reticulum of the cell. Cardiomyocytes isolated from adult rats were stained with anti-STIM1 antibody (Sigma Aldrich) and were co-stained with anti-SERC2 ATPase antibody to better define the compartment to which STIM1 localizes. The cells were then washed with PBS and were then incubated with the respective fluorescent secondary antibodies. As shown in Figure 10B, STIM1 colocalizes with SERCA indicating that STIM1 is present in the SR compartment of the cardiomyocytes.

3.2. Store-operated calcium entry requires STIM1 in neonatal cardiomyocytes

The expression and immunofluorescence experiments show the presence of STIM1 in both neonatal and adult cardiomyocytes. In order to investigate if STIM1 can induce store-operated Ca^{2+}-entry in cardiomyocytes as observed in other non-excitable cells, the endogenous expression of STIM1 was manipulated using adenoviruses that can either overexpress STIM1 or silence *Stim1* expression. To investigate the effects of manipulated STIM1 expression on store-operated Ca^{2+} entry, we monitored intracellular Ca^{2+}-concentration using Fura-2AM in isolated NRCMs and in cardiomyocytes from *Stim1$^{-/-}$* mice. Seventy-two hours before measurements, neonatal rat cardiomyocytes were infected with adenoviruses encoding STIM1 or a short hairpin to silence endogenous STIM1. On the day of measurement, the cells were exposed to Ca^{2+}-free buffer and thapsigargin, a SERCA inhibitor that causes depletion of calcium in the SR. Then $CaCl_2$ was added as an extracellular source for SOCE typically resulting in Ca^{2+}-influx, which is measured by Fura-2. Adenovirus-driven overexpression of *Stim1* significantly increased the Ca^{2+}-influx in NRCM upon exposure to an exogenous source of Ca^{2+} after thapsigargin induced store depletion (Figure 11A, red tracing). A reciprocal effect was observed upon partial silencing of *Stim1* in NRCM (Figure 11A, green tracing). This effect was also observed in neonatal cardiomyocytes isolated from *Stim1$^{-/-}$* mice (Figure 11B).
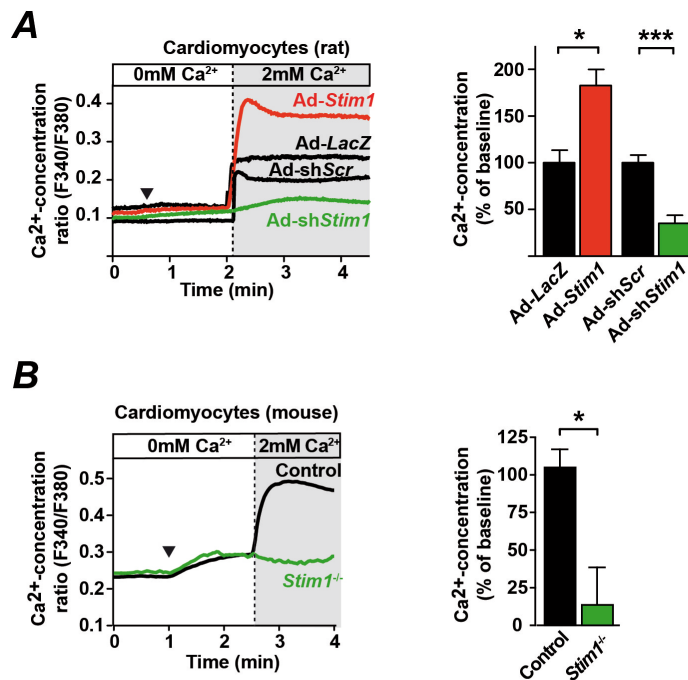
Figure 11. Role of STIM1 in store-operated Ca^{2+}-entry in neonatal cardiomyocytes.
(A) Fluorescence analysis of Ca^{2+}-entry in neonatal rat cardiomyocytes were measured by using Fura-2AM. Representative tracings of the Fura-2 emission in neonatal cardiomyocytes after SR-store depletion using thapsigargin and susequent switch to Ca^{2+}-containing buffer. 72 hours before measurements, cardiomyocytes were infected with adenovirus overexpressing STIM1 (Ad-*Stim1*) and a short hairpin to silence endogenous STIM1 (Ad-sh*Stim1*). Adenovirus overexpressing ß-galactosidase (Ad-*LacZ*) and a sh-scrambled sequence (Ad-sh*Scr*) served as controls (Ad-*Stim1* n=45; Ad-*LacZ* n=15; Ad-sh*Stim1* n=40; Ad-sh*Scr* n=34). Arrow indicates addition of thapsigargin. *Right*, quantitative measurement on these recordings. **(B)** Ca^{2+}-entry in cardiomyocytes isolated from *Stim1$^{-/-}$* mice (n=11) and wildtype controls (n=53). Data are mean ± s.e.m., and * P<0.05, ** P< 0.01 and *** P<0.001.

The cardiomyocyte isolates typically contain < 20% non-cardiomyocyte cells, the majority of which are cardiac fibroblasts. We controlled for the potential contribution of these non-cardiomyocyte cells to these results by performing similar Fura measurements on neonatal rat cardiac fibroblasts. Alteration of STIM1 expression in neonatal cardiac fibroblasts (NRCF) either using Ad-*Stim1* or Ad-sh*Stim1* was confirmed by western blot (Figure 12A). *Ca^{2+}* flux changes in these cells were similar to that of NRCM upon overexpression but were not affected by *Stim1* silencing (Figure 12B), excluding a significant contribution from the non-cardiomyocytes to our findings. Also the cell proliferation experiments indicate that STIM1 does not have a significant role in cardiac fibroblasts (Figure 12C).

Together these results reiterated that STIM1 is required for SOCE in cardiomyocytes in the presence of an SERCA inhibitor.
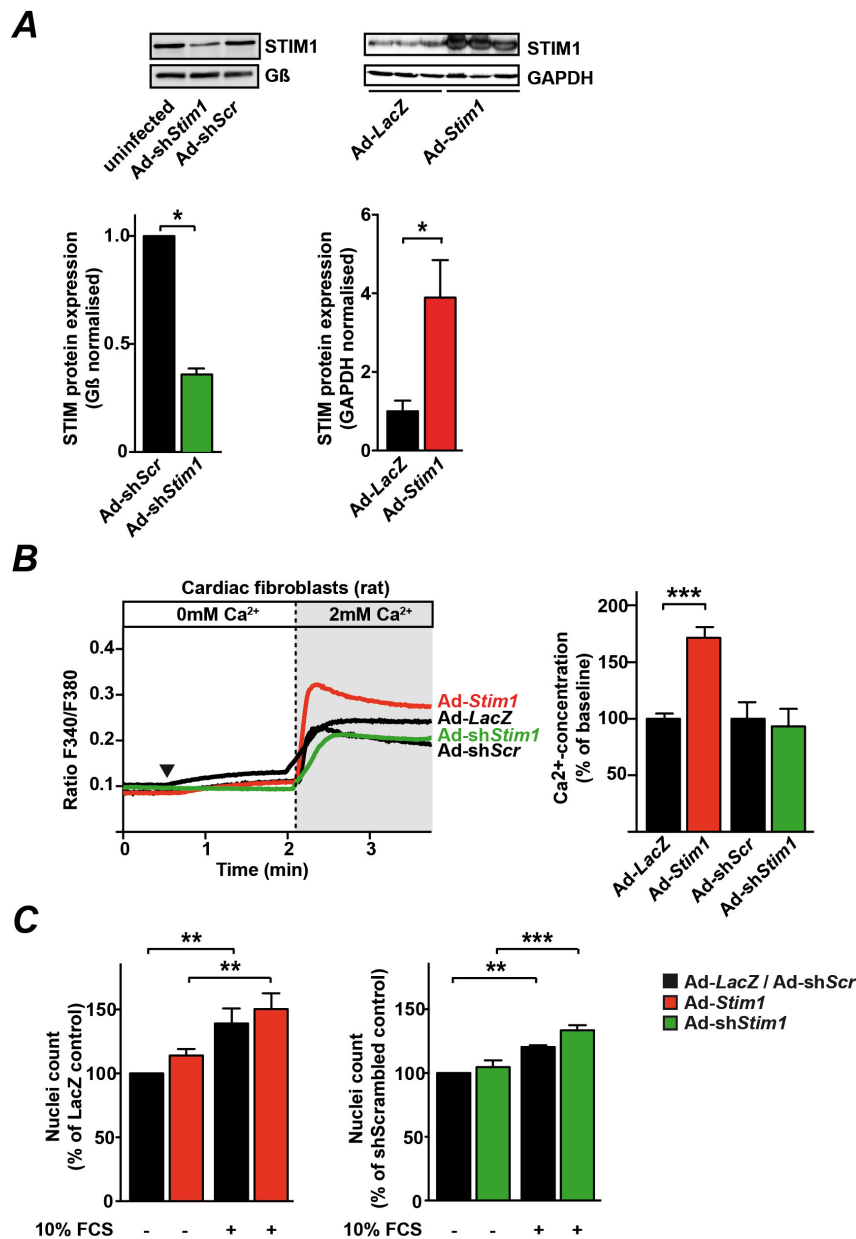
Figure 12. Role of STIM1 in cardiac fibroblast SOC and cell proliferation.
(A) Western blot detecting STIM1 in cardiac fibroblasts 72 hours after infection with Ad-sh*Stim1* (*left*) and with Ad-*Stim1*
(*right*) and quantitative analysis of the results. n = 3 per group. **(B)** Fluorescence analysis of Ca²⁺ entry in neonatal rat
cardiac fibroblasts. *Left*, representative tracings of the Fura-2 emission ratio in CFs infected with Ad-*Stim1* (red) and
Ad-sh*Stim1* (green). Arrow indicates addition of thapsigargin. Silencing STIM1 did not influence SOC entry (Ad-*Stim1*
n=63; Ad-*LacZ* n=56; Ad-sh*Stim1* n=7; Ad-sh*Scr* n=14). Arrow indicates addition of thapsigargin. *Right*, quantitative
analysis of the experiments. **(C)** Proliferation assay on fibroblasts infected with Ad-*Stim1* (red) or Ad-sh*Stim1* (green) and
stimulated for 48 hours with 10%FCS. Data are mean ± s.e.m., and * P<0.05, ** P< 0.01 and *** P<0.001.

3.3. Drug-induced store depletion induces clustering of endogenous STIM1

Our previous results indicate that STIM1 is essential for SOCE in neonatal

cardiomyocytes. We determined the localization of endogenous STIM1 after drug-

induced store depletion by immunostaining. Wild-type neonatal rat and mouse

cardiomyocytes were kept in Ca²⁺-free buffer for 60 min after which they were

treated with 8 μM thapsigargin for 10 min until cell fixation with 4% PFA. The cells

were stained for STIM1, α-actinin and DAPI. As detected by immunostaining with an anti-STIM1 antibody using a confocal microscopy, thapsigargin-induced store depletion of wild-type rat and mouse cardiomyocytes enhanced the clustering of STIM1 into puncta. The cells were also stained for α-actinin, a cardiomyocyte marker (Figure 13).
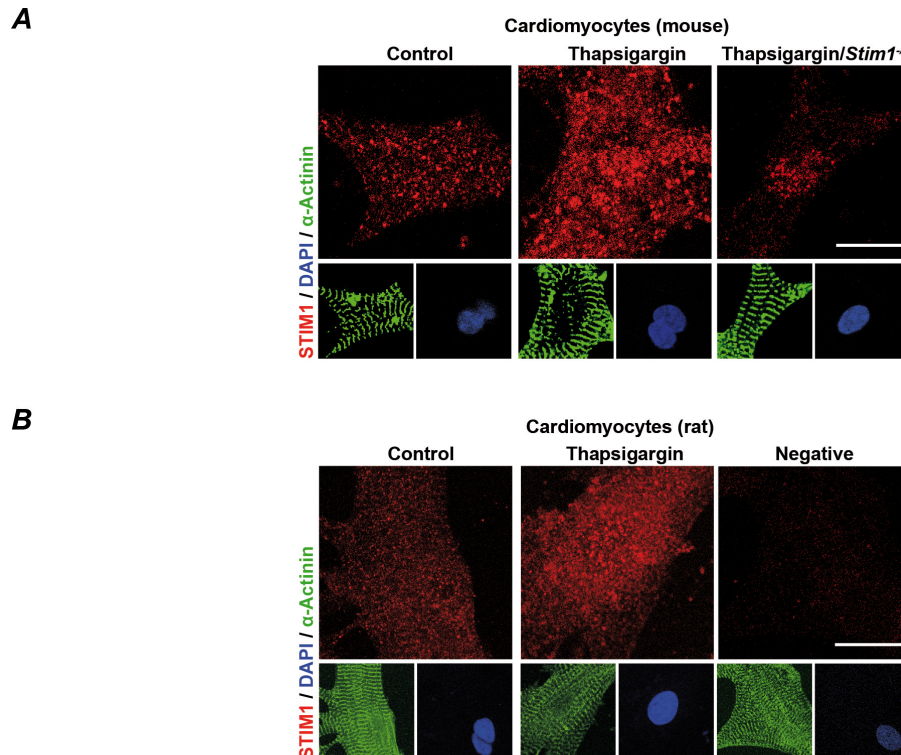

Figure 13. Drug-induced store-depletion causes clustering of STIM1 in NRCM.
(A) Detection of endogenous STIM1 in isolated neonatal mouse cardiomyocytes. Cardiomyocytes from Stim1$^{-/-}$ mice served as negative control. Immunofluorescent staining for STIM1 using a C-terminal antibody (red) and for α-actinin (green). Nuclei were stained with DAPI. **(B)** Detection of endogenous STIM1 in isolated neonatal rat cardiomyocytes. Immunofluorescent staining for STIM1 using an N-terminal antibody (red) and for α-actinin (green). Nuclei were stained with DAPI. Scale bar represents 10 µm.

It has been shown previously that STIM1 is a transmembrane Ca^{2+} sensor within the endoplasmic reticulum, which upon store depletion translocates to regions close to plasma membrane and triggers the SOC influx [69,70]. In this study, STIM1 translocation upon store depletion was studied using total internal reflection (TIRF) microscopy.

TIRF is based on total internal reflection and makes use of an evanescent wave that excites fluorophores in regions immediately adjacent to the glass-water interface. Total internal reflection is an optical phenomenon that occurs when an incident light strikes a medium boundary at an angle larger than a critical angle with respect to the normal of the refracting surface. The evanescent wave thus generated is

internally reflected. This electromagnetic wave decays exponentially and therefore can penetrate to only distances of approximately 150 nm into the sample. This enables selective visualization of surface regions such as the plasma membrane and cytosolic regions just beneath the plasma membrane surface.

Neonatal rat cardiomyocytes grown on coverslips (approximately 0.17 mm thick) were kept in Ca^{2+}-free buffer for 60 min and then were treated with 8 µM thapsigargin for 10 min. The cells were then fixed with 4% PFA, stained for STIM1 and α-actinin and were mounted on a glass slide. PBS was used as a mounting medium as the refractive index is near to that of water (refractive index of water is 1.31). The TIRF images were taken using a TILL Photonics iMIC microscope (Graefelfing, Germany) and were processed using the ImageJ software. As shown in Figure 4, thapsigargin treatment of NRCMs resulted in the redistribution of STIM1 into puncta in regions very close to the plasma membrane (Figure 14). The short time of thapsigargin treatment until cell fixation (< 10 min) attributes the increase in the signal intensities to the distribution and clustering of STIM1 rather than upregulated *Stim1* expression.
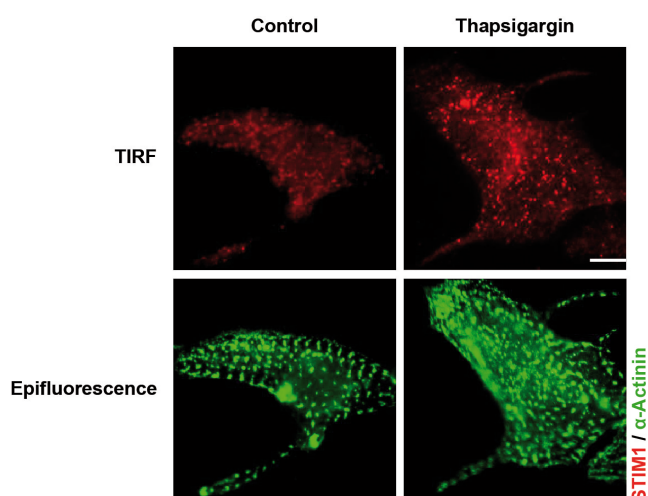

Figure 14. STIM1 translocation in neonatal cardiomyocytes.
Microscopic detection of endogenous STIM1 using total internal reflection microscopy in NRCMs. Immunofluorescent staining for STIM1 (red) and α-actinin (green). Scale bar represents 5 µm.

3.4. Effects of altered expression of *Stim1* on cardiomyocyte hypertrophy

It has been shown previously in neonatal cardiomyocytes that overexpressing *Stim1* increased the Ca^{2+}-influx upon addition of exogenous Ca^{2+} after thapsigargin treatment, while silencing of *Stim1* reversed this effect. This encouraged studying the effects of altered *Stim1* expression on cardiomyocyte growth as a result of the

changes in the intracellular Ca^{2+} levels affected by the SOC channels. NRCMs were infected with adenoviruses either overexpressing STIM1 or silencing *Stim1* and were incubated under basal and hypertrophy-inducing conditions (50 μM phenylephrine) for 48 hours. The cells were the fixed with 4% PFA and were stained with an anti-α-actinin antibody and DAPI. Goat anti-mouse Alexafluor 488 was used as a secondary antibody. The cardiomyocyte area, as visualized by the cytosolic staining with α-actinin, was then measured using automated microscopy.

NRCMs overexpressing STIM1 (Ad-*Stim1)* were significantly larger than cardiomyocytes infected with adenovirus encoding ß-galactosidase (Ad-*LacZ*) (Figure 15A). Significant increase in the expression of atrial natriuretic factor (ANF) was observed in NRCMs overexpressing STIM1 compared to controls (Figure 15B). When cells were treated with an SOCE inhibitor, SKF-96365, the cell sizes of NRCM infected with Ad-*Stim1* were comparable to those infected with Ad-*LacZ*. This could suggest that STIM1 induces hypertrophy by interacting with other SOC proteins such as ORAI and TRP.
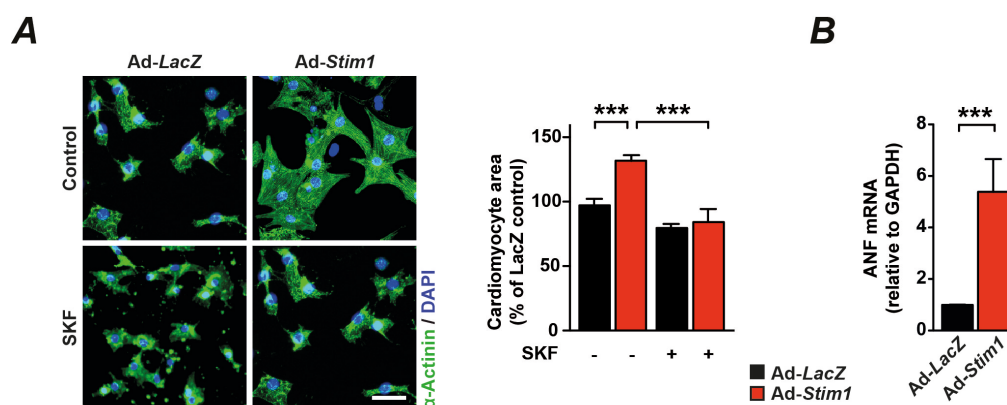

Figure 15. Overexpression of STIM1 leads to cardiomyocyte hypertrophy.
(A) Immunofluorescent analysis of neonatal rat cardiomyocytes infected with adenoviral vectors encoding either ß-galactosidase (Ad-*LacZ*) or STIM1 (Ad-*Stim1*) at a multiplicity of infection of 10 and treated with SOCE inhibitor SKF96365 and control (DMSO; solvent for dissolving SKF96365). Cells are stained with α-actinin (green) and DAPI (blue). Scalebar represents 50 μm. **(B)** Expression of atrial natriuretic factor in Ad-*Stim1* and Ad-*LacZ* infected NRCMs under basal conditions (0.1% FCS). Data are from 3 to 6 independent experiments with 3 replicates each. Data are mean ± s.e.m., and * $P<0.05$, ** $P<0.01$ and *** $P<0.001$.

Pathological cardiac hypertrophy is typically characterized by activation of the Ca^{2+}-dependent signalling pathways via calcineurin-NFAT axis. In order to determine if STIM1 is an activator of the NFAT pathway, an NFAT-dependent luciferase reporter system was used. The construct was a gift from Prof Molkentin which contains nine copies of the NFAT-binding site from the IL4 promoter cloned immediately upstream of the α-MHC promoter followed by a luciferase gene [147] (Figure 16A). Increase in

NFAT activity is directly proportional to the luciferase activity measured. NRCMs were infected with adenovirus overexpressing STIM1 and 24 hours later the cells were transfected with the 9xNFAT-TATA-luciferase reporter construct followed by incubation with SOCE inhibitor (SKF96365) for 48 hours. Overexpression of STIM1 in neonatal cardiomyocytes significantly increased NFAT activation compared to the LacZ-overexpressing controls (Figure 16B). In addition, SKF96365 inhibited STIM1-induced NFAT activation.
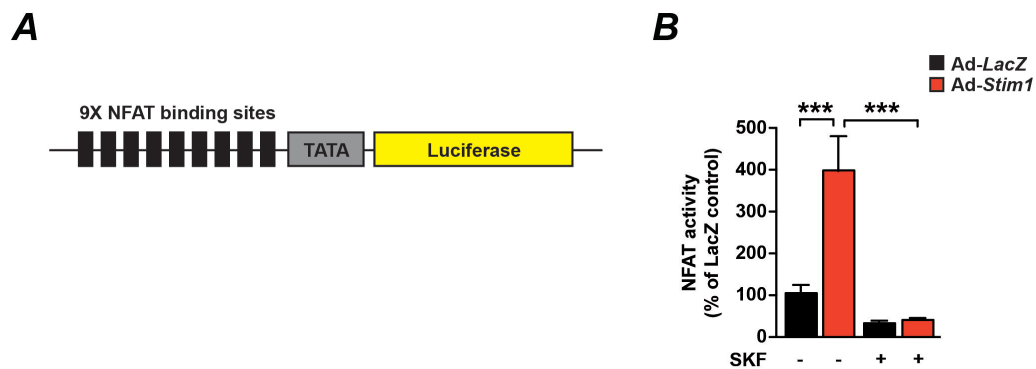

Figure 16. Overexpression of STIM1 leads to cardiomyocyte hypertrophy via NFAT.
(A) Schematic representation of 9X NFAT-TATA-Luciferase reporter construct (modified from Braz et al, JCI 2003).
(B) Determination of NFAT activity in NRCMs overexpressing STIM1 in the presence and absence of SOCE inhibitor, SKF96365. Data are from 3 independent experiments with 3 replicates per group and are mean ± s.e.m., and * $P<0.05$, ** $P<0.01$ and *** $P<0.001$.

The functional impact on NFAT activation and hypertrophy was further investigated in NRCMs after silencing *Stim1*. Reduction of *Stim1* expression prevented phenylephrine-induced cardiomyocyte hypertrophy (Figure 17A). Additional parameters such as NFAT activity and ANF expression were significantly lower in NRCMs infected with Ad-sh*Stim1* than the Ad-sh*Scr* control (Figure 17B). These results indicate that STIM1 is required for cardiomyocyte hypertrophy.
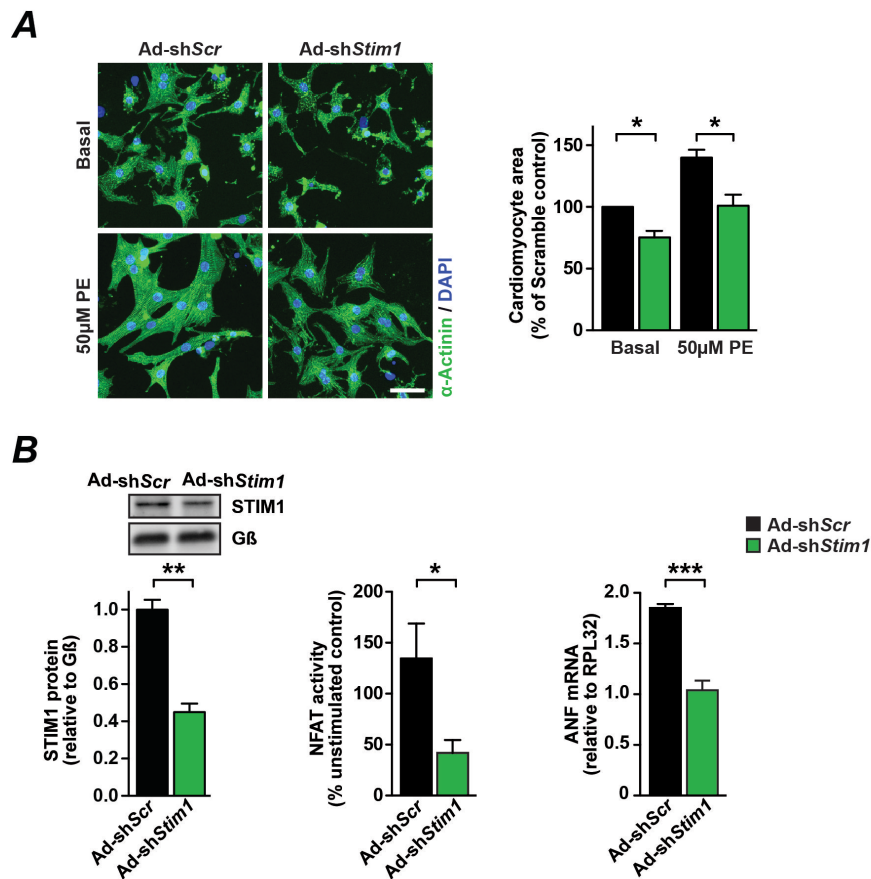
Figure 17. Effects of silencing *Stim1* on cardiomyocyte growth.
(A) Silencing of endogenous *Stim1* using a short hairpin adenovirus (Ad-sh*Stim1*) significantly prevented phenylephrine-induced cardiomyocyte hypertrophy. Scalebar represents 100 μm. **(B)** Effects of NFAT activity and atrial natriuretic factor expresssion on PE-induced NRCMs infected with Ad-sh*Stim1*. Ad-sh*Scr* was used as control. n = 3 - 4 independent experiments with 3 replicates each. Data are mean ± s.e.m., and * P<0.05, ** P<0.01 and *** P<0.001.

3.5. STIM1 is upregulated in heart failure

It was further investigated whether endogenous STIM1 levels are altered under pathological cardiac hypertrophy. In a classic model of cardiac hypertrophy mice overexpressing the ß1-adrenergic receptor (ß1-TG mice) [145], STIM1 was found to be upregulated in the 10-months old transgenic mice compared to wild-type controls (Figure 18).
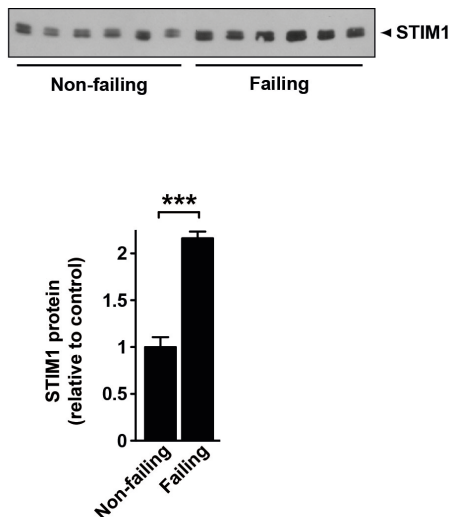
Figure 18. STIM1 is upregulated in heart failure.
Western blot analysis of STIM1 protein expression in 10-months old non-failing (wild-type) and failing (ß1-AR transgenic mice) hearts. n=6 animals per group.

3.6. Effects of *Stim1* silencing *in vivo*

Previous results indicate that STIM1 is upregulated in pathological cardiac hypertrophy *in vivo* and manipulation of *Stim1* expression in neonatal cardiomyocytes altered their growth significantly *in vitro*. Figure 11B showed that the store operated Ca^{2+}-influx was diminished in neonatal cardiomyocytes isolated from *Stim1*$^{-/-}$ mice. The majority of the mice lacking STIM1 died within few hours after birth and the surviving animals exhibited pronounced growth retardation, which is in agreement with the literature [99]. The maximal age of the mice in our colony was 4 weeks. The early mortality of these mice did not allow us to apply any cardiac disease model. Therefore, we assessed the cardiac phenotype of *Stim1*$^{-/-}$ mice compared to the wildtype controls by conducting echocardiography and also post-mortem analysis at 3 weeks of age.

Echocardiography revealed that *Stim1*$^{-/-}$ mice had normal cardiac function and dimensions (Figure 19C). There was no difference in the heart weight to body weight ratio, but *Stim1*$^{-/-}$ mice achieved only 50% of the body weight of the wildtype mice. Heart weight to tibia length ratios were significantly lower in *Stim1*$^{-/-}$ mice than wildtype littermates (Figure 19B). Although neonatal cardiomyocytes from *Stim1*$^{-/-}$ mice exhibited a diminished SOCE influx, there was no cardiac dysfunction in these mice at 3 weeks of age.
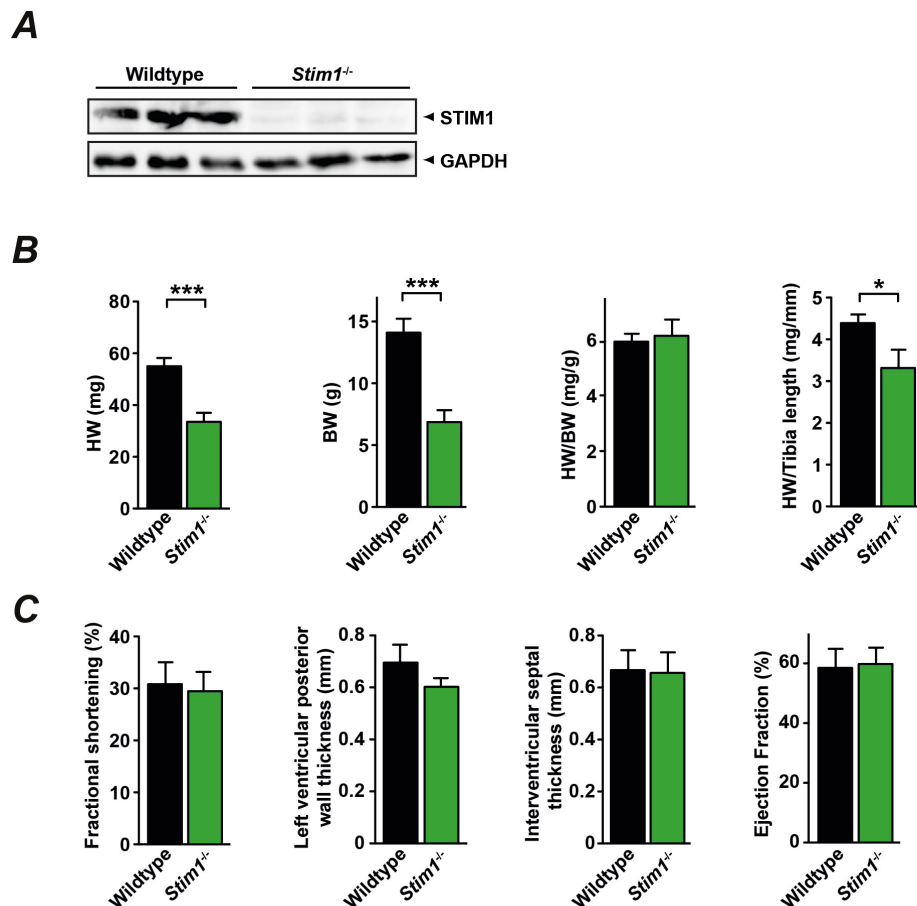
Figure 19. *Stim1*-deficient mice.
(A) Western blot detecting STIM1 in heart lysates from *Stim1*-deficient and wildtype mice. **(B)** Heart weight (HW), body weight (BW), heart weight/body weight (HW/BW) and heart weight/tibia length (HW/TL) ratios of 3-weeks old *Stim1* knockout mice. Wildtype n=9; *Stim1*$^{-/-}$ n=5. **(C)** Echocardiographic analysis on these mice. Wildtype n=6; *Stim1*$^{-/-}$ n=5. Data are mean ± s.e.m., and * P<0.05, ** P<0.01 and *** P<0.001.

The limitations posed by the *Stim1*$^{-/-}$ mice prompted us to investigate the effects of silencing endogenous *Stim1* in a disease model of cardiac hypertrophy *in vivo*. In a collaborative study with Dr. Jean-Sebastien Hulot (INSERM, Paris), the effects of adeno-associated virus (AAV)-mediated silencing of *Stim1* were studied in a rat model of pressure overload induced hypertrophy. Dr. Hulot performed these experiments and showed that *Stim1* silencing protected the rats from pressure-induced hypertrophy. The results from this study are discussed in Chapter 4 of this report.

3.7. STIM1 and its associating partners

Previous results have shown that store operated Ca^{2+}entry occurs in neonatal cardiomyocytes and in hypertrophied adult cardiomyocytes, and that STIM1 is sufficient and necessary for cardiac hypertrophy. A SOCE inhibitor, SKF96365,

significantly prevented STIM1-induced cardiomyocyte growth and also the NFAT activity in NRCMs overexpressing STIM1 (Figure 15A). This suggests that STIM1 does not confer cardiomyocyte growth by itself but requires association with other SOC partner molecules such as TRP and ORAI. It was then intended to identify the molecular components that make up the SOC complex that can interact with STIM1 under hypertrophic conditions. The interaction of STIM1 with ORAI and TRP proteins has been well studied in non-excitable cells. The influence of these proteins on STIM1-induced hypertrophy was studied by manipulating their expression in combination with STIM1 overexpressing adenoviruses.

ORAI1 is located in the plasma membrane and is a Ca^{2+}-selective ion channel that gets activated upon coupling with STIM1 on store depletion and allows for Ca^{2+} entry into the cell. In order to determine their functional importance in *Stim1*-induced hypertrophy, NRCMs were infected with adenovirus overexpressing ORAI1 at a multiplicity of infection 10 alone or in combination with STIM1 and cardiomyocyte cell size and NFAT activity were analyzed. Despite that the NFAT activity was significantly higher in cells infected with Ad-*Stim1* and Ad-*Orai1* than that of Ad-*Stim1* alone, the cell sizes of the two groups were similar. Overexpression of ORAI1 alone did not have an influence on cell size or NFAT activity and was comparable to the LACZ overexpressing controls. The loss of function of ORAI proteins in STIM1-induced hypertrophy was determined by use of adenoviruses overexpressing short hairpin RNA against ORAI1 (Ad-sh*Orai1*) *and* ORAI3 (Ad-sh*Orai3*) at a multiplicity of infection 100. Silencing ORAI1 or ORAI3 partially inhibited STIM1 induced effects on cardiomyocyte hypertrophy. This indicates that STIM1 requires ORAI proteins to confer hypertrophy on cardiac myocytes (Figure 20B).
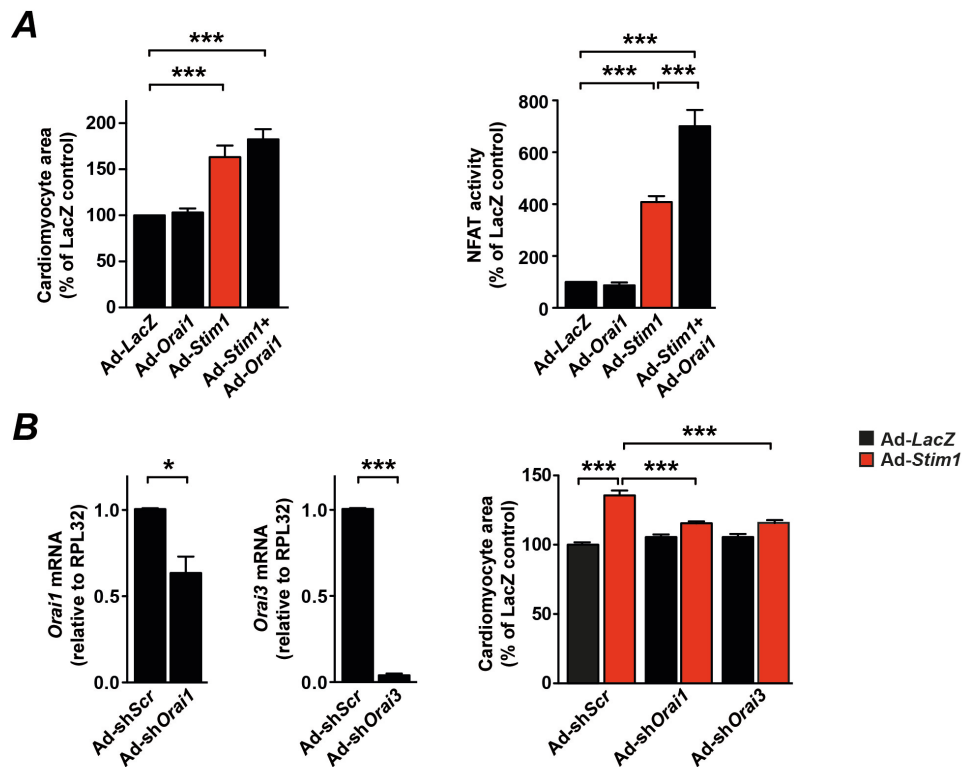
Figure 20. Role of ORAI1 in STIM1-dependent cardiomyocyte hypertrophy.
(A) Effect of ORAI1 overexpression on cardiomyocyte hypertrophy and NFAT activity. **(B)** Effects of *Orai* silencing on STIM1-dependent cardiomyocyte growth. *Left and middle*, relative expression of *Orai1* and *Orai3* in cardiomyocytes 72 hours after infection with respective adenoviral silencing vectors (Ad-sh*Orai1* and Ad-sh*Orai3*). Ad-sh*Scr* was used as control. *Right*, effects of ORAI1 silencing on STIM1-induced cardiomyocyte hypertrophy. n = 2 - 4 independent experiments with 3 replicates each. Data are mean ± s.e.m., and * P<0.05, ** P< 0.01 and *** P<0.001.

The SOC inhibitor used in this study, SKF96365, can also inhibit TRPC channels. Several studies in the literature have shown STIM1-TRPC interactions [136,137]. The physiological relevance of TRPCs in STIM1-mediated cardiomyocyte hypertrophy was investigated using an siRNA approach. There are seven isoforms of TRPC channels known in the literature – TRPC 1 to 7. TRPC-2, -5 and -7 were not investigated, as they were not detected in the heart using real-time PCR. The siRNA sequences for TRPC 1, 4 and 6 were derived from the literature whereas the sequences for TRPC3 were designed using Dharmacon siRNA design software. Specific TRPC siRNAs were purchased from Sigma Aldrich and their influence on STIM1-induced hypertrophy was investigated.

After 24 hours from seeding of the cells, NRCMs were transfected with si*Trpc1* (100 nM), si*Trpc3* (25 nM), si*Trpc4* (50 nM) and si*Trpc6* (50 nM) using lipofectamine. Concentration-matched siNeg (Sigma Aldrich) was used as respective control. 24 hours after transfection, the cells were infected with Ad-*Stim1* or Ad-*LacZ*. Medium was replaced to NRCM containing 0.1% FCS after 24 hours of infection and the cells were incubated for 48 hours before they were fixed.

Cardiomyocyte hypertrophy was then analyzed as described previously. Preliminary results showed that si*Trpc1* and si*Trpc3* significantly inhibited STIM1-dependent cardiomyocyte hypertrophy. However, si*Trpc4 and* si*Trpc6* did not prevent STIM1-mediated cardiomyocyte hypertrophy.
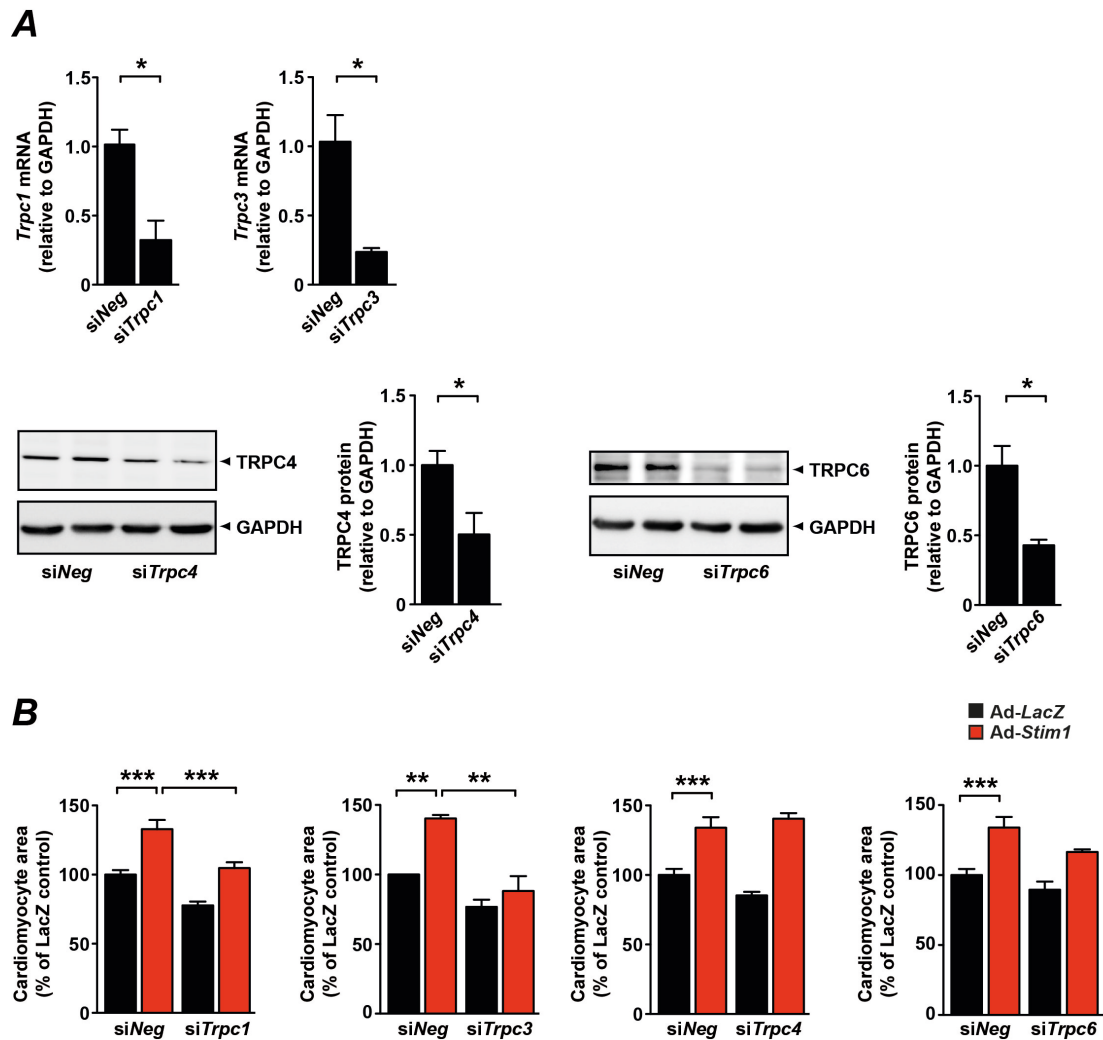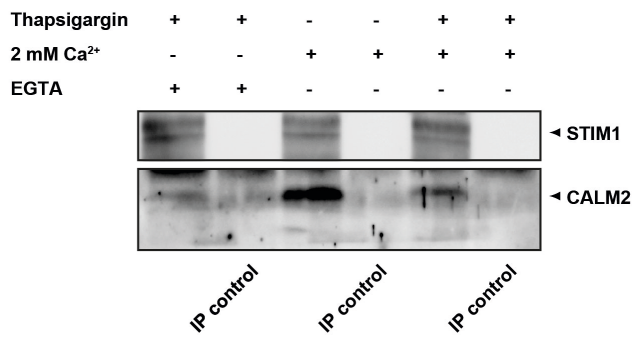

Figure 21. Effect of *Trpc* silencing in *Stim1*-dependent cardiomyocyte hypertrophy.
(A) Western blot and qPCR analysis of TRPC1, TRPC3, TRPC4 and TRPC6 in cardiomyocytes 72 hours after transfection with respective siRNA. **(B)** Effects of TRPC silencing on STIM1-induced cardiomyocyte hypertrophy. n = 2 - 3 independent experiments with 3 replicates each. Data are mean ± s.e.m., and * P<0.05, ** P< 0.01 and *** P<0.001.

The above results indicate that ORAI and TRP proteins play a crucial role in STIM1-induced cardiomyocyte hypertrophy and might form the molecular components of the SOCE. Upon coupling of STIM1 with either of these proteins, there is increase in Ca^{2+} influx and activation of NFAT that induces a pro-hypertrophic transcriptional program. The molecular mechanism that bridges the upstream Ca^{2+} influx and the downstream NFAT-induced gene transcription remains to be elucidated.

It is known that calcineurin induces NFAT translocation by dephosphorylation, and that calcineurin is activated by Ca^{2+}-CALM2 complex. Calmodulin2 is localized in regions very close to the plasma membrane and can be activated upon binding to Ca^{2+} ions entering into the cell. In order to bridge the gap existing between STIM-mediated Ca^{2+} entry and the subsequent NFAT activation, co-immunoprecipitation experiments were performed to study if there exist molecular interactions exist between the STIM1-SOCE complex that is formed at the plasma membrane and CALM2. NRCM lysates under 3 states – basal (Ca^{2+} high), store depletion (Ca^{2+} absent) and store depletion (Ca^{2+} high) – were examined for endogenous interactions of STIM1 with CALM2. Store depletion was induced using thapsigargin. The cells were lysed in IP lysis buffer and the protein concentrations were estimated using BCA assay. 300 μg of protein lysates were cleared using 50 μl 'Invitrogen' Protein-G magnetic beads and were then incubated with 2 μg of 'Sigma' Anti-STIM1 antibody overnight at 4°C. At the next day, the cell lysates were incubated with 50 μl 'Invitrogen' Protein-G magnetic beads for 3 hours at 4°C. The tubes were then placed on the Dynamag spin magnet, where the beads will migrate to the side facing the magnet facilitating easy removal of the supernatant. The immunoprecipitated STIM1 protein complex was then dissociated from the beads using 50 μl of 1X Lamelli buffer and analysed using a western blot.

It can be seen from Figure 3 that STIM1 co-immunoprecipitated CALM2 in neonatal cardiomyocytes. In the presence of high Ca^{2+} under basal conditions, CALM2 co-immunoprecipitated with STIM1. CALM2 did not co-immunoprecipitate under store depletion in the absence of Ca^{2+} but precipitated in the presence of high Ca^{2+}.

IP : Anti-STIM1 antibody

Thapsigargin	+	+	-	-	+	+
2 mM Ca²⁺	-	-	+	+	+	+
EGTA	+	+	-	-	-	-

◄ STIM1

◄ CALM2

IP control   IP control   IP control

Input

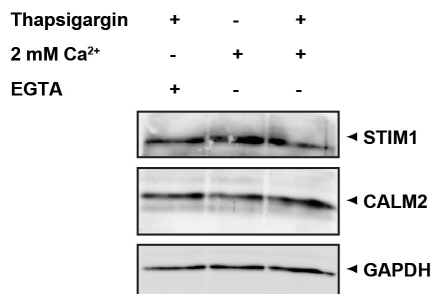| Thapsigargin | + | - | + |
| 2 mM Ca²⁺ | - | + | + |
| EGTA | + | - | - |

◄ STIM1

◄ CALM2

◄ GAPDH

Figure 22. STIM1 interacts with calmodulin.
Co-immunoprecipitation analysis of neonatal rat cardiomyocytes under basal and drug-induced store depletion in the presence and absence of 2 mM Ca²⁺. *Top*, immunoblots detecting STIM1 and calmodulin (CALM2) after immunoprecipitation with anti-STIM1 antibody. *Bottom*, immunoblots detecting STIM1, CALM2 and GAPDH on lysates used for the co-immunoprecitation experiment.

Calcineurin is the main activator of the pro-hypertrophic NFAT signalling pathway and therefore it was in our interest to investigate if STIM1 interacts with calcineurin. Co-immunoprecipitation experiments were performed on thapsigargin-treated NRCM both in the presence and absence of Ca²⁺. The NRCM lysates were immunoprecipitated with anti-STIM1 antibody and the gels were blotted for CALM2 and calcineurin B (PPP3CB), which is the small regulatory subunit B of calcineurin. In the presence of high Ca²⁺, there was increase in interaction of CALM2 and PPP3CB with STIM1.
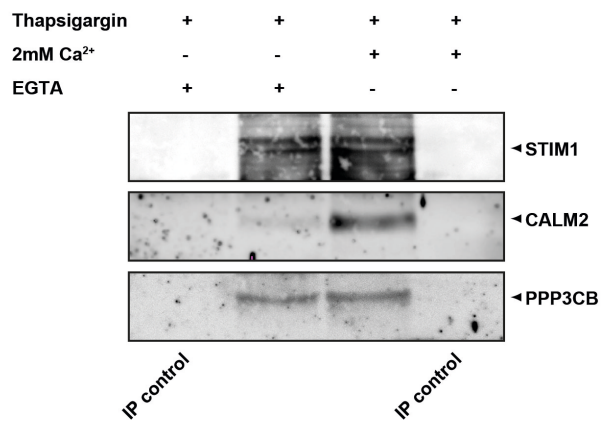
IP : Anti-STIM1 antibody

Thapsigargin	+	+	+	+
2mM Ca^{2+}	-	-	+	+
EGTA	+	+	-	-

◄STIM1
◄CALM2
◄PPP3CB

IP control   IP control

Figure 23. Increase in STIM1 interaction with CALM2 and CALN after drug-induced store depletion under high Ca^{2+}.
Co-immunoprecipitation analysis of neonatal rat cardiomyocytes under drug-induced store depletion in the presence and absence of 2mM Ca^{2+}. Immunoblots detecting STIM1, calmodulin (CALM2) and calcineurin B (PPP3CB) after immunoprecipitation with anti-STIM1 antibody.

4. Discussion

Ca^{2+} release from the endoplasmic reticulum and the subsequent influx of extracellular Ca^{2+} into the cytosol known as the store-operated Ca^{2+} entry is the major Ca^{2+} signalling pathway in non-excitable cells [62,63], and STIM1 has been identified as key regulator of SOCE [112,148]. We first analyzed the expression of *Stim1* in neonatal and adult cardiac cells – cardiomyocytes (CM) and cardiac fibroblasts (CF) that are the major cell types in the heart. *Stim1* expression was expressed approximately two-fold higher in neonatal cardiomyocytes than the adult cells. This might suggest STIM1-dependent SOC influx played a critical role in maintenance of Ca^{2+} homeostasis in perinatal hearts till the time the neonatal cells differentiated into adult cells with highly organized T-tubular structure containing voltage-gated Ca^{2+} channels and other ion channels [59]. The existence of SOCE in neonatal cardiomyocytes but not in healthy adult cells [79] would contribute to this hypothesis. Maturation of cardiomyocytes by differentiation is fundamental for proper cardiac function and Ca^{2+} homeostasis in adult cells [149,150]. Loss of *Stim1* in mice affected skeletal muscle structure and function. The mice suffered from perinatal lethality as a result of congenital myopathy despite showing normal Mendelian ratios (~25%) for *Stim1*-deficient mice. These mice displayed increased central nucleation, reduced SERCA1 and myosin heavy chain in hind limb muscles that attributes to severe muscle weakness [151]. Conditional deletion of *Stim1* in skeletal muscles showed profound growth delay, reduced myonuclear proliferation, perinatal lethality and impaired muscle differentiation [152]. *Stim1* expression in CF, which was lower than that in CM at neonatal age, was significantly increased in adult cells (Figure 10A). Cardiac fibroblasts comprise 30% of the total cell population at day 1 after birth, which then increases to about 64% at day 15. Conversely, cardiomyocytes were observed at 62% and 30% in day 1 and day 15 hearts respectively [153].
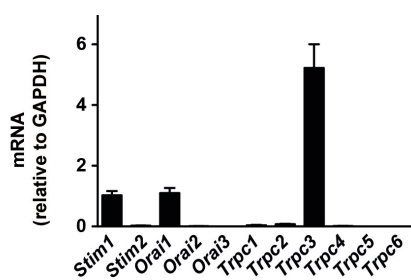

Figure 24. mRNA expression profile of *Stim*, *Orai* and *Trpc* family members in mouse heart.
Relative expression of *Stim*, *Orai* and *Trpc* family members in left ventricular lysates from adult FVB mice (n=4). Data are normalised to *Stim1* expression.

Another isoform of STIM1 known as STIM2 is also expressed in the heart (Figure 24). Due to their high structural similarity to that of STIM1 (~ 58% homology), an intriguing question that might arise here is the contribution of STIM2 to SOC-mediated influx. STIM2 overexpression completely abrogated endogenous SOCE in several cell types such as HEK, PC12, A7r5 and Jurkat T cells [100] but upon co-expression with ORAI1 resulted in large increases in SOCE [102]. Moreover, overexpression of STIM2 in *Stim1*-deficient T cells could partially restore SOCE that was initially absent [154]. However, overexpression of STIM2 increased basal Ca^{2+} levels while their endogenous inhibition lowered basal cytosolic and ER Ca^{2+} levels. Also STIM2 was present in aggregated and active state under resting conditions with full stores [102]. STIM2 formed punctae at a much faster rate than STIM1 suggesting that STIM2 is activated at partial store depletion while STIM1 is activated under extensive store depletion [102,155]. STIM1 requires about 40 seconds to translocate to ER-PM junctions and activate SOCE [90]. Taken together, STIM2 maintains basal cytosolic and ER Ca^{2+} levels and synergistically with STIM1-mediated SOCE, while STIM1 appears to be activated only upon strong receptor mediated SOC influx.

Although SOCE was identified in both neonatal and adult cardiomyocytes as early as 2002 [79,156], their physiological relevance in inducing cardiac hypertrophy and also the role of STIM1 in this Ca^{2+} influx in cardiomyocytes is not clearly understood. To address these questions, we analyzed the effects of altered STIM1 expression on SOC currents and also its cellular localization under store depletion.

4.1. STIM1 translocation leads to activation of SOCE in cardiomyocytes

The effects on SOCE currents were determined by measuring the intracellular Ca^{2+} concentration in cells upon drug-induced store depletion in Ca^{2+}-free medium followed by exogenous addition of Ca^{2+}. These currents were abrogated in the presence of SOCE inhibitors but not with L-type Ca^{2+} channel inhibitors in cardiomyocytes [79], indicating that the Ca^{2+}-influx was via the store operated route. For silencing, adenoviruses overexpressing short hairpins against *Stim1* were used. We tested three constructs out of which Ad-sh*Stim1*-2 provided maximal knockdown (data not shown). Ad-sh*Scr1* was used as control for all experiments. Overexpression of STIM1 resulted in a significant 80% increase in SOCE currents compared to LACZ control while silencing *Stim1* diminished this current in neonatal cardiomyocytes (Figure 11A). A similar approached recent study investigating the

effect of manipulated STIM1 expression on cardiomyocytes reproduced our findings [157,158].

In our experiments overexpression of STIM1 alone was sufficient to induce a significant increase in SOCE but did not require co-expression of ORAI1 for significant enhancement of SOC influx as reported in previous studies on HEK cells [73,112]. However, a study of SOCE in HeLa cells supports our data wherein STIM1 alone was sufficient for enhanced SOCE activity [159]. This was also shown using HeLa cells in the very first study that identified STIM1 as a molecular component of SOCE [69]. This can be attributed to the fact that our experiments were conducted on NRCMs and not on HEK cells that are known to have little or no endogenous SOCE due to very low amounts of endogenous ORAI1 present [160]. The presence of endogenous SOCE in neonatal cardiomyocytes or HeLa cells can be seen in cells either overexpressing LACZ (Figure 11A) or transfected with control plasmids [159], respectively. Overexpression of EYFP tagged STIM1 in HEK cells enhanced SOCE and translocation to ER-PM junction upon thapsigargin treatment [161]. Also constitutively active mutant of STIM1 generated by a mutation in the EF hand rendered constitutive localization of STIM1 in ER-PM junctions and also enhanced SOCE even when the stores were full. This suggests a STIM1-mediated and store-independent SOCE [69,161].

Conversely, silencing of *Stim1* expression diminished SOCE and was in agreement to previous studies performed on several cell types [162–166], including cardiomyocytes [167].

Cardiac fibroblasts, like the cardiomyocytes, exhibit spontaneous Ca^{2+} oscillations (30-60% of cultured cells) via LTCC, NCX, IP_3R, PMCA and SOC [168]. Although LTCC-mediated spontaneous Ca^{2+} oscillations were also observed in cardiac fibroblasts, it was not possible to completely abolish the current using the LTCC inhibitor nifedipine suggesting a lesser role for these channels [168] similar to that observed in pre-adipocyte cells [169]. Thapsigargin treatment on Ad-*LacZ* or Ad-sh*Scr* infected CFs confirmed the presence of endogenous SOCE (Figure 12B). Cardiac fibroblasts exhibited similar increases in SOCE currents upon STIM1 overexpression as cardiomyocytes but silencing *Stim1* did not affect its currents. Endogenous SOC currents were abolished in the presence of an SOCE inhibitor La^{3+} [169]. Taken together, this might suggest that either endogenous STIM1 does not significantly contribute to Ca^{2+} oscillations in CFs or that sufficient silencing of *Stim1* expression

was not achieved leading to a significant portion of STIM1 still retained in CFs for SOCE activity.

Several reports have shown that STIM1 regulates SOCE by translocating to regions very close to the plasma membrane where it interacts with its SOC partner proteins such as ORAI and TRP [69,70,115]. For the first time, this study confirmed translocation of endogenous STIM1 in neonatal cardiomyocytes upon thapsigargin-induced intracellular store depletion (Figure 13). Thapsigargin treatment redistributed STIM1 into puncta-like structures in close proximity to the plasma membrane, as reported in previous studies [96–98]. Thus STIM1 and its molecular component form channel clusters in the SR-PM junctions. Other stress factors such as oxidative stress [170] and ATP depletion [171] can influence STIM1 oligomerization and therefore CRAC activation.

In summary, it was determined that SOCE was prevalent and robust in neonatal cardiomyocytes, and that STIM1 was sufficient and necessary for SOCE activation.

4.2. STIM1 induces cardiac hypertrophy

In cardiomyocytes, Ca^{2+}-dependent signalling cascades govern muscle contraction and long-term remodelling of the heart by altering Ca^{2+}-dependent gene transcription. Our results suggest STIM1-dependent SOCE as a potential mechanism to alter Ca^{2+} in cardiomyocytes. How does this small Ca^{2+} influx mediated by SOC channels in the presence of large and rapid Ca^{2+} oscillations during excitation-contraction coupling could instigate a functional remodelling of the cardiomyocyte? How does SOCE act as a leak current to activate Ca^{2+}-calmodulin-dependent growth pathways? Which transcription factors are involved? Answers to these questions are critical to understand STIM1-dependent cardiac growth. Calmodulin is the main signal transducer for many Ca^{2+} signalling pathways including transcriptional control. A computational mathematical model predicted high Ca^{2+}-calmodulin oscillations in the dyadic clefts and very low amounts in the cytosol [172]. This is due to high buffering of Ca^{2+} at the dyadic clefts for every cycle of excitation-contraction coupling. Moreover, CamKII activity at the dyadic clefts oscillated in line with increases in local Ca^{2+} during excitation-contraction coupling but low Ca^{2+}-calmodulin levels prevented their activity in the cytosol. Calcineurin activity, a main regulator of cardiac hypertrophy, was found at saturated levels both at the dyadic clefts and cytosol under normal low frequency oscillations (1 Hz) but increased under high frequency oscillations [172].

Agonists binding to G protein-coupled receptors (G_q) on the plasma membrane initiate IP_3-induced SR store depletion, thereby leading STIM1 translocation and SOCE activation. It gives rise to transient oscillations in cytosolic Ca^{2+} that provide long-term signals for cell maintenance without triggering the toxic effects of prolonged Ca^{2+} increases [173]. Therefore, a coordinated function of SR Ca^{2+} release and SOCE activation is crucial to produce cytosolic oscillations and control transcription [173,174].

SOCE contributes only a small fraction of global Ca^{2+}, typically inducing a local subplasmalemmal Ca^{2+} rise. This local contribution of SOCE to Ca^{2+} oscillations is critical for transcriptional control [175]. Despite mast cells showing similar leukotriene C4-induced Ca^{2+} oscillations both in the presence or absence of SOCE blockers, only transient stimulation of thapsigargin for 4 min resulted in increased transcription *c-fos* gene while absence of SOCE blocker failed to induce a *c-fos* expression [176]. In another study, mutant lymphocytes with defective CRAC channel activity showed close correlation between the severities of CRAC defect, Ca^{2+} influx and Ca^{2+}-dependent gene transcription [177]. This implicates that the local Ca^{2+} contribution by SOCE is crucial for transcriptional regulation and long-term cellular responses.

A sustained increase in Ca^{2+} oscillations is essential for initiation of a hypertrophic stimulus in cardiomyocytes [178]. Dolmetsch *et al* [179] observed that amplitude and duration of Ca^{2+} oscillations determined differential activation of pro-inflammatory transcription factors – NFAT, NFkB and JNK. NFkB and JNK required large Ca^{2+} transients for activation while NFAT could be activated by low sustained Ca^{2+} plateau. Ca^{2+} oscillations effectively reduced Ca^{2+} thresholds required for activation of transcription factors thereby increasing signal sensitivities also under low stimulations. Rapid oscillations are required for effective activation of the transcription factor NFAT [180].

Among all the Ca^{2+}-dependent signalling pathways involved in cardiac hypertrophy, the CALM2-mediated PPP3CA-NFAT pathway is the most important. Overexpression of either CALM or PPP3CA in the heart resulted in cardiac hypertrophy in mice, although the mechanism of CALM overexpression involved the PPP3CA pathway [181,182]. Prolonged increases in the frequency of Ca^{2+} oscillations were sufficient to activate NFAT translocation leading to a hypertrophic stimulus [178]. Stimulation of cardiomyocytes either with angiotensin, aldosterone, norepinephrine or pacing at low frequency of 2 Hz resulted in sustained increase in frequency of

spontaneous Ca^{2+} transients followed by NFAT translocation and hypertrophy. Using a PPP3CA inhibitor, cyclosporine, NFAT translocation and hypertrophy was inhibited even in the presence of high Ca^{2+} transients [178]. Imbalances in the shifts between dephosphorylated and phosphorylated NFAT induced by sustained local Ca^{2+} concentrations leads to NFAT translocation into the nucleus and hypertrophy. Consistent with these reports, overexpression of STIM1 in neonatal cardiomyocytes enhanced NFAT activation by dephosphorylation followed by increased ANF expression leading to cardiomyocyte hypertrophy (Figure 15 and 16). Atrial natriuretic factor (ANF) is a well-characterized cardiac hypertrophy marker [183]. Conversely, reciprocal effects were observed upon silencing *Stim1* (Figure 17). Two independent groups also obtained similar results on the role of STIM1 on cardiomyocyte hypertrophy [157,158].

In support to STIM1 mediating cardiac hypertrophy, endogenous levels of STIM1 are increased in several heart failure models such as ß1-adrenergic receptor transgenic mice (Figure 18) and pressure overload induced cardiac hypertrophy [184].

4.3. Silencing *Stim1* prevents pressure overload-induced cardiac hypertrophy
Stim1-deficient mice mostly died perinatally while the ones that survived suffered from pronounced growth retardation and enlargement of the spleen [99]. The mice displayed decreased heart weights, diminished SOCE but did not display any cardiac dysfunction at three weeks of age (Figure 19). This was consistent with findings from Stiber *et al* where *Stim1*-deficient mice suffered from perinatal lethality, and the skeletal muscle was characterized by diminished SOC and skeletal myopathy [151]. In human patients, lack of STIM1 expression was characterized by immunodeficiency and congenital myopathy [185]. Targeted deletion of *Stim1* in smooth muscle cells displayed defects in muscle development and contractility as a result of reduced SOCE [186]. Smooth muscle targeted *Stim1* knockout mice displayed high mortality (about 50% at day 30) while perinatal lethality was observed in *Stim1-Stim2* double knockout mice. This indicates a partial rescue of SOCE by *Stim2* in the absence of *Stim1*. Conditional deletion of *Stim1* in skeletal muscles resulted in growth delay, myonuclear proliferation, perinatal lethality and contractile dysfunction [152]. Although the mice displayed normal excitation-contraction coupling, it was not able to withstand neurohormonal agonist stimulations. *Stim1*-deficient myocytes displayed reduced SR Ca^{2+} content and alterations in proteins that regulate SERCA such as upregulation of an endogenous

SERCA inhibitor, sarcolipin. Sarcolipin was found to be highly expressed in neonates of skeletal muscle targeted *Stim1* knockout mice resulting in reduced SR Ca^{2+} content and decreased SOCE activity [187]. This indicates that STIM1 is required for the hypertrophic growth and differentiation of neonatal skeletal muscle cells. The maximal age of the whole animal *Stim1*^{-/-} mice was about 4 weeks and did not facilitate external induction of heart failure either by agonist stimulation or transverse aortic constriction. Therefore, an inducible-targeted deletion of *Stim1* in cardiomyocytes will provide a better tool to investigate their role in pathological cardiac remodelling.

It was previously described that STIM1 was upregulated in heart failure (Figure 18) as a result of re-entry of SOCE activity under pathological conditions in an adult heart [184]. In order to investigate the effects of silencing *Stim1* on cardiac hypertrophy *in vivo*, a cardiotrophic adeno-associated virus of serotype 9 (AAV9) [188] encoding a short hairpin RNA against *Stim1* (AAV9-sh*Stim1*) were injected into a rat model of pressure overload-induced hypertrophy (Figure 25).
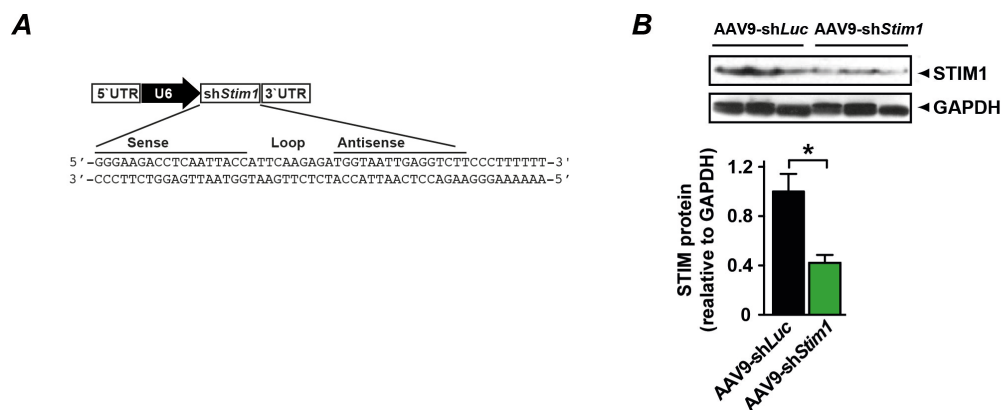

Figure 25. Generation of AAV9-sh*Stim1* vector.
(A) Scheme of AAV9 vector containing short hairpin RNA against *Stim1* (AAV9-sh*Stim1*). **(B)** Western blot analysis on AAV9-sh*Stim1* and AAV9-sh*Luc* treated rats. Data are mean ± s.e.m., and * P<0.05, ** P<0.01 and *** P<0.001. Data are from JS Hulot.

Reduced *Stim1* expression after AAV9-sh*Stim1* injection prevented cardiac hypertrophy (Figure 26B) and myocardial fibrosis (Figure 26D). In agreement with the results from 2 independent groups [158,167], reducing *Stim1* expression interfered with the response of cardiomyocytes to prohypertrophic receptor agonists by preventing SOCE that re-entered in hypertrophic cardiomyocytes [184].
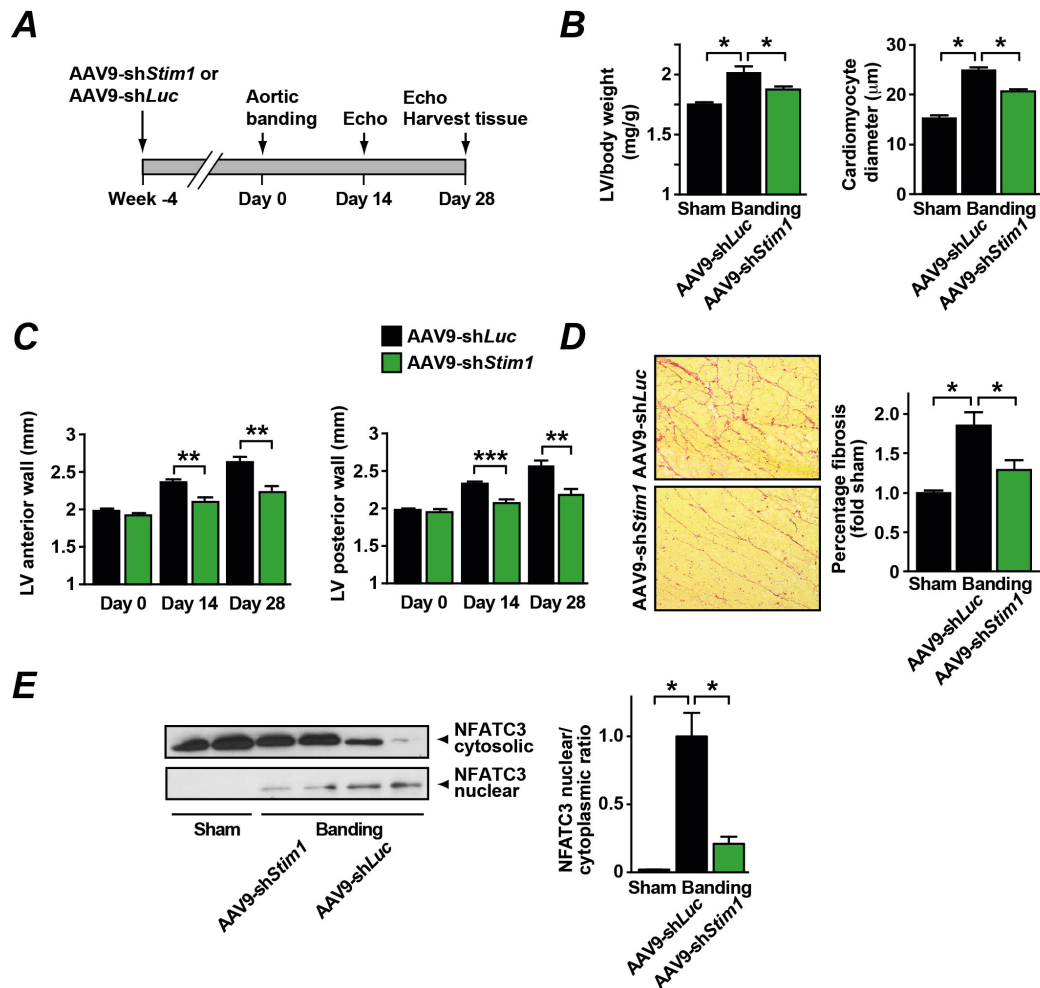
Figure 26. Silencing *Stim1* protects rats from pressure overload-induced hypertrophy.
(A) Experimental strategy of silencing *Stim1* in a rat model of heart failure. **(B)** Left ventricular weight/body weight ratio of AAV9-sh*Stim1* and AAV9-sh*Luc* treated rats (n=8 per group). Average cardiomyocyte diameter in each group (>20 cells per animal; n=4 animals per group). **(C)** Echocardiographic analysis on the mice at 2 weeks and 4 weeks after surgery (n=8 animals per group). **(D)** Sirius red staining for interstitial fibrosis in left ventricular section of the hearts (n=5 animals per group). **(E)** Quantitative analysis of NFAT in subcellular fractions by immunoblot analysis. Data are mean ± s.e.m., and * P<0.05, ** P<0.01 and *** P<0.001. Data are from JS Hulot.

4.4. STIM1-mediated gating of ORAI and TRP channels

Several reports have identified ORAI1 as the as the other functional component of SOC [79,124,158,167]. The interaction of STIM1 with ORAI, not only induces the opening of the SOC channels but also increases the Ca^{2+} selectivity of the channel [189]. The formation of the junctional complexes between STIM1 and ORAI is crucial for the local Ca^{2+} environment in the cell. Store depletion influences STIM1, ORAI1 and LTCC channels within the same junctional complex wherein STIM1 reciprocally regulates these channels [190]. Also STIM1 influences ORAI1 turnover by insertion and retention in the junctional complexes while facilitating internalization of the LTCC channels.

The coupling of STIM1-ORAI1 is a steady-state event influenced by the local Ca^{2+} environment. Ca^{2+} present in the junctional space provides a strong feedback

control on STIM1-ORAI1 coupling. Similar to how the SR store depletion initiates SOCE, the SR refilling is essential for its deactivation. Increased ER luminal Ca^{2+} levels is the sole mechanism that mediates disaggregation of STIM1 [191].

Apart from ORAI1, ORAI3 has been known to be involved in SOCE but the contribution of ORAI2 to SOCE is not clear. In the absence of ORAI1, ORAI3 but not ORAI2 could mimic ORAI1 [103,111]. Also, gating of ORAI3 channels by STIM1 has been shown in HEK293 cells [192]. In our study, silencing either *Orai1* or *Orai3*, partially but significantly, decreased STIM1-induced cardiomyocyte hypertrophy suggesting a possible interaction between STIM1 and the ORAI1/3 channels (Figure 20B). However, Ad-sh*Orai1* decreased *Orai3* by 50% while Ad-sh*Orai3* decreased *Orai1* mRNA levels by 20% (data not shown). Voelkers *et al* [158] observed that silencing *Orai1* and not *Stim1* could diminish SOCE and decrease cardiomyocyte hypertrophy even under basal conditions. In contrast, our results showed that *Orai1* knockdown alone did not have an effect on SOCE or cardiac cell size (Figure 11A, 17 and 20B). This implicates STIM1 as the major molecular component of the SOC channel. However, partial inhibition of cardiomyocyte hypertrophy after *Orai* silencing suggests a possible involvement of other channel proteins in the formation of SOC complex.

Before the discovery of STIM1 and ORAI1, TRPC channels were thought to function as store-operated channels. However, their role in SOCE is highly controversial. TRPCs are non-selective cation channels with properties distinct from those of Ca^{2+}-selective CRAC currents. Therefore, ORAI channels that exhibit high selectivity to Ca^{2+} can be cited as strong evidence that ORAI1 is the partner of STIM1. Whereas most studies implicate STIM1-induced activation of TRPCs [193–195], other reports provide a strong evidence contradicting this hypothesis [190,196].

STIM1 regulates most of TRPC proteins either directly (TRPC 1/4/5) or indirectly (TRPC 3/6), and all TRPC channels are implicated in SOCE activation [193–195]. Based on their expression in the heart (Figure 24) and their relevance in SOCE, we identified TRPC1, TRPC3, TRPC4 and TRPC6 for siRNA knockdown approach. Knocking down endogenous *Trpc1* and *Trpc6* partially prevented STIM1-induced hypertrophy but that of *Trpc3* completely prevented this effect (Figure 21B). Silencing *Trpc4* did not have any effect of cardiomyocyte hypertrophy. *Trpc1*, *Trpc3* and *Trpc6* have been identified to contain conserved NFAT consensus sequences in their promoters. Thapsigargin treatment in the presence of high Ca^{2+} resulted in upregulation of TRPC1 and TRPC3 in cardiomyocytes [197,198] and also in vascular

smooth muscle cells [199] in a PPP3CA-NFAT-dependent manner. Absence of extracellular Ca^{2+} prevented this upregulation of the genes.

It is interesting that silencing *Orai1*, *Orai3*, *Trpc1* or *Trpc3* prevented STIM1-induced hypertrophy. This reveals important aspects on interdependence of these channels with each other. STIM1 enhanced heteromultimerization of TRPC1 with TRPC3 and TRPC4 with TRPC6 [137]. Expression of ORAI1 in stably expressing TRPC3 and TRPC6 HEK cells increased SOCE significantly indicating interaction and requirement of a functional ORAI1 channel [138]. Expression of ORAI1 together with TRPC1 evoked significant SOCE activation while individual expression did not show any effect [200]. Thapsigargin treatment resulted in enhancement of Co-IP of expressed ORAI1-STIM1-TRPC3-IP_3R1 in which TRPC3 played a central role mediating the interaction of ORAI1 and IP_3R in HEK293 cells [201]. This clearly indicates interdependence between STIM, ORAI and TRP proteins for effective SOCE activation. In summary, a functional ORAI is required for SOCE activation involving TRPC1 and TRPC3.

Recent reports on LTCC and SOCE gating have revealed that they are reciprocally regulated. STIM1 inhibited Ca^{2+} entry via LTCC gating and caused long-term internalization of these channels [202], and reciprocally regulated ORAI1 channels [190]. This finding links the two major Ca^{2+} signalling pathways in both excitable and non-excitable cells together which to this date was thought to act independently. This raises questions whether LTCC-mediated Ca^{2+} entry was also involved in the pro-hypertrophic induction by STIM1. It was previously reported that use of LTCC inhibitor protected the hearts from cardiomyopathy [203]. Pro-hypertrophic signalling of STIM1, despite the inhibition of LTCC gating, significantly attributes the increase in cytosolic Ca^{2+} and hypertrophy to SOC-mediated Ca^{2+} influx.

4.5. STIM1 interacts with calmodulin and calcineurin

In CoIP experiments, STIM1 demonstrated high affinity binding to CALM2 in the presence of high Ca^{2+} (Figure 22). The polybasic tails of the STIM proteins, STIM1 and STIM2, are rich in basic and hydrophobic residues as observed in other calmodulin binding motifs. Using isothermal titration chemistry, it has been shown that the polybasic C-terminal end of both STIM1 and STIM2 bind to calmodulin in a Ca^{2+}-dependent manner [204,205]. Binding affinity of STIM1 to calmodulin was greatly reduced in the absence of Ca^{2+}. Although a short polybasic tail of human STIM1 (amino acid 667 -685) was demonstrated to have high affinity for CALM binding in

the presence of Ca^{2+} [204], homology searches between STIM1 polybasic tail and calmodulin target proteins did not find a match. Therefore, it can either be that STIM1 has a novel calmodulin binding site or an indirect interaction through one of its SOC partner proteins such as ORAI [206] and TRPC [193–195,207,208]. Co-immunoprecipitation experiments on STIM1 mutants carrying mutations at the calmodulin binding sites or live-cell FRET imaging experiments between STIM1 and CALM could help to better understand their interactions.

Meanwhile, Mullins *et al* identified a region in the N-terminal end of ORAI1 that binds to calmodulin in a Ca^{2+}-dependent manner facilitating CDI [206]. At high Ca^{2+}, overexpression of Ca^{2+}-insensitive CALM mutants inhibited the fast inactivation of the SOC channels [206]. A recent report indicates that the two lobes of CALM can bind to N- and C-terminal ends of two adjacent ORAI1 proteins [209]. ORAI1 thus exists as dimer at resting state but forms a tetramer upon SOCE activation [107]. For SOCE activation, STIM1 interacts with both the N- and C-terminal ends of ORAI1 [74]. Increase in SOC influx results in a high pool of activated local Ca^{2+}-CALM around the STIM1-ORAI1 SOC channel. High affinity C-terminal lobe of CALM first interacts with an ORAI1 protein of one dimer followed by interaction of N-terminal end of CALM with the neighbouring ORAI1 of the second dimer, thereby displacing STIM1 from the SOC complex and inactivating the channel [209]. Also interaction of Ca^{2+}-CALM with TRP proteins resulted in conformational changes resulting in blockade of the current [194]. Also inhibition of CALM by calmidazolium enhanced SOCE suggesting that CALM is involved in Ca^{2+}-dependent inactivation of STIM1-SOC [210]. Parvez *et al* [101] demonstrated that Ca^{2+}-bound CALM and not apoCALM was able to inhibit STIM2-mediated Ca^{2+} currents at high intracellular Ca^{2+} levels. This in agreement with our finding that STIM1 co-immunoprecipitated CALM2 only in the presence of high Ca^{2+} influx, indicating a fully functional SOC channel.

In this report it has been shown that CALM2 binding to STIM1 increased under store depletion at high Ca^{2+} (Figure 22) which in turn also increased PPP3CB tethering to STIM1 (Figure 23). PPP3CB was anchored to STIM1 also under basal conditions, but SOCE activation and increased CALM2 binding to STIM1 could trigger the downstream NFAT signalling pathway. This mechanism might be similar to LTCC facilitation wherein local Ca^{2+} signals and a high local pool of CALM could activate PPP3CA tethered to the channel leading to LTCC facilitation [211,212].

4.6. Conclusion

In conclusion, this is the first report showing translocation of endogenous STIM1 in neonatal rat cardiomyocytes from a diffused state in the ER to distinct puncta at ER-PM junctions after store depletion. Overexpression of STIM1 resulted in increased SOC influx and cardiomyocyte cell size in a PPP3CA-NFAT dependent manner thereby suggesting the involvement of SOCE in cardiac remodelling. Conversely, silencing *Stim1* prevented phenylephrine-induced cardiomyocyte hypertrophy *in vitro* and pressure overload-induced hypertrophy *in vivo*. Our results confirm that STIM1 either directly interacts or forms a heteromultimeric SOC complex involving ORAI1, ORAI3, TRPC1 and TRPC3 proteins. Taken together, our results implicate an important role for STIM1 in cardiomyocyte hypertrophy and also suggest a new therapeutic entry point for cardiac disease (Figure 27).
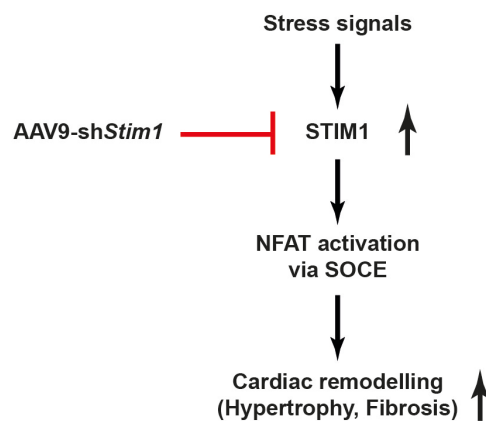
Figure 27. Proposed mechanism underlying NFAT-mediated cardiac remodelling through STIM1.

5. Summary / Zusammenfassung

Ca^{2+} is the ubiquitous second messenger that not only modulates excitation-contraction coupling in cardiomyocytes, but is also an important trigger for transcriptional activation during pathological cardiac remodelling. Store-operated Ca^{2+} entry is a potential route regulating Ca^{2+} trafficking in cardiomyocytes through stromal interaction molecule 1 (STIM1), a Ca^{2+} sensor protein in the SR membrane that is capable of triggering SOCE. In this study we investigated whether STIM1 is involved in cardiac remodelling both *in vitro* and *in vivo*.

Consistent with earlier reports, we observed that drug-inducible SOCE was abundant and robust in neonatal rat cardiomyocytes, and largely depended on STIM1. To investigate the effect of STIM1 on SOCE and cardiomyocyte hypertrophy, we manipulated its expression in neonatal cardiomyocytes using adenoviruses either overexpressing STIM1 or a short hairpin against *Stim1*. Levels of STIM1 correlated directly with the amplitude of SOC-mediated Ca^{2+} influx and cardiac cell size. In agreement with SOCE activation, endogenous STIM1 proteins translocated to ER-PM junctions upon drug-induced store depletion. Although STIM1-mediated SOCE was absent in adult cardiomyocytes, it re-entered in cardiac disease. Adeno-associated virus mediated silencing of *Stim1* protected rats from pressure overload induced cardiac hypertrophy suggesting that STIM1 is critical for cardiomyocyte hypertrophy both *in vitro* and *in vivo*.

Our results show that STIM1 promotes cardiomyocyte hypertrophy by interacting with calmodulin and calcineurin and triggering NFAT-mediated transcriptional activation of prohypertrophic genes. A siRNA-based approach identified ORAI1, ORAI3, TRPC1 and TRPC3 to be involved in STIM1-induced cardiac hypertrophy. In summary, our findings suggest that STIM1 promotes cardiac hypertrophy via the calcineurin-NFAT pathway by forming a heteromultimeric SOC complex involving ORAI1, ORAI3, TRPC1 and TRPC3. STIM1 was both sufficient and necessary for cardiomyocyte hypertrophy and provides a new therapeutic entry point for cardiac disease.

Calcium (Ca^{2+}) ist ein ubiquitär vorkommender sekundärer Botenstoff, der nicht nur die elektromechanische Kopplung in Kardiomyozyten moduliert, sondern auch die Transkriptionsaktivität in Herzmuskelzellen reguliert. Ein Weg, über den Ca^{2+} in Kardiomyozyten gelangt, ist der speicherabhängige Ca^{2+}-Einstrom (store-operated Ca^{2+} entry, SOCE), der durch den Calciumsensor STIM1 (stromal interaction molecule 1) in der Membran des sarkoplasmatischen Retikulums getriggert wird. Im Rahmen dieser Arbeit wurde die Rolle von STIM1 bei kardialen Umbauprozessen *in vitro* und *in vivo* analysiert.

Wie in früheren Veröffentlichungen beschrieben, konnten auch wir stimulationsabhängig SOCE in neonatalen Rattenkardiomyozyten nachweisen. Eine zentrale Rolle für diesen Ca^{2+}-Strom spielte STIM1. Wie für Aktivierung des SOCE typisch formierte sich endogenes STIM1 nach agonistinduzierter Speicherleerung in ER-PM-Verbindungspunkten. Während in adulten Kardiomyozyten kein STIM1-vermittelter SOCE beobachtbar war, wurde er bei kardialen Erkrankungen re-initiiert. Um den Einfluss von STIM1 auf den SOCE sowie auf das hypertrophe Wachstum von Kardiomyozyten zu untersuchen, wurde das Protein in neonatalen Kardiomyozyten durch Infektion mit *Stim1*-kodierendem Adenovirus überexprimiert. Das Expressionsniveau von STIM1 korrelierte direkt mit der Amplitude des SOCE und der Größe der Herzmuskelzellen. Umgekehrt waren Ratten durch Herabregulation von endogenem STIM1 (durch Applikation von adenoassoziiertem Virus, der ein *Stim1*-shRNA-Konstrukt exprimierte) von Aortenkonstriktion-induzierter Kardiomyozytenhypertrophie geschützt. Somit scheint STIM1 sowohl *in vitro* als auch *in vivo* ein zentraler Faktor für die Hypertrophieentwicklung zu sein.

STIM1 fördert Kardiomyozytenhypertrophie, indem es mit Calmodulin und Calcineurin interagiert und damit über NFAT-Aktivierung die Transkription prohypertropher Gene aktiviert. Mittels eines siRNA-basierten Ansatzes konnten ORAI1, ORAI3, TRPC1 und TRPC3 als weitere Proteine identifiziert werden, die bei einer STIM1-induzierten Hypertrophie eine Rolle spielen.

Zusammenfassend lassen unsere Daten darauf schließen, dass STIM1 Kardiomyozytenhypertrophie durch Aktivierung des Calcineurin-NFAT-Signalwegs fördert. Dabei bildet STIM1 einen heteromultimeren SOC-Komplex mit ORAI1, ORAI3, TRPC1 und TRPC3. STIM1 erwies sich sowohl als hinreichend als auch als notwendig für das Entstehen kardialer Hypertrophie und könnte damit einen neuen Angriffspunkt für die Therapie von Herzerkrankungen darstellen.

6. Bibliography

1. Swynghedauw, B. Molecular mechanisms of myocardial remodeling. *Physiological reviews* **79**, 215–62 (1999).

2. Kang, P. M. & Izumo, S. Apoptosis in heart: basic mechanisms and implications in cardiovascular diseases. *Trends in molecular medicine* **9**, 177–82 (2003).

3. Krayenbuehl, H. P. *et al.* Left ventricular myocardial structure in aortic valve disease before, intermediate, and late after aortic valve replacement. *Circulation* **79**, 744–55 (1989).

4. Heineke, J. & Molkentin, J. D. Regulation of cardiac hypertrophy by intracellular signalling pathways. *Nature reviews. Molecular cell biology* **7**, 589–600 (2006).

5. Bers, D. M. Calcium cycling and signaling in cardiac myocytes. *Annual review of physiology* **70**, 23–49 (2008).

6. Solaro, R. J. & Rarick, H. M. Troponin and tropomyosin: proteins that switch on and tune in the activity of cardiac myofilaments. *Circulation research* **83**, 471–80 (1998).

7. Hove-Madsen, L. & Bers, D. M. Sarcoplasmic reticulum Ca2+ uptake and thapsigargin sensitivity in permeabilized rabbit and rat ventricular myocytes. *Circulation research* **73**, 820–8 (1993).

8. Li, L., Chu, G., Kranias, E. G. & Bers, D. M. Cardiac myocyte calcium transport in phospholamban knockout mouse: relaxation and endogenous CaMKII effects. *The American journal of physiology* **274**, H1335–47 (1998).

9. Bassani, J. W., Bassani, R. A. & Bers, D. M. Relaxation in rabbit and rat cardiac cells: species-dependent differences in cellular mechanisms. *The Journal of physiology* **476**, 279–93 (1994).

10. Bers, D. M. Calcium Fluxes Involved in Control of Cardiac Myocyte Contraction. *Circulation Research* **87**, 275–281 (2000).

11. Guatimosim, S. *et al.* Local Ca(2+) signaling and EC coupling in heart: Ca(2+) sparks and the regulation of the [Ca(2+)](i) transient. *Journal of molecular and cellular cardiology* **34**, 941–50 (2002).

12. Langer, G. A. & Peskoff, A. Calcium concentration and movement in the diadic cleft space of the cardiac ventricular cell. *Biophysical journal* **70**, 1169–82 (1996).

13. Sipido, K. R., Callewaert, G. & Carmeliet, E. Inhibition and rapid recovery of Ca2+ current during Ca2+ release from sarcoplasmic reticulum in guinea pig ventricular myocytes. *Circulation research* **76**, 102–9 (1995).

14. Peterson, B. Z., DeMaria, C. D., Adelman, J. P. & Yue, D. T. Calmodulin is the Ca2+ sensor for Ca2+ -dependent inactivation of L-type calcium channels. *Neuron* **22**, 549–58 (1999).

15. Somlyo, A. V & Somlyo, A. P. Electromechanical and pharmacomechanical coupling in vascular smooth muscle. *The Journal of pharmacology and experimental therapeutics* **159**, 129–45 (1968).

16. Bolton, T. B. Mechanisms of action of transmitters and other substances on smooth muscle. *Physiological reviews* **59**, 606–718 (1979).

17. Berridge, M. J., Bootman, M. D. & Roderick, H. L. Calcium signalling: dynamics, homeostasis and remodelling. *Nature reviews. Molecular cell biology* **4**, 517–29 (2003).

18. Komori, S. & Bolton, T. B. Calcium release induced by inositol 1,4,5-trisphosphate in single rabbit intestinal smooth muscle cells. *The Journal of physiology* **433**, 495–517 (1991).

19. Pacaud, P. & Bolton, T. B. Relation between muscarinic receptor cationic current and internal calcium in guinea-pig jejunal smooth muscle cells. *The Journal of physiology* **441**, 477–99 (1991).

20. Poggioli, J., Sulpice, J. C. & Vassort, G. Inositol phosphate production following alpha 1-adrenergic, muscarinic or electrical stimulation in isolated rat heart. *FEBS letters* **206**, 292–8 (1986).

21. Gambassi, G., Spurgeon, H. A., Ziman, B. D., Lakatta, E. G. & Capogrossi, M. C. Opposing effects of alpha 1-adrenergic receptor subtypes on Ca2+ and pH homeostasis in rat cardiac myocytes. *The American journal of physiology* **274**, H1152–62 (1998).

22. Bootman, M. D. & Lipp, P. Ringing changes to the "bell-shaped curve". *Current biology : CB* **9**, R876–8 (1999).

23. Bootman, M. D., Lipp, P. & Berridge, M. J. The organisation and functions of local Ca(2+) signals. *Journal of cell science* **114**, 2213–22 (2001).

24. Rodriguez, P. & Kranias, E. G. Phospholamban: a key determinant of cardiac function and dysfunction. *Archives des maladies du coeur et des vaisseaux* **98**, 1239–43 (2005).

25. Yano, K. & Zarain-Herzberg, A. Sarcoplasmic reticulum calsequestrins: structural and functional properties. *Molecular and cellular biochemistry* **135**, 61–70 (1994).

26. Bassani, J. W., Yuan, W. & Bers, D. M. Fractional SR Ca release is regulated by trigger Ca and SR Ca content in cardiac myocytes. *The American journal of physiology* **268**, C1313–9 (1995).

27. Rahamimoff, H. Na(+)-Ca2+ exchanger: the elusive protein. *Current topics in cellular regulation* **31**, 241–71 (1990).

28. Bers, D. M., Barry, W. H. & Despa, S. Intracellular Na+ regulation in cardiac myocytes. *Cardiovascular research* **57**, 897–912 (2003).

29. Litwin, S. E., Li, J. & Bridge, J. H. Na-Ca exchange and the trigger for sarcoplasmic reticulum Ca release: studies in adult rabbit ventricular myocytes. *Biophysical journal* **75**, 359–71 (1998).

30. Goldhaber, J. I. & Philipson, K. D. Cardiac sodium-calcium exchange and efficient excitation-contraction coupling: implications for heart disease. *Advances in experimental medicine and biology* **961**, 355–64 (2013).

31. Zhao, X. L., Gutierrez, L. M., Chang, C. F. & Hosey, M. M. The alpha 1-subunit of skeletal muscle L-type Ca channels is the key target for regulation by A-kinase and protein phosphatase-1C. *Biochemical and biophysical research communications* **198**, 166–73 (1994).

32. Marx, S. O. *et al.* PKA phosphorylation dissociates FKBP12.6 from the calcium release channel (ryanodine receptor): defective regulation in failing hearts. *Cell* **101**, 365–76 (2000).

33. Zhang, R., Zhao, J. & Potter, J. D. Phosphorylation of both serine residues in cardiac troponin I is required to decrease the Ca2+ affinity of cardiac troponin C. *The Journal of biological chemistry* **270**, 30773–80 (1995).

34. Gautel, M., Zuffardi, O., Freiburg, A. & Labeit, S. Phosphorylation switches specific for the cardiac isoform of myosin binding protein-C: a modulator of cardiac contraction? *The EMBO journal* **14**, 1952–60 (1995).

35. Tada, M. & Toyofuku, T. SR Ca(2+)-ATPase/phospholamban in cardiomyocyte function. *Journal of cardiac failure* **2**, S77–85 (1996).

36. Babu, Y. S., Bugg, C. E. & Cook, W. J. Structure of calmodulin refined at 2.2 A resolution. *Journal of molecular biology* **204**, 191–204 (1988).

37. Black, D. J., Leonard, J. & Persechini, A. Biphasic Ca2+-dependent switching in a calmodulin-IQ domain complex. *Biochemistry* **45**, 6987–95 (2006).

38. Stemmer, P. M. & Klee, C. B. Dual calcium ion regulation of calcineurin by calmodulin and calcineurin B. *Biochemistry* **33**, 6859–66 (1994).

39. Maier, L. S. *et al.* Dynamic changes in free Ca-calmodulin levels in adult cardiac myocytes. *Journal of molecular and cellular cardiology* **41**, 451–8 (2006).

40. Wu, X. & Bers, D. M. Free and bound intracellular calmodulin measurements in cardiac myocytes. *Cell calcium* **41**, 353–64 (2007).

41.   Alseikhan, B. A., DeMaria, C. D., Colecraft, H. M. & Yue, D. T. Engineered calmodulins reveal the unexpected eminence of Ca2+ channel inactivation in controlling heart excitation. *Proceedings of the National Academy of Sciences of the United States of America* **99**, 17185–90 (2002).

42.   Yamaguchi, N., Xu, L., Pasek, D. A., Evans, K. E. & Meissner, G. Molecular basis of calmodulin binding to cardiac muscle Ca(2+) release channel (ryanodine receptor). *The Journal of biological chemistry* **278**, 23480–6 (2003).

43.   Yuan, W. & Bers, D. M. Ca-dependent facilitation of cardiac Ca current is due to Ca-calmodulin-dependent protein kinase. *The American journal of physiology* **267**, H982–93 (1994).

44.   Wehrens, X. H. T., Lehnart, S. E., Reiken, S. R. & Marks, A. R. Ca2+/calmodulin-dependent protein kinase II phosphorylation regulates the cardiac ryanodine receptor. *Circulation research* **94**, e61–70 (2004).

45.   Dolmetsch, R. E., Lewis, R. S., Goodnow, C. C. & Healy, J. I. Dolmetsch_Diff activtn of TF by ca transients_Nat 1997.pdf.

46.   Klee, C. B., Ren, H. & Wang, X. Regulation of the calmodulin-stimulated protein phosphatase, calcineurin. *The Journal of biological chemistry* **273**, 13367–70 (1998).

47.   Aitken, A., Klee, C. B. & Cohen, P. The structure of the B subunit of calcineurin. *European journal of biochemistry / FEBS* **139**, 663–71 (1984).

48.   Anglister, J. *et al.* 1H, 13C, 15N nuclear magnetic resonance backbone assignments and secondary structure of human calcineurin B. *Biochemistry* **33**, 3540–7 (1994).

49.   Kakalis, L. T., Kennedy, M., Sikkink, R., Rusnak, F. & Armitage, I. M. Characterization of the calcium-binding sites of calcineurin B. *FEBS letters* **362**, 55–8 (1995).

50.   Okamura, H. *et al.* Concerted dephosphorylation of the transcription factor NFAT1 induces a conformational switch that regulates transcriptional activity. *Molecular cell* **6**, 539–50 (2000).

51.   McKinsey, T. A., Zhang, C. L., Lu, J. & Olson, E. N. Signal-dependent nuclear export of a histone deacetylase regulates muscle differentiation. *Nature* **408**, 106–11 (2000).

52.   Wilkins, B. J. *et al.* Calcineurin/NFAT coupling participates in pathological, but not physiological, cardiac hypertrophy. *Circulation research* **94**, 110–8 (2004).

53.   Berridge, M. J. Remodelling Ca2+ signalling systems and cardiac hypertrophy. *Biochemical Society transactions* **34**, 228–31 (2006).

54.   Wilkins, B. J. & Molkentin, J. D. Calcium-calcineurin signaling in the regulation of cardiac hypertrophy. *Biochemical and biophysical research communications* **322**, 1178–91 (2004).

55.   Wu, X. *et al.* Local InsP3-dependent perinuclear Ca2+ signaling in cardiac myocyte excitation-transcription coupling. *The Journal of clinical investigation* **116**, 675–82 (2006).

56.   Shannon, T. R., Wang, F., Puglisi, J., Weber, C. & Bers, D. M. A mathematical treatment of integrated Ca dynamics within the ventricular myocyte. *Biophysical journal* **87**, 3351–71 (2004).

57.   Tomaselli, G. F. & Marbán, E. Electrophysiological remodeling in hypertrophy and heart failure. *Cardiovascular research* **42**, 270–83 (1999).

58.   Chen, X. *et al.* L-type Ca2+ channel density and regulation are altered in failing human ventricular myocytes and recover after support with mechanical assist devices. *Circulation research* **91**, 517–24 (2002).

59.   Orchard, C. & Brette, F. t-Tubules and sarcoplasmic reticulum function in cardiac ventricular myocytes. *Cardiovascular research* **77**, 237–44 (2008).

60.   Sitsapesan, R. & Williams, A. J. Regulation of the gating of the sheep cardiac sarcoplasmic reticulum Ca(2+)-release channel by luminal Ca2+. *The Journal of membrane biology* **137**, 215–26 (1994).

61.   Lewis, R. S. Calcium signaling mechanisms in T lymphocytes. *Annual review of immunology* **19**, 497–521 (2001).

62.   Putney, J. W. A model for receptor-regulated calcium entry. *Cell calcium* **7**, 1–12 (1986).

63.   Takemura, H. & Putney, J. W. Capacitative calcium entry in parotid acinar cells. *The Biochemical journal* **258**, 409–12 (1989).

64.   Feske, S., Giltnane, J., Dolmetsch, R., Staudt, L. M. & Rao, A. Gene regulation mediated by calcium signals in T lymphocytes. *Nature immunology* **2**, 316–24 (2001).

65.   Hoth, M. & Penner, R. Depletion of intracellular calcium stores activates a calcium current in mast cells. *Nature* **355**, 353–6 (1992).

66.   Parekh, A. B. Functional consequences of activating store-operated CRAC channels. *Cell calcium* **42**, 111–21 (2007).

67.   Parekh, A. B. & Putney, J. W. Store-operated calcium channels. *Physiological reviews* **85**, 757–810 (2005).

68.   Dirksen, R. T. Checking your SOCCs and feet: the molecular mechanisms of Ca2+ entry in skeletal muscle. *The Journal of physiology* **587**, 3139–47 (2009).

69. Liou, J. *et al.* STIM is a Ca2+ sensor essential for Ca2+-store-depletion-triggered Ca2+ influx. *Current biology : CB* **15**, 1235–41 (2005).

70. Zhang, S. L. *et al.* STIM1 is a Ca2+ sensor that activates CRAC channels and migrates from the Ca2+ store to the plasma membrane. *Nature* **437**, 902–5 (2005).

71. Feske, S. *et al.* A mutation in Orai1 causes immune deficiency by abrogating CRAC channel function. *Nature* **441**, 179–85 (2006).

72. Vig, M. *et al.* CRACM1 is a plasma membrane protein essential for store-operated Ca2+ entry. *Science (New York, N.Y.)* **312**, 1220–3 (2006).

73. Mercer, J. C. *et al.* Large store-operated calcium selective currents due to co-expression of Orai1 or Orai2 with the intracellular calcium sensor, Stim1. *The Journal of biological chemistry* **281**, 24979–90 (2006).

74. Park, C. Y. *et al.* STIM1 clusters and activates CRAC channels via direct binding of a cytosolic domain to Orai1. *Cell* **136**, 876–90 (2009).

75. Zhou, Y. *et al.* STIM1 gates the store-operated calcium channel ORAI1 in vitro. *Nature structural & molecular biology* **17**, 112–6 (2010).

76. Hoth, M. & Penner, R. Calcium release-activated calcium current in rat mast cells. *The Journal of physiology* **465**, 359–86 (1993).

77. Lepple-Wienhues, A. & Cahalan, M. D. Conductance and permeation of monovalent cations through depletion-activated Ca2+ channels (ICRAC) in Jurkat T cells. *Biophysical journal* **71**, 787–94 (1996).

78. Bakowski, D. & Parekh, A. B. Monovalent cation permeability and Ca(2+) block of the store-operated Ca(2+) current I(CRAC)in rat basophilic leukemia cells. *Pflügers Archiv : European journal of physiology* **443**, 892–902 (2002).

79. Hunton, D. L. *et al.* Capacitative calcium entry contributes to nuclear factor of activated T-cells nuclear translocation and hypertrophy in cardiomyocytes. *The Journal of biological chemistry* **277**, 14266–73 (2002).

80. Uehara, A., Yasukochi, M., Imanaga, I., Nishi, M. & Takeshima, H. Store-operated Ca2+ entry uncoupled with ryanodine receptor and junctional membrane complex in heart muscle cells. *Cell calcium* **31**, 89–96 (2002).

81. Kentish, J. C. *et al.* Calcium release from cardiac sarcoplasmic reticulum induced by photorelease of calcium or Ins(1,4,5)P3. *The American journal of physiology* **258**, H610–5 (1990).

82. Freichel, M. *et al.* Store-operated cation channels in the heart and cells of the cardiovascular system. *Cell Physiol Biochem.* **9**, 270–83 (1999).

83. Roos, J. *et al.* STIM1, an essential and conserved component of store-operated Ca2+ channel function. *The Journal of cell biology* **169**, 435–45 (2005).

84. Oritani, K. & Kincade, P. W. Identification of stromal cell products that interact with pre-B cells. *The Journal of cell biology* **134**, 771–82 (1996).

85. Hogan, P. G., Lewis, R. S. & Rao, A. Molecular basis of calcium signaling in lymphocytes: STIM and ORAI. *Annual review of immunology* **28**, 491–533 (2010).

86. Feske, S. CRAC channelopathies. *Pflügers Archiv : European journal of physiology* **460**, 417–35 (2010).

87. Stathopulos, P. B., Zheng, L., Li, G.-Y., Plevin, M. J. & Ikura, M. Structural and mechanistic insights into STIM1-mediated initiation of store-operated calcium entry. *Cell* **135**, 110–22 (2008).

88. Zheng, L., Stathopulos, P. B., Li, G.-Y. & Ikura, M. Biophysical characterization of the EF-hand and SAM domain containing Ca2+ sensory region of STIM1 and STIM2. *Biochemical and biophysical research communications* **369**, 240–6 (2008).

89. Peterson, A. J. *et al.* A domain shared by the Polycomb group proteins Scm and ph mediates heterotypic and homotypic interactions. *Molecular and cellular biology* **17**, 6683–92 (1997).

90. Liou, J., Fivaz, M., Inoue, T. & Meyer, T. Live-cell imaging reveals sequential oligomerization and local plasma membrane targeting of stromal interaction molecule 1 after Ca2+ store depletion. *Proceedings of the National Academy of Sciences of the United States of America* **104**, 9301–6 (2007).

91. Luik, R. M., Wu, M. M., Buchanan, J. & Lewis, R. S. The elementary unit of store-operated Ca2+ entry: local activation of CRAC channels by STIM1 at ER-plasma membrane junctions. *The Journal of cell biology* **174**, 815–25 (2006).

92. Stathopulos, P. B., Li, G.-Y., Plevin, M. J., Ames, J. B. & Ikura, M. Stored Ca2+ depletion-induced oligomerization of stromal interaction molecule 1 (STIM1) via the EF-SAM region: An initiation mechanism for capacitive Ca2+ entry. *The Journal of biological chemistry* **281**, 35855–62 (2006).

93. Stathopulos, P. B. & Ikura, M. Structurally delineating stromal interaction molecules as the endoplasmic reticulum calcium sensors and regulators of calcium release-activated calcium entry. *Immunological reviews* **231**, 113–31 (2009).

94. Shen, W.-W., Frieden, M. & Demaurex, N. Local cytosolic Ca2+ elevations are required for stromal interaction molecule 1 (STIM1) de-oligomerization and termination of store-operated Ca2+ entry. *The Journal of biological chemistry* **286**, 36448–59 (2011).

95. Muik, M. *et al.* A Cytosolic Homomerization and a Modulatory Domain within STIM1 C Terminus Determine Coupling to ORAI1 Channels. *The Journal of biological chemistry* **284**, 8421–6 (2009).

96. Hewavitharana, T. *et al.* Location and function of STIM1 in the activation of Ca2+ entry signals. *The Journal of biological chemistry* **283**, 26252–62 (2008).

97. Orci, L. *et al.* From the Cover: STIM1-induced precortical and cortical subdomains of the endoplasmic reticulum. *Proceedings of the National Academy of Sciences of the United States of America* **106**, 19358–62 (2009).

98. Lur, G. *et al.* Ribosome-free terminals of rough ER allow formation of STIM1 puncta and segregation of STIM1 from IP(3) receptors. *Current biology : CB* **19**, 1648–53 (2009).

99. Varga-Szabo, D. *et al.* The calcium sensor STIM1 is an essential mediator of arterial thrombosis and ischemic brain infarction. *The Journal of experimental medicine* **205**, 1583–91 (2008).

100. Soboloff, J. *et al.* STIM2 is an inhibitor of STIM1-mediated store-operated Ca2+ Entry. *Current biology : CB* **16**, 1465–70 (2006).

101. Parvez, S. *et al.* STIM2 protein mediates distinct store-dependent and store-independent modes of CRAC channel activation. *FASEB journal : official publication of the Federation of American Societies for Experimental Biology* **22**, 752–61 (2008).

102. Brandman, O., Liou, J., Park, W. S. & Meyer, T. STIM2 is a feedback regulator that stabilizes basal cytosolic and endoplasmic reticulum Ca2+ levels. *Cell* **131**, 1327–39 (2007).

103. Gwack, Y. *et al.* Biochemical and functional characterization of Orai proteins. *The Journal of biological chemistry* **282**, 16232–43 (2007).

104. Prakriya, M. *et al.* Orai1 is an essential pore subunit of the CRAC channel. *Nature* **443**, 230–3 (2006).

105. Vig, M. *et al.* CRACM1 multimers form the ion-selective pore of the CRAC channel. *Current biology : CB* **16**, 2073–9 (2006).

106. Frischauf, I. *et al.* Molecular determinants of the coupling between STIM1 and Orai channels: differential activation of Orai1-3 channels by a STIM1 coiled-coil mutant. *The Journal of biological chemistry* **284**, 21696–706 (2009).

107. Mignen, O., Thompson, J. L. & Shuttleworth, T. J. Orai1 subunit stoichiometry of the mammalian CRAC channel pore. *The Journal of physiology* **586**, 419–25 (2008).

108. Penna, A. *et al.* The CRAC channel consists of a tetramer formed by Stim-induced dimerization of Orai dimers. *Nature* **456**, 116–20 (2008).

109. Lis, A. *et al.* CRACM1, CRACM2, and CRACM3 are store-operated Ca2+ channels with distinct functional properties. *Current biology : CB* **17**, 794–800 (2007).

110. Lee, K. P. *et al.* Molecular determinants of fast Ca2+-dependent inactivation and gating of the Orai channels. *Proceedings of the National Academy of Sciences of the United States of America* **106**, 14687–92 (2009).

111. Gwack, Y. *et al.* Hair loss and defective T- and B-cell function in mice lacking ORAI1. *Molecular and cellular biology* **28**, 5209–22 (2008).

112. Soboloff, J. *et al.* Orai1 and STIM reconstitute store-operated calcium channel function. *The Journal of biological chemistry* **281**, 20661–5 (2006).

113. Muik, M. *et al.* Dynamic coupling of the putative coiled-coil domain of ORAI1 with STIM1 mediates ORAI1 channel activation. *The Journal of biological chemistry* **283**, 8014–22 (2008).

114. Calloway, N., Vig, M., Kinet, J.-P., Holowka, D. & Baird, B. Molecular clustering of STIM1 with Orai1/CRACM1 at the plasma membrane depends dynamically on depletion of Ca2+ stores and on electrostatic interactions. *Molecular biology of the cell* **20**, 389–99 (2009).

115. Wu, M. M., Buchanan, J., Luik, R. M. & Lewis, R. S. Ca2+ store depletion causes STIM1 to accumulate in ER regions closely associated with the plasma membrane. *The Journal of cell biology* **174**, 803–13 (2006).

116. Yuan, J. P. *et al.* SOAR and the polybasic STIM1 domains gate and regulate Orai channels. *Nature cell biology* **11**, 337–43 (2009).

117. Li, Z. *et al.* Mapping the interacting domains of STIM1 and Orai1 in Ca2+ release-activated Ca2+ channel activation. *The Journal of biological chemistry* **282**, 29448–56 (2007).

118. Li, Z. *et al.* Graded activation of CRAC channel by binding of different numbers of STIM1 to Orai1 subunits. *Cell research* **21**, 305–15 (2011).

119. Cosens, D. J. & Manning, A. Abnormal electroretinogram from a Drosophila mutant. *Nature* **224**, 285–7 (1969).

120. Sidi, S., Friedrich, R. W. & Nicolson, T. NompC TRP channel required for vertebrate sensory hair cell mechanotransduction. *Science (New York, N.Y.)* **301**, 96–9 (2003).

121. Minke, B. & Selinger, Z. The inositol-lipid pathway is necessary for light excitation in fly photoreceptors. *Society of General Physiologists series* **47**, 201–17 (1992).

122. Clapham, D. E. TRP channels as cellular sensors. *Nature* **426**, 517–24 (2003).

123. Seth, M. *et al.* TRPC1 channels are critical for hypertrophic signaling in the heart. *Circulation research* **105**, 1023–30 (2009).

124. Ohba, T. *et al.* Upregulation of TRPC1 in the development of cardiac hypertrophy. *Journal of molecular and cellular cardiology* **42**, 498–507 (2007).

125. Kuwahara, K. *et al.* TRPC6 fulfills a calcineurin signaling circuit during pathologic cardiac remodeling. *The Journal of clinical investigation* **116**, 3114–26 (2006).

126. Bush, E. W. *et al.* Canonical transient receptor potential channels promote cardiomyocyte hypertrophy through activation of calcineurin signaling. *The Journal of biological chemistry* **281**, 33487–96 (2006).

127. Ambudkar, I. S. & Ong, H. L. Organization and function of TRPC channelosomes. *Pflügers Archiv : European journal of physiology* **455**, 187–200 (2007).

128. Ward, M.-L. *et al.* Stretch-activated channels in the heart: contributions to length-dependence and to cardiomyopathy. *Progress in biophysics and molecular biology* **97**, 232–49 (2008).

129. Maroto, R. *et al.* TRPC1 forms the stretch-activated cation channel in vertebrate cells. *Nature cell biology* **7**, 179–85 (2005).

130. Nakayama, H., Wilkin, B. J., Bodi, I. & Molkentin, J. D. Calcineurin-dependent cardiomyopathy is activated by TRPC in the adult mouse heart. *FASEB journal : official publication of the Federation of American Societies for Experimental Biology* **20**, 1660–70 (2006).

131. Wu, X., Eder, P., Chang, B. & Molkentin, J. D. TRPC channels are necessary mediators of pathologic cardiac hypertrophy. *Proceedings of the National Academy of Sciences of the United States of America* **107**, 7000–5 (2010).

132. Onohara, N. *et al.* TRPC3 and TRPC6 are essential for angiotensin II-induced cardiac hypertrophy. *The EMBO journal* **25**, 5305–16 (2006).

133. Ver Heyen, M. *et al.* Replacement of the muscle-specific sarcoplasmic reticulum Ca(2+)-ATPase isoform SERCA2a by the nonmuscle SERCA2b homologue causes mild concentric hypertrophy and impairs contraction-relaxation of the heart. *Circulation research* **89**, 838–46 (2001).

134. Shan, D., Marchase, R. B. & Chatham, J. C. Overexpression of TRPC3 increases apoptosis but not necrosis in response to ischemia-reperfusion in adult mouse cardiomyocytes. *American journal of physiology. Cell physiology* **294**, C833–41 (2008).

135. Alicia, S., Angélica, Z., Carlos, S., Alfonso, S. & Vaca, L. STIM1 converts TRPC1 from a receptor-operated to a store-operated channel: moving TRPC1 in and out of lipid rafts. *Cell calcium* **44**, 479–91 (2008).

136. Huang, G. N. *et al.* STIM1 carboxyl-terminus activates native SOC, I(crac) and TRPC1 channels. *Nature cell biology* **8**, 1003–10 (2006).

137. Yuan, J. P., Zeng, W., Huang, G. N., Worley, P. F. & Muallem, S. STIM1 heteromultimerizes TRPC channels to determine their function as store-operated channels. *Nature cell biology* **9**, 636–45 (2007).

138. Liao, Y. *et al.* Orai proteins interact with TRPC channels and confer responsiveness to store depletion. *Proceedings of the National Academy of Sciences of the United States of America* **104**, 4682–7 (2007).

139. Cheng, K. T., Liu, X., Ong, H. L. & Ambudkar, I. S. Functional requirement for Orai1 in store-operated TRPC1-STIM1 channels. *The Journal of biological chemistry* **283**, 12935–40 (2008).

140. Ng, L. C. *et al.* TRPC1 and Orai1 interact with STIM1 and mediate capacitative Ca2+ entry caused by acute hypoxia in mouse pulmonary arterial smooth muscle cells. *American journal of physiology. Cell physiology* **303**, C1156–72 (2012).

141. Ong, H. L. *et al.* Dynamic assembly of TRPC1-STIM1-Orai1 ternary complex is involved in store-operated calcium influx. Evidence for similarities in store-operated and calcium release-activated calcium channel components. *The Journal of biological chemistry* **282**, 9105–16 (2007).

142. Liao, Y. *et al.* Functional interactions among Orai1, TRPCs, and STIM1 suggest a STIM-regulated heteromeric Orai/TRPC model for SOCE/Icrac channels. *Proceedings of the National Academy of Sciences of the United States of America* **105**, 2895–900 (2008).

143. Potier, M. & Trebak, M. New developments in the signaling mechanisms of the store-operated calcium entry pathway. *Pflügers Archiv : European journal of physiology* **457**, 405–15 (2008).

144. Jentzsch, C. *et al.* A phenotypic screen to identify hypertrophy-modulating microRNAs in primary cardiomyocytes. *Journal of molecular and cellular cardiology* **52**, 13–20 (2012).

145. Engelhardt, S., Hein, L., Wiesmann, F. & Lohse, M. J. Progressive hypertrophy and heart failure in beta1-adrenergic receptor transgenic mice. *Proceedings of the National Academy of Sciences of the United States of America* **96**, 7059–64 (1999).

146. Hein, S. *et al.* Progression from compensated hypertrophy to failure in the pressure-overloaded human heart: structural deterioration and compensatory mechanisms. *Circulation* **107**, 984–91 (2003).

147. Braz, J. C. *et al.* Targeted inhibition of p38 MAPK promotes hypertrophic cardiomyopathy through upregulation of calcineurin-NFAT signaling. *The Journal of clinical investigation* **111**, 1475–86 (2003).

148. Putney, J. W. Capacitive calcium entry: sensing the calcium stores. *The Journal of cell biology* **169**, 381–2 (2005).

149. Gregorio, C. C. & Antin, P. B. To the heart of myofibril assembly. *Trends in cell biology* **10**, 355–62 (2000).

150. Conway, S. J., Kruzynska-Frejtag, A., Kneer, P. L., Machnicki, M. & Koushik, S. V What cardiovascular defect does my prenatal mouse mutant have, and why? *Genesis (New York, N.Y. : 2000)* **35**, 1–21 (2003).

151. Stiber, J. *et al.* STIM1 signalling controls store-operated calcium entry required for development and contractile function in skeletal muscle. *Nature cell biology* **10**, 688–97 (2008).

152. Li, T. *et al.* STIM1-Ca(2+) signaling is required for the hypertrophic growth of skeletal muscle in mice. *Molecular and cellular biology* **32**, 3009–17 (2012).

153. Banerjee, I., Fuseler, J. W., Price, R. L., Borg, T. K. & Baudino, T. a Determination of cell types and numbers during cardiac development in the neonatal and adult rat and mouse. *American journal of physiology. Heart and circulatory physiology* **293**, H1883–91 (2007).

154. Oh-Hora, M. *et al.* Dual functions for the endoplasmic reticulum calcium sensors STIM1 and STIM2 in T cell activation and tolerance. *Nature immunology* **9**, 432–43 (2008).

155. Bird, G. S. *et al.* STIM1 is a calcium sensor specialized for digital signaling. *Current biology : CB* **19**, 1724–9 (2009).

156. Hunton, D. L., Zou, L., Pang, Y. & Marchase, R. B. Adult rat cardiomyocytes exhibit capacitative calcium entry. *American journal of physiology. Heart and circulatory physiology* **286**, H1124–32 (2004).

157. Luo, X. *et al.* STIM1-dependent store-operated Ca^{2+} entry is required for pathological cardiac hypertrophy. *Journal of molecular and cellular cardiology* **52**, 136–47 (2012).

158. Voelkers, M. *et al.* Orai1 and Stim1 regulate normal and hypertrophic growth in cardiomyocytes. *Journal of molecular and cellular cardiology* **48**, 1329–34 (2010).

159. Walsh, C. M., Doherty, M. K., Tepikin, A. V & Burgoyne, R. D. Evidence for an interaction between Golli and STIM1 in store-operated calcium entry. *The Biochemical journal* **430**, 453–60 (2010).

160. Chiu, T.-Y., Teng, H.-C., Huang, P.-C., Kao, F.-J. & Yang, D.-M. Dominant role of Orai1 with STIM1 on the cytosolic entry and cytotoxicity of lead ions. *Toxicological sciences : an official journal of the Society of Toxicology* **110**, 353–62 (2009).

161. Smyth, J. T., Dehaven, W. I., Bird, G. S. & Putney, J. W. Ca2+-store-dependent and -independent reversal of Stim1 localization and function. *Journal of cell science* **121**, 762–72 (2008).

162. Li, J. *et al.* Interactions, functions, and independence of plasma membrane STIM1 and TRPC1 in vascular smooth muscle cells. *Circulation research* **103**, e97–104 (2008).

163. Lu, W., Wang, J., Peng, G., Shimoda, L. A. & Sylvester, J. T. Knockdown of stromal interaction molecule 1 attenuates store-operated Ca2+ entry and Ca2+ responses to acute hypoxia in pulmonary arterial smooth muscle. *American journal of physiology. Lung cellular and molecular physiology* **297**, L17–25 (2009).

164. Ng, L. C. *et al.* TRPC1 and STIM1 mediate capacitative Ca2+ entry in mouse pulmonary arterial smooth muscle cells. *The Journal of physiology* **587**, 2429–42 (2009).

165. Potier, M. *et al.* Evidence for STIM1- and Orai1-dependent store-operated calcium influx through ICRAC in vascular smooth muscle cells: role in proliferation and migration. *FASEB journal : official publication of the Federation of American Societies for Experimental Biology* **23**, 2425–37 (2009).

166. Takahashi, Y. *et al.* Functional role of stromal interaction molecule 1 (STIM1) in vascular smooth muscle cells. *Biochemical and biophysical research communications* **361**, 934–40 (2007).

167. Ohba, T. *et al.* Essential role of STIM1 in the development of cardiomyocyte hypertrophy. *Biochemical and biophysical research communications* **389**, 172–6 (2009).

168. Chen, J.-B. *et al.* Multiple Ca2+ signaling pathways regulate intracellular Ca2+ activity in human cardiac fibroblasts. *Journal of cellular physiology* **223**, 68–75 (2010).

169. Hu, R. *et al.* Characterization of calcium signaling pathways in human preadipocytes. *Journal of cellular physiology* **220**, 765–70 (2009).

170. Grupe, M., Myers, G., Penner, R. & Fleig, A. Activation of store-operated I(CRAC) by hydrogen peroxide. *Cell calcium* **48**, 1–9 (2010).

171. Chvanov, M. *et al.* ATP depletion induces translocation of STIM1 to puncta and formation of STIM1-ORAI1 clusters: translocation and re-translocation of STIM1 does not require ATP. *Pflügers Archiv : European journal of physiology* **457**, 505–17 (2008).

172. Saucerman, J. J. & Bers, D. M. Calmodulin binding proteins provide domains of local Ca2+ signaling in cardiac myocytes. *Journal of molecular and cellular cardiology* **52**, 312–6 (2012).

173.	Berridge, M. J. Inositol trisphosphate and calcium oscillations. *Biochemical Society symposium* 1–7 (2007).doi:10.1042/BSS0740001

174.	Putney, J. W. & Bird, G. S. Cytoplasmic calcium oscillations and store-operated calcium influx. *The Journal of physiology* **586**, 3055–9 (2008).

175.	Mancarella, S., Wang, Y. & Gill, D. L. Calcium signals: STIM dynamics mediate spatially unique oscillations. *Current biology : CB* **19**, R950–2 (2009).

176.	Chang, W.-C., Nelson, C. & Parekh, A. B. Ca2+ influx through CRAC channels activates cytosolic phospholipase A2, leukotriene C4 secretion, and expression of c-fos through ERK-dependent and -independent pathways in mast cells. *FASEB journal : official publication of the Federation of American Societies for Experimental Biology* **20**, 2381–3 (2006).

177.	Fanger, C. M., Hoth, M., Crabtree, G. R. & Lewis, R. S. Characterization of T cell mutants with defects in capacitative calcium entry: genetic evidence for the physiological roles of CRAC channels. *The Journal of cell biology* **131**, 655–67 (1995).

178.	Colella, M. *et al.* Ca2+ oscillation frequency decoding in cardiac cell hypertrophy: role of calcineurin/NFAT as Ca2+ signal integrators. *Proceedings of the National Academy of Sciences of the United States of America* **105**, 2859–64 (2008).

179.	Dolmetsch, R. E., Lewis, R. S., Goodnow, C. C. & Healy, J. I. Differential activation of transcription factors induced by Ca2+ response amplitude and duration. *Nature* **386**, 855–8 (1997).

180.	Dolmetsch, R. E., Xu, K. & Lewis, R. S. Calcium oscillations increase the efficiency and specificity of gene expression. *Nature* **392**, 933–6 (1998).

181.	Gruver, C. L., DeMayo, F., Goldstein, M. A. & Means, A. R. Targeted developmental overexpression of calmodulin induces proliferative and hypertrophic growth of cardiomyocytes in transgenic mice. *Endocrinology* **133**, 376–88 (1993).

182.	Molkentin, J. D. *et al.* A calcineurin-dependent transcriptional pathway for cardiac hypertrophy. *Cell* **93**, 215–28 (1998).

183.	Urbain, R. *et al.* [Left ventricular accumulation of messenger ribonucleic acid coding for the natriuretic atrial factor in various experimental models of cardiac hypertrophy in rats]. *Archives des maladies du coeur et des vaisseaux* **82**, 1089–92 (1989).

184.	Hulot, J.-S. *et al.* Critical role for stromal interaction molecule 1 in cardiac hypertrophy. *Circulation* **124**, 796–805 (2011).

185.	Picard, C. *et al.* STIM1 mutation associated with a syndrome of immunodeficiency and autoimmunity. *The New England journal of medicine* **360**, 1971–80 (2009).

186. Mancarella, S. *et al.* Targeted STIM deletion impairs calcium homeostasis, NFAT activation, and growth of smooth muscle. *FASEB journal : official publication of the Federation of American Societies for Experimental Biology* 1–14 (2012).doi:10.1096/fj.12-215293

187. Seth, M. *et al.* Dynamic regulation of sarcoplasmic reticulum Ca(2+) stores by stromal interaction molecule 1 and sarcolipin during muscle differentiation. *Developmental dynamics : an official publication of the American Association of Anatomists* **241**, 639–47 (2012).

188. Inagaki, K. *et al.* Robust systemic transduction with AAV9 vectors in mice: efficient global cardiac gene transfer superior to that of AAV8. *Molecular therapy : the journal of the American Society of Gene Therapy* **14**, 45–53 (2006).

189. McNally, B. a & Prakriya, M. Permeation, selectivity and gating in store-operated CRAC channels. *The Journal of physiology* **590**, 4179–91 (2012).

190. Wang, Y. *et al.* The calcium store sensor, STIM1, reciprocally controls Orai and CaV1.2 channels. *Science (New York, N.Y.)* **330**, 105–9 (2010).

191. Deng, X., Wang, Y., Zhou, Y., Soboloff, J. & Gill, D. L. STIM and Orai: dynamic intermembrane coupling to control cellular calcium signals. *The Journal of biological chemistry* **284**, 22501–5 (2009).

192. Bergsmann, J. *et al.* Molecular determinants within N terminus of Orai3 protein that control channel activation and gating. *The Journal of biological chemistry* **286**, 31565–75 (2011).

193. Tang, J. *et al.* Identification of common binding sites for calmodulin and inositol 1,4,5-trisphosphate receptors on the carboxyl termini of trp channels. *The Journal of biological chemistry* **276**, 21303–10 (2001).

194. Singh, B. B., Liu, X., Tang, J., Zhu, M. X. & Ambudkar, I. S. Calmodulin regulates Ca(2+)-dependent feedback inhibition of store-operated Ca(2+) influx by interaction with a site in the C terminus of TrpC1. *Molecular cell* **9**, 739–50 (2002).

195. Yildirim, E., Dietrich, A. & Birnbaumer, L. The mouse C-type transient receptor potential 2 (TRPC2) channel: alternative splicing and calmodulin binding to its N terminus. *Proceedings of the National Academy of Sciences of the United States of America* **100**, 2220–5 (2003).

196. Varga-Szabo, D. *et al.* Store-operated Ca(2+) entry in platelets occurs independently of transient receptor potential (TRP) C1. *Pflügers Archiv : European journal of physiology* **457**, 377–87 (2008).

197. Ohba, T. *et al.* Biochemical and Biophysical Research Communications Essential role of STIM1 in the development of cardiomyocyte hypertrophy. *Biochemical and Biophysical Research Communications* **389**, 172–176 (2009).

198. Feng, S.-L. *et al.* Activation of calcium-sensing receptor increases TRPC3 expression in rat cardiomyocytes. *Biochemical and biophysical research communications* **406**, 278–84 (2011).

199. Morales, S. *et al.* Calcium controls smooth muscle TRPC gene transcription via the CaMK/calcineurin-dependent pathways. *American journal of physiology. Cell physiology* **292**, C553–63 (2007).

200. Kim, M. S. *et al.* Native Store-operated Ca2+ Influx Requires the Channel Function of Orai1 and TRPC1. *The Journal of biological chemistry* **284**, 9733–41 (2009).

201. Woodard, G. E., López, J. J., Jardín, I., Salido, G. M. & Rosado, J. A. TRPC3 regulates agonist-stimulated Ca2+ mobilization by mediating the interaction between type I inositol 1,4,5-trisphosphate receptor, RACK1, and Orai1. *The Journal of biological chemistry* **285**, 8045–53 (2010).

202. Park, C. Y., Shcheglovitov, A. & Dolmetsch, R. The CRAC channel activator STIM1 binds and inhibits L-type voltage-gated calcium channels. *Science (New York, N.Y.)* **330**, 101–5 (2010).

203. Semsarian, C. *et al.* The L-type calcium channel inhibitor diltiazem prevents cardiomyopathy in a mouse model. *The Journal of clinical investigation* **109**, 1013–20 (2002).

204. Bauer, M. C., O'Connell, D., Cahill, D. J. & Linse, S. Calmodulin binding to the polybasic C-termini of STIM proteins involved in store-operated calcium entry. *Biochemistry* **47**, 6089–91 (2008).

205. Shen, X. *et al.* Scanning the human proteome for calmodulin-binding proteins. *Proceedings of the National Academy of Sciences of the United States of America* **102**, 5969–74 (2005).

206. Mullins, F. M., Park, C. Y., Dolmetsch, R. E. & Lewis, R. S. STIM1 and calmodulin interact with Orai1 to induce Ca2+-dependent inactivation of CRAC channels. *Proceedings of the National Academy of Sciences of the United States of America* **106**, 15495–500 (2009).

207. Zhang, Z. *et al.* Activation of Trp3 by inositol 1,4,5-trisphosphate receptors through displacement of inhibitory calmodulin from a common binding domain. *Proceedings of the National Academy of Sciences of the United States of America* **98**, 3168–73 (2001).

208. Trost, C., Bergs, C., Himmerkus, N. & Flockerzi, V. The transient receptor potential, TRP4, cation channel is a novel member of the family of calmodulin binding proteins. *The Biochemical journal* **355**, 663–70 (2001).

209. Liu, Y. *et al.* Crystal structure of calmodulin binding domain of orai1 in complex with ca2+*calmodulin displays a unique binding mode. *The Journal of biological chemistry* **287**, 43030–41 (2012).

210. Galán, C., Dionisio, N., Smani, T., Salido, G. M. & Rosado, J. a The cytoskeleton plays a modulatory role in the association between STIM1 and the Ca2+ channel subunits Orai1 and TRPC1. *Biochemical pharmacology* **82**, 400–10 (2011).

211. Mori, M. X., Erickson, M. G. & Yue, D. T. Functional stoichiometry and local enrichment of calmodulin interacting with Ca2+ channels. *Science (New York, N.Y.)* **304**, 432–5 (2004).

212. Tandan, S. *et al.* Physical and functional interaction between calcineurin and the cardiac L-type Ca2+ channel. *Circulation research* **105**, 51–60 (2009).

7. Publications and conferences attended

7.1. Publications

Hulot JS, Fauconnier J, **Ramanujam D**, Chaanine A, Aubart F, Sassi Y, Merkle S, Cazorla O, Ouillé A, Dupuis M, Hadri L, Jeong D, Mühlstedt S, Schmitt J, Braun A, Bénard L, Saliba Y, Laggerbauer B, Nieswandt B, Lacampagne A, Hajjar RJ, Lompré AM, Engelhardt S. Critical role for stromal interaction molecule 1 in cardiac hypertrophy. *Circulation* **124**, 796–805 (2011).

7.2. Conferences and seminars attended

Ramanujam D, Sassi Y, Merkle S, Mühlstedt S, Dupuis M, Fauconnier J, Hulot JS, Schmitt J, Braun A, Nieswandt B, Engelhardt S. A critical role for STIM in cardiomyocyte hypertrophy. 77. Jahrestagung der Deutschen Gesellschaft für Kardiologie, 27-30.04.2011, Mannheim – **Presentation**

Ramanujam D, Fauconnier J, Sassi Y, Merkle S, Mühlstedt S, Dupuis M, Schmitt J, Braun A, Nieswandt B, Hulot JS, Engelhardt S. A critical role for STIM in cardiomyocyte hypertrophy *in vitro* and *in vivo*. 77. Jahrestagung der Deutschen Gesellschaft für Experimentelle und Klinische Pharmakologie und Toxikologie, 30.03-01.04.2011, Frankfurt am Main – **Poster**

Ramanujam D, Merkle S, Mühlstedt S, Dupuis M, Sassi Y, Schmitt J, Braun A, Nieswandt B, Engelhardt S. Investigation of Stim1-dependent calcium entry in cardiac myocytes. 76. Jahrestagung der Deutschen Gesellschaft für Experimentelle und Klinische Pharmakologie und Toxikologie, 23-25.03.2010, Mainz – **Poster**

8. Appendix

8.1. Acknowledgement

8.2. Lebenslauf

Name:	Deepak Prabhu RAMANUJAM
Geburtstag/-ort:	26.10.1984 in Chennai, India
Addresse:	Maistrasse 20, 80337 München
Telefon:	0176 83295360
Email:	ramanujam@ipt.med.tum.de

Studium und Praktika

02/2007 - 02/2008　　Biomedical Immunology (M.Sc.) an der University of East London (United Kingdom).

Masterthesis: Streptococcal superantigen induced inhibition of T regulatory cells ability to suppress T effector responses targeting myelin proteolipid protein (04/2007 – 09/2007).
Betreuer: Dr. Nadia Terrazzini and Dr. John Wright

07/2002 - 05/2006　　Industrial Biotechnology (B.Tech.) an der Government College of Technology – Anna University (India).

Bachelorthesis: Detection of human papilloma virus (HPV) signals in the peripheral blood of cervical cancer patients (12/2005 – 05/2006).
Betreuer: Prof. Muthukumaran Sivanandham

Praktikum am Madras Diabetes Research Foundation (04/2005 – 05/2005).
Betreuer: Dr. Muthuswamy Balasubramanyam

Industrie praktikum am Orchid Chemicals and Pharmaceuticals Limited (05/2004).

Promotion

12/2008 - heute　　Doktorarbeit am Institut fur Pharmakologie und Toxikologie der Technische Universität München.
Titel: Characterisation of stromal interaction molecule 1 (STIM1) in the myocardium.
Betreuer: Prof. Dr. Dr. Stefan Engelhardt.

07/2011 – heute　　Mitglied der TUM Graduate School der Technische Universität München.